THE ELECTRON SPIN RESONANCE STUDIES OF SOME FREE RADICALS

A Thesis

presented by

Ian McLaren Brown, B.Sc.

to the

University of St. Andrews

in application for the Degree

of Doctor of Philosophy

DECLARATION

I hereby declare that the following Thesis is based on the results of experiments carried out by me, that the Thesis is my own composition, and that it has not previously been presented for a Higher Degree.

CERTIFICATE

I certify that Ian McLaren Brown, B.Sc., has spent nine terms as a research student in the Physical Laboratory of the United College of St. Salvator and St. Leonard in the University of St. Andrews, that he has fulfilled the conditions of Ordinance No. 16 of the University Court of St. Andrews and that he is qualified to submit the accompanying Thesis in application for the Degree of Doctor of Philosophy.

Research Supervisor.

CAREER

I matriculated in the United College of St. Salvator and St. Leonard in the University of St. Andrews in October 1953 and followed a course leading to graduation in June 1957 with the Degree of Bachelor of Science with First Class Honours in Natural Philosophy. In October 1957 I was admitted by the Senatus Academicus of the same University as a research student in the Department of Natural Philosophy in the same College and have since then been engaged in the work which is the subject of this Thesis.

TABLE OF CONTENTS

TABLE OF CONTENTS

TABLE OF CONTENTS

TABLE OF CONTENTS

TABLE OF CONTENTS

LIST OF ILLUSTRATIONS

LIST OF ILLUSTRATIONS

LIST OF ILLUSTRATIONS

CHAPTER I

INTRODUCTION

1.1 Free Radicals.

It is well established that the chemical and physical properties of a molecule are attributable to the outer shell electrons of the constituent atoms. In general these outer shell or valence electrons are paired off with antiparallel spins. There does exist, however, a class of molecules wherein at least one valence electron is unpaired. The molecules of this class are called free radicals.

It might be supposed from Classical Chemistry, reasoning that, since the unpaired electrons are in the valence shells, the reactivity would be enhanced because of a tendency for pairing with unpaired electrons of other atoms. This is not always correct. For instance, it is true that some radicals are so reactive that to study their physical properties certain trapping techniques have to be adopted. Such work has recently been carried out in the National Bureau of Standards' Free Radical

Programme (1957-60) where radicals have been produced in the gas phase and trapped in an inert matrix at low temperatures. On the other hand, it must be borne in mind that there are radical types, e.g. Diphenylpicrylhydrazyl, with inherent stability which Pauling and Wheland have shown[1] to be due to delocalisation of the unpaired electrons throughout the molecule. We therefore see that the free radical nature does not necessarily imply high chemical reactivity. One feature that is common among radicals, however, is their paramagnetism and consequently their ability to show the phenomenon of electron spin resonance (e.s.r.).

1.2 The Resonance Phenomenon.

When a d.c. magnetic field is applied across a free radical sample of spin ½, it removes the double degeneracy of the magnetic states. The splitting between the resulting Zeeman levels is ΔE where $\Delta E = g \beta H_o$. g is called the spectroscopic splitting factor which varies only slightly from radical to radical. β is the Bohr magneton. H_o is the value of the magnetic field.

If the sample is also simultaneously subjected to an alternating field at right angles to the steady field,

magnetic dipole transitions will be induced by the former. Treating the alternating field as a time-dependent perturbation, it can be shown[2] from standard quantum mechanical theory that the probability of such transitions is appreciable only when the frequency ν_o of the a.c. magnetic field is the same as the transition frequency $\frac{\Delta E}{h}$ where h is Planck's constant. i.e. There is a resonance condition

$$h\nu_o = g\beta H_o \qquad (1.1)$$

These transitions can be induced from the lower to the upper level or vice versa so that the net transfer from the lower to the upper per unit time, N_{12} is given by:

$$N_{12} = \rho_{12}N_1 - \rho_{21}N_2 \qquad (1.2)$$

where N_1 is the number of electrons in the lower Zeeman level and N_2 is the number in the upper level. ρ_{12} is the transition probability per unit time of inducing transitions from the lower to the upper level by the alternating magnetic field. ρ_{21} is the corresponding transition probability for transitions from the upper to the lower level. From time-dependent perturbation theory

$$\rho_{12} = \rho_{21} = \rho(\nu).$$

$\rho(\nu)$ is a function of frequency (see 1.12) but is appreciable only when $\nu = \nu_o$.

Expression (1.2) therefore reduces to

$$N_{12} = (N_1 - N_2)\,\rho(\nu_o). \qquad (1.2)$$

The free radical system will be in equilibrium so that the Maxwell-Boltzmann distribution gives

$$\frac{N_1}{N_2} = e - \frac{\Delta E}{kT}. \qquad (1.3)$$

This implies that N_{12} is positive and hence the overall process is absorptive of energy.

The power absorbed in each transition = $h\nu_o$ so that the total power absorbed $= N_{12}\, h\nu_o$

$$= N_1 \frac{h^2\nu_o^2}{kT}\rho(\nu_o) \qquad (h\nu \ll kT)$$

$$= \frac{N}{2}\frac{h^2\nu_o^2}{kT}\,\rho(\nu_o) \qquad (1.4)$$

where $N = N_1 + N_2$.

Furthermore, for a system of total spin S, the time-dependent perturbation theory shows the existence of a selection rule that limits transitions to those between the levels differing in the z component of S by ± 1.

1.3 E.S.R. Absorption Characteristics.

Since in free radicals the difference in energy between the ground state and the first excited orbital state is much larger than kT, from the Maxwell-Boltzmann

distribution, it is seen that only the ground state will be populated. Thus e.s.r. is associated with this state only and the information about it is contained in the following characteristics of the e.s.r. spectrum.

(a) The g-value, i.e. the spectroscopic splitting factor.

(b) The presence of structure. If the unpaired electron is in the vicinity of nuclear spins, the magnetic interactions may cause hyperfine structure.

(c) The line width. The absorption line will have a line width due to the interactions experienced by the unpaired electron in the intra and intermolecular fields. These interactions provide the relaxation processes which keep the spin system in thermal equilibrium with the lattice. If $\Delta\nu$ is the line width in c/s, τ the total relaxation time of the spin system, then

$$\Delta\nu = \frac{1}{\tau} \qquad (1.5)$$

(d) The anisotropy of the spectrum. If investigations are carried out on a free radical in the single crystal form, the interactions on the unpaired electron will depend on the orientation of the external magnetic field with respect to the crystal axes. Hence the g-value, hyperfine structure and line width will show anisotropies that will

reflect the local symmetry about the unpaired electron.

Even although transition metals and rare earth elements are also paramagnetic, it is possible to distinguish them from free radicals by these characteristics of their e.s.r. spectra. Thus polycrystalline samples of most radicals show narrow lines (1 ~ 15 oe) with g-values all within a few tenths of one per cent of the free electron value 2.00229, whereas in transition metals, g-values can vary from one to six and line widths as great as 476 oe. have been reported[3]. In addition, in a single crystal or in dilute solution, the radical may show hyperfine structure that is indicative of its molecular structure.

1.4 General Experimental Procedure.

Due to the dependence of the power absorbed in v_o^2 (see 1.4), to obtain large detectable e.s.r. absorptions it is worth while working at microwave frequencies and making use of conventional waveguide techniques. A simple apparatus would consist of a microwave oscillator, usually a reflex klystron, coupled with waveguide of suitable dimensions to a cavity resonator. The free radical speciman is placed in this cavity at a region of maximum r.f. magnetic field. The d.c. field is applied perpendicular to the latter, across the sample and is homogeneous enough

to prevent broadening of the spectra. Magnetic absorptions will effect changes in cavity Q which can be detected as voltage changes from a crystal rectifier monitoring either the reflected or transmitted wave from the cavity. The presence of the cavity renders the apparatus very frequency sensitive so it is preferable to keep the microwave frequency constant and obtain the absorptions as a function of the magnetic field. This can be done by recording them as 50 c/s pulses on an oscilloscope while sweeping the magnetic field at 50 c/s about the resonance value.

1.5 An Estimate of the Minimum Number of Radicals Detectable.

An estimate will now be made of the minimum number of radicals that can be detected by a spectrometer limited by thermal noise only.

Feher has shown[4] that for a system using a reflection cavity and a magic-tee bridge, the maximum e.s.r. signal ΔV at the crystal rectifier is determined by

$$\frac{\Delta V}{V} = \frac{\sqrt{2}}{4} \frac{\Delta Q_o}{Q_o} \qquad (1.6)$$

where V is the available voltage from the klystron, Q_o is the unloaded Q of the cavity and ΔQ_o is the change in Q_o due to e.s.r. absorption. The rest of the calculation

differs from that made by Feher[4] but the final result is comparable with his for the same operating conditions of the spectrometer.

$$\text{The cavity } Q = \frac{2\pi\nu_o \cdot \text{Energy stored in the cavity}}{\text{The power absorbed in the walls + the paramagnetic power loss.}} \qquad (1.7)$$

Substitution of (1.4) for the paramagnetic loss gives:

$$\text{The cavity } Q = \frac{\frac{\nu_o}{4}\int_{V_c} H_1^2 \, d\,Vc}{\text{Wall losses} + \frac{N}{2}\frac{h^2\nu_o^2}{kT}\rho(\nu_o)} \qquad (1.8)$$

$$= Q_o - \Delta Q_o,$$

where V_c is the volume of the cavity, and H_1 is the amplitude of the r.f. magnetic field whose direction is along the x-axis while that of the splitting field is along the z-axis.

If the paramagnetic loss is much less than the wall losses ΔQ_o reduces to

$$\Delta Q_o = 2N\frac{h^2\nu_o}{kT}\frac{\rho(\nu_o)\,Q_o^2}{\int_{V_c} H_1^2 dV_c}V \qquad (1.9)$$

Putting this value of ΔQ_o into (1.6) gives

$$\Delta V = \frac{\sqrt{2}}{2}\frac{N\,h^2\nu_o}{kT}\frac{\rho(\nu_o)\,Q_o}{\int_{V_c} H_1^2 dV_c}V \qquad (1.10)$$

There is a minimum detectable value of N, N_{min} when ΔV is comparable with the thermal noise $\sqrt{2kT_d\Delta f R_o}$, Δf being the

bandwidth of the detector, T_d the temperature of the detector and R_o the characteristic impedance of the waveguide so that

$$N_{min} = \left(\frac{kT_d\Delta f}{2P_o}\right)^{\frac{1}{2}} \frac{2kT}{h^2\nu_o} \frac{\int_{V_c} H_1^2 dV_c}{Q_o \rho(\nu_o)} \qquad (1.11)$$

From time-dependent perturbation theory[5]

$$\rho(\nu) = \frac{g^2\beta^2}{h^2} \pi^2 \frac{\int_{V_s} H_1^2 dV_s}{V_s} |\langle +\tfrac{1}{2}| S_x | -\tfrac{1}{2}\rangle|^2 g(\nu) \qquad (1.12)$$

where V_s is the volume of the sample. $\langle +\frac{1}{2}|S_x|-\frac{1}{2}\rangle$ is the matrix element of the x-component of spin, S_x, between the states with S_z values $\pm\frac{1}{2}$ and $|\langle +\frac{1}{2}|S_x|-\frac{1}{2}\rangle|^2 = \frac{1}{4}$.

$g(\nu)$ is the line shape function which satisfies the equation

$$\int_0^\infty g(\nu)\, d\nu = 1 \qquad (1.13)$$

so that

$$g(\nu_o) \approx \frac{1}{\Delta\nu} \qquad (1.13a)$$

where $\Delta\nu$ is the line width.

Substituting (1.13a) into (1.12) and the resulting expression for $\rho(\nu_o)$ into (1.11) gives

$$N_{min} = \left(\frac{kT_d\Delta f}{2P_o}\right)^{\frac{1}{2}} \frac{2kT}{Q_o\nu_o} \frac{V_s}{\eta} \frac{\Delta\nu}{\beta^2\pi^2} \qquad (1.14)$$

where η is the filling factor here defined as

$$\eta = \frac{\int_{V_s} H_1^2 dV_s}{\int_{V_c} H_1^2 dV_c} \qquad (1.15)$$

For the following operating conditions of an x-band

spectrometer:

P_o = 50 m.w., Q_o = 4,000, Δf = 10 k c/s, $T = T_d = 300^oK$ and for a rectangular H_{012} cavity $\frac{V_s}{\eta}$ = 6 cm^3 substituted into (1.14) gives

$$N_{min} = 2 \times 10^{12} \text{ spins of D.P.P.H. of line width 2 oe} \qquad (1.16)$$

Also since $Q_o \propto \frac{1}{\nu_o^{\frac{1}{2}}}$ and $\eta \propto \frac{1}{V_c} \propto \nu_o^3$ expression (1.14) shows that

$$N_{min} \propto \frac{1}{\nu_o^{\frac{7}{2}}} \qquad (1.17)$$

1.6 Object of this Thesis.

It was the purpose of this work to investigate the e.s.r. properties of certain organic molecular complexes that contain free radicals. The formation of these compounds involves the mechanism of a transfer of a single electron from a donor to an acceptor molecule. Since both these molecules initially have an even number of paired electrons the radicals formed have two unpaired electrons per complex molecule. These complexes are therefore synonymously called charge-transfer, donor-acceptor or biradical molecular complexes[6] and the processes that give rise to them are known as charge-transfer or univalent redox reactions. Primarily, it was attempted to obtain the hyperfine spectra of these complexes and so unequivocally

identify them. As will be seen in Chapter II, the resolution of hyperfine structure is inhibited when the radicals are studied in concentrated polycrystalline form. Therefore, because no single crystals have been grown, the compounds have been studied in dilute solutions.

Chapter II discusses in detail the interactions mentioned in 1.3 with special emphasis on the hyperfine structure and the mechanisms modifying it.

Chapter III describes the apparatus designed and built for this research.

Chapter IV reports the results of the experiments and interprets them where possible.

CHAPTER II

THE THEORY INVOLVED IN E.S.R. ABSORPTION

This chapter will deal with a discussion of the interactions which influence the e.s.r. absorption characteristics of free radicals.

II.1 The General Hamiltonian.

The ground state of any quantum mechanical system can be obtained, in principle, from a solution of the time-independent Schrodinger wave equation,

$$\mathcal{H} \Psi_o = E_o \Psi_o \qquad (2.1)$$

where $\mathcal{H}$ is the complete Hamiltonian of the system, E_o is the lowest energy eigenvalue, and Ψ_o is the wave function corresponding to E_o.

For a system consisting of a single molecule, the Born-Oppenheimer theorem[7] can be assumed to be valid, so that for the purpose of determining the electronic motions, the nuclei can be considered as fixed in their equilibrium positions. As in this thesis work all radicals were investigated either in solids or solutions, the magnetic moments associated with molecular rotation as a whole, will be here

neglected. Hence, for a free radical molecule in an external magnetic field, $\mathcal{H}$ will reduce to

$$\mathcal{H} = T_e + V_e + \mathcal{H}_m \qquad (2.2)$$

where T_e is the kinetic energy operator of the electrons, V_e is the operator for the potential energy due to electrostatic electron-electron and nucleus-electron interaction, and $\mathcal{H}_m$ is the operator for the interactions between the electron spins and orbital moments, the electron and nuclear spins and all the interactions involving the external magnetic field. We shall also neglect nuclear quadrupole moments.

As $\mathcal{H}_m$ is a weak interaction operator, it can be considered as a perturbation term that can remove magnetic degeneracies of the ground state. E.s.r. transitions will involve energies ΔE which to a first order are given by

$$\Delta E = \langle \Psi_o^o | \mathcal{H}_m | \Psi_o^o \rangle \qquad (2.3)$$

where

$$(T_e + V_e)\Psi_o^o = E_o^o \Psi_o^o \qquad (2.4)$$

i.e. Ψ_o^o is the unperturbed eigenfunction of the ground state energy E_o^o.

In molecules where the exact form of Ψ_o^o is difficult to obtain because of the complexity of V_e in equation (2.4), it is necessary to adopt a simplified mathematical model.

The theory involved in e.s.r. can be formulated in terms of this model through expression (2.3). The experimentally-obtained quantities can then be used to appraise the validity of the approximation to Ψ_o^o and, at the same time, may point to further refinements.

A usual mathematical approximation of Ψ_o^o is its expression as a single product of one-electron functions φ_i, spin-orbitals, antisymmetrised in the form of a single Slater determinant.

i.e. $$\Psi_o^o = [(2N+1)!]^{-\frac{1}{2}} \sum_P (-1)^p P_{\varphi_1 \cdots \varphi_{2N+1}} \qquad (2.5)$$

p is the parity of the permutation P and the sum is over all (2N+1) permutations, where (2N+1) is the odd number of electrons in the free radical molecule. They will be restricted to the lowest (N+1) orbitals. The unpaired electron will then singly occupy the $(N+1)^{th}$ orbital, so that Ψ_o^o will describe a doublet state. Further, φ_i is a function $\psi_i(r_i)$ of the space co-ordinates r_i of the i^{th} electron multiplied by a function $\eta_i(\xi_i)$ of the spin co-ordinate ξ_i of the i^{th} electron.

$$\text{i.e.} \quad \varphi_i = \psi_i(r_i)\eta_i(\xi_i) \qquad (2.6)$$

The ψ_i's are called molecular orbitals which are often approximated by linear combinations of atomic orbitals[8] u_n

$$\text{i.e. } \psi_i = \sum_n c_n u_n \qquad (2.7)$$

The use of molecular orbitals implies that $(T_e + V_e)$ of equation (2.4) can be written to a good approximation in the form $\sum_i h\,eff_i$ where

$$h\,eff_i\ \psi_i = \varepsilon_i \psi_i \qquad (2.8)$$

The one electron Hamiltonian $h\,eff_i$ describes the average smoothed out field on the i^{th} electron.

Application of the Variation Principle[8] to the ψ_i's gives a set of equations from which the c's of equation (2.7) can be obtained for a given ε_i, namely

$$\Sigma\, c_n\, (\beta_{mn} - \varepsilon_i S_{mn}) = 0 \qquad (2.9)$$

The ε_i's are evaluated from the secular determinant

$$|\beta_{mn} - \varepsilon_i S_{mn}| = 0 \qquad (2.10)$$

where

$$\beta_{mn} = \langle u_m | h_{eff} | u_n \rangle$$

$$S_{mn} = \langle u_m | u_n \rangle$$

The following assumptions characteristic of the Hückel theory[9] render the above solutions more easily obtainable.

(1) All $S_{mn} = 0$

(2) All $\beta_{mm} = \alpha$

(3) $\beta_{mn} = 0$ for non-neighbouring atoms

$= \beta$ for neighbouring atoms.

In this theory, h_{eff} is not explicitly defined, but α and β are used as parameters, which are adjusted to fit the experimental results. The c's are of the most interest in magnetic resonance, as will be shown in Section II.5. They express the delocalisation of an electron throughout the molecule when it is in a molecular orbital ψ_i.

II.2 Quenching of Orbital Angular Momenta.

The total Hamiltonian of a molecule does not possess spherical symmetry, so that it will not commute with the orbital angular momentum operator. Orbital angular momentum quantumnumbers will then not specify the eigenstates. In effect, the highly directional and usually lowly symmetrical effective electric fields of the chemical bonds remove the orbital degeneracy associated with the isolated atoms through a Stark splitting. On application of an external magnetic field, the magnetic splitting will constitute only a small perturbation ($\sim$ 1 cm^{-1}) compared to this Stark splitting (10^5 cm^{-1}). No microwave magnetic dipole transitions can therefore be induced between or from the excited orbital levels ($h\nu \ll kT \ll 10^5$ cm^{-1}) so that orbital momenta play no direct part in the e.s.r. spectra of free radicals. This effect is known as the "quenching" of the orbital momenta. On the other hand,

the electric fields only affect the spins indirectly, through the spin-orbit coupling, but they still may remove some of the spin degeneracy. Without a detailed knowledge of the electric fields and spin-orbit coupling, it is therefore difficult to predict what the energy levels will be within kT of the ground state, the region of interest in magnetic resonance. Fortunately, however, there are two theorems which elucidate the behaviour of the ground state of paramagnetic in such circumstances - Kramers' and the Jahn-Teller theorems. The former states that a molecule with an odd number of electrons will always have at least a double degeneracy in the eigenstates, including spin. The latter states that a non-linear molecule will adjust itself, by nuclear displacements, to remove all orbital degeneracies left after the Stark splitting, but not the Kramers' degeneracy. Hence, a free radical molecule with a single unpaired electron will possess a singlet orbital ground state with double spin degeneracy and will therefore, in principle, always show e.s.r.

II.3 The Spin-Hamiltonian.

To facilitate the interpretation of e.s.r. data, Pryce[10] and Abragam and Pryce[11] have introduced a formal Hamiltonian, the spin-Hamiltonian, which reduces the

problem to one containing as few parameters as possible. This Hamiltonian describes only the levels associated with e.s.r. and is expressed in terms of an effective spin S' where (2S'+1) equals the observed multiplicity. For systems whose ground state is a single orbital level - as is the case for a free radical (Section II.2)-the effective spin is equal to the true spin.

The general expression for the spin-Hamiltonian $\mathcal{H}_s$ for a paramagnetic system in a crystal can be written[12]

$$\mathcal{H}_s = \beta(g_z H_z S_z + g_x H_x S_x + g_y H_y S_y + D\{S_z^2 - \tfrac{1}{3}S(S+1)\}$$
$$+ E(S_x^2 - S_y^2) + A_z S_z I_z + A_x S_x I_x + A_y S_y I_y$$
$$- g_N \beta_N \underline{H}.\underline{I} \qquad (2.12)$$

where H_z is the z component of the magnetic field, S_z is the total z component of the effective electron spin angular momentum operator, I_z is the z component of the nuclear spin angular momentum operator, g_N is the nuclear g-value, β_N is the nuclear magneton and D,E and the x,y and z components of g and A are parameters whose values are chosen to fit the experimental data for a particular system.

The first three terms are the main splitting terms describing the interactions between the magnetic field and the unpaired electron spins. The deviation of g from

the free-electron value (2.0023) is a measure of the effect of the electric fields on the spins through the spin-orbit coupling. It is small in free radicals (<0.1%) because of orbital quenching. As the magnitude of the unquenched orbital moment can be different for different directions of H due to electric field symmetries, g can be anisotropic.

The operator terms containing D and E formally represent the zero magnetic field splittings of the spin levels that can arise due to asymmetric electric fields. The three terms in A account for the nucleus-electron spin interactions with the possibility of anisotropic coupling. $g_N\beta_N\underline{H}.\underline{I}$ is the operator for the direct interaction between the magnetic field and the nuclear moment, and is usually negligible compared with the other terms in (2.12).

II.4 Nuclear Degeneracy.

When several nuclear moments in a molecule are concerned in the hyperfine structure, two types of nuclei can be distinguished by the number of hyperfine lines and their relative intensities. Consider as a simplified form of (2.12) for a free radical, the isotropic spin-Hamiltonian $\mathcal{H}_s$ where

$$\mathcal{H}_s = g\beta H_z S_z + \sum_n A_n S_z I_{nz} \qquad (2.13)$$

(a) Equivalent Nuclei. When the nuclei are chemically equivalent, the A's in (2.13) are all equal. Each spin level will be split into (2I+1) nuclear levels, where I is the total nuclear spin = $\sum_n I_n$. According to the strong field ($g\beta H >> A$) selection rules

$$\Delta S_z = \pm 1 \qquad (2.14)$$

$$\Delta I_{nz} = 0 \text{ for all } n$$

there will be (2I+1) lines separated by $\frac{A}{h}$ mc/s. If the nuclei are all protons, the relative intensities are given by the coefficients of a binomial distribution.

(b) Non-equivalent Nuclei. The A's are all different. Consider $A_1 > A_2 > A_n$.

Through interactions with I_1, each spin level splits into $(2I_1+1)$ levels. Through interaction with I_2 each of these levels splits into $(2I_2+1)$ levels. Hence the total number of levels for each spin level = $\prod_n (2I_n+1)$. With the selection rules (2.14), the number of hyperfine lines is then $\prod_n (2I_n+1)$.

II.5 The Relation between the Hyperfine Splitting Factor and Theoretical Entities.

The hyperfine coupling parameter A in (2.12) and (2.13) can be related to theoretical quantities of Section II.1

by use of the general hyperfine interaction operator[25] $\mathcal{H}_H$

$$\mathcal{H}_H = \sum_n g\beta g_N\beta_N \left[\frac{\underline{S}\cdot\underline{I}_n}{r_{kn}^3} - \frac{3(\underline{S}\cdot\underline{r})(\underline{I}_n\cdot\underline{r})}{r_{kn}^5}\right] - \frac{8\pi}{3}\underline{S}\cdot\underline{I}_n\delta(r_{kn}) \quad (2.15)$$

where S is the electron spin operator, I_n the nuclear spin operator of the n^{th} nucleus, g_N the nuclear g-value, β_N the nuclear magneton, r_{kn} the distance between the k^{th} electron and the n^{th} nucleus and $\delta(r_{kn})$ the Dirac delta function. The first two terms describe the anisotropic dipole-dipole interactions between the unpaired electrons and the nuclei in the molecule. The third term is the isotropic Fermi Contact term which arises from relativistic effects[13]. In solutions where the molecular tumbling frequency is often much larger than the hyperfine splitting frequency, the effect of the anisotropic term will be averagdd out to zero[14]. $\mathcal{H}_H$ is then isotropic, as is the spin-Hamiltonian for the system (i.e. of the form 2.13). The presence of the Dirac δ-function requires that the wave function of the unpaired electron possesses a finite value at the nucleus, if it is to contribute hyperfine structure of the Contact type. This can only be so if the wave function has some atomic s character.

On equating the hyperfine splitting in (2.13) to the expectation value of the Fermi part, $\mathcal{H}_F$, of (2.15), we

obtain for the n^{th} nucleus

$$a_n = \frac{A_n}{h} = \frac{\langle \Psi | \mathcal{H}_F | \Psi \rangle}{h S_z I_{nz}}$$

where Ψ is the ground state electronic wave function.

From (2.15) a_n reduces to

$$a_n = \frac{8\pi g}{3h} \beta g_N \beta_N \langle \Psi | \delta(r_{kn}) | \Psi \rangle \qquad (2.16)$$

II.5.1 Configuration Interaction.

The stability of aromatic radicals ions suggests that the molecular orbital of the unpaired electron in them is, to a zero order, a π orbital. Such an orbital, constructed from linear combinations of p_z atomic orbitals (equation 2.7) has a node in the plane of the ring. The matrix element in (2.16) and therefore the Contact hyperfine interaction is then zero.

Jarrett[15], Weissman[16] and McConnell[17] have accounted for the observed aromatic radical isotropic splittings by considering higher order effects in obtaining the ground state electronic wave function. In particular, McConnell[17] has carried out a first-order perturbation calculation on a system where the unpaired electron is restricted entirely to the molecular orbitals of an isolated CH bond and has obtained the correct order of magnitude predictions for

the splittings.

Thus, for the isolated CH bond, the ground state electronic wave function Ψ is written

$$\Psi = \Psi_i + \lambda\Psi_e \qquad (2.17)$$

where Ψ_i is the zero order ground state function corresponding to the configuration $(1\sigma_B)^2(2\sigma_B)^2p_z$ of the carbon hydrogen linkage. It is of the form (2.5) and is an eigenfunction of S_z with eigenvalue $\frac{1}{2}$. Ψ_e is an excited state wave function corresponding to the configuration $(1\sigma_B)^2(2\sigma_B 2p_z 2\sigma_A)$ and is an eigenfunction of S_z with eigenvalue $\frac{1}{2}$. It is this part of Ψ that gives rise to the hyperfine splitting, where σ_B is a bonding σ orbital between the carbon and hydrogen atom and σ_A is an antibonding σ orbital.

This type of mixing is known as σ-π exchange and is the means whereby the electron principally in a p_z orbital can get into the σ shells. It is brought about by electrostatic repulsions between the electrons in addition to those accounted for by (2.8).

McConnell has shown[17] that Q, the hyperfine splitting for the CH fragment, is given by

$$Q = \sqrt{\frac{2}{6}}\,\frac{\lambda}{(1 - S_o^2)^{\frac{1}{2}}}\,a_H \qquad (2.18)$$

where a_H is the hyperfine splitting if the unpaired electron is wholly in a 1s hydrogen orbital. From molecular beam experiments[18] a_H = 1420 mc/s. S_o is the overlap integral between an sp^3 carbon hybrid orbital and a 1s hydrogen atom orbital.

An estimation of λ from atomic exchange and overlap integrals gives Q to be within -10 to -100 mc/s. The empirical value is -63 mc/s.

II.5.2 The McConnell Relation.

In aromatic radicals, the unpaired electron will not be confined to one CH bond, but will be delocalised among the atoms of the ring. McConnell has shown[17] that the hyperfine splitting a_n, due to the proton attached to the n^{th} carbon atom, is related to the unpaired electron density at the n^{th} carbon ring atom, ρ_n, by the expression

$$a_n = \rho_n Q \qquad (2.19)$$

assuming that Q of (2.18) is the same for all CH bonds in the ring.

Thus, on estimating Q and measuring the hyperfine splittings, the relationship (2.19) affords an accurate means of obtaining information on the unpaired electron distribution throughout the molecule. In the Hückel

approximation, the unpaired electron density is the probability of finding an unpaired electron in a p_z orbital centred on the carbon atom n and is equal to c_n^2 (see equation 2.7).

$$\text{i.e. } a_n = c_n^2 Q \qquad (2.19a)$$

McConnell has further generalised[17] this concept of unpaired electron density to wave functions that do not depend on the one electron approximation. (2.19) will still hold if for ρ_n is substituted the spin densities, i.e. expectation value of the spin density operator $(\rho_n)_{op}$ defined by the equation

$$(\rho_n)_{op} \sum_k S_{kz} = \sum_k \Delta_n(k) S_{kz} \qquad (2.20)$$

$\Delta_n(k)$ is an "atomic orbital delta function" which equals 1 when electron k is in a p_z atomic orbital centred on carbon atom n and is zero elsewhere.

The Hückel theory gives good predictions of spin densities in even alternant hydrocarbons, but not in odd alternant systems. Thus, the overall hyperfine splitting for a system of N carbon atoms to each of which are attached one proton is $\sum_n |a_n|$ where

$$\sum_n |a_n| = \sum_n |\rho_n| Q \qquad (2.21)$$

From Hückel theory $\sum_n \rho_n = 1$ and $\rho_n > 0$.

Therefore, the total spread of the spectra from aromatic hydrocarbon radical ions should be constant and equal to Q. In odd alternant systems, however, the total splitting is found[19] to be larger than Q, so that if (2.19) is still to hold, ρ_n must have a negative value at certain carbon sites in the molecule. Their physical significance is that at these sites the unpaired electron density has a polarisation which is opposite to the total spin polarisation of the molecule. In these cases $\sum_n |\rho_n| > 1$ but still $\sum_n \rho_n = 1$.

The use of better approximations to the ground state electronic wave function than those of Hückel, viz. (2.5), (2.6), (2.7) and (2.11), such as the Löwdin[20] wave functions or the inclusion of π-π interaction[17] do in fact give negative spin density predictions at certain carbon atoms. These are the sites where Hückel theory gives zero spin density.

II.5.3 Hyperconjugation.

Hyperfine splitting can be produced by the protons of a methyl group attached to a ring system, e.g. the methyl group protons in tolu-p-benzosemiquinone[21]. This splitting cannot be explained by a σ-π exchange interaction involving excited levels of the CH bonds in the methyl

group, as described in Section II.5.1, because the π system of the aromatic ring does not extend to the methyl carbon. The way in which mixing of the 1s hydrogen orbitals into the π system can take place, is by direct overlap of the $2p_z$ ring carbon orbital and the 1s methyl hydrogen orbital. To prevent overlap contributions from cancelling, the mixed wave functions must possess the same symmetry. It is, therefore, necessary in mixing with a $2p_z$-orbital to choose a methyl group M.O. of the form $h_1 - \frac{1}{2}(h_2 + h_3)$, where h_n is the 1s orbital of the n^{th} hydrogen atom of the methyl group.

This type of mixing mechanism is called hyperconjugation and the splitting produced as a consequence is usually of the same order as that produced by σ-π configuration interaction. Furthermore, McLachlan has shown[22] with a valence bond argument that the hyperfine splitting a_H for a methyl proton is related to the spin density ρ on the carbon (or nitrogen) atom to which the methyl group is attached. The relationship is

$$a_H = Q\rho \qquad (2.22)$$

which is similar to the McConnell relation (2.19) for protons attached to ring carbon atoms. The best semi-empirical value for Q for the methyl protons in Wurster's

blue ion is +70 mc/s (+25 oe).

II.6 Exchange.

Dirac has shown that the isotropic exchange interaction $\mathcal{H}_e$ can be written in the form[23]

$$\mathcal{H}_e = \sum_{i \neq j} J_{ij} \underline{S}_i \cdot \underline{S}_j \qquad (2.23)$$

where J_{ij} is the exchange integral between the i^{th} and j^{th} electron in the system and its sign determines whether the parallel or antiparallel spin alignment state is lower.

Due to this form of $\mathcal{H}_e$, there will be no contribution from paired electrons. The isotropic electron exchange interaction in free radicals is of two types, inter and intramolecular exchange. The former will be discussed in II.7.3.

II.6.1 Intramolecular Exchange.

This interaction operator has to be included in the spin-Hamiltonian for one molecule when it has more than one unpaired electron. It is, therefore, of importance in the biradical molecular complexes described in this thesis.

For a molecule with two unpaired electron spins s_1 and s_2, the isotropic exchange $\mathcal{H}_e$ can be written

FIGURE I. THE POSSIBLE LOWEST ENERGY LEVELS FOR A MOLECULE WITH TWO UNPAIRED ELECTRONS.

(a) A BIRADICAL

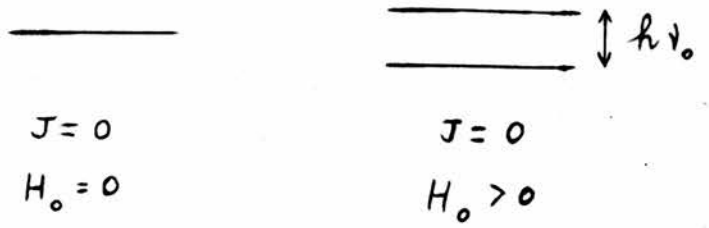

(b) A MOLECULE WITH A TRIPLET STATE

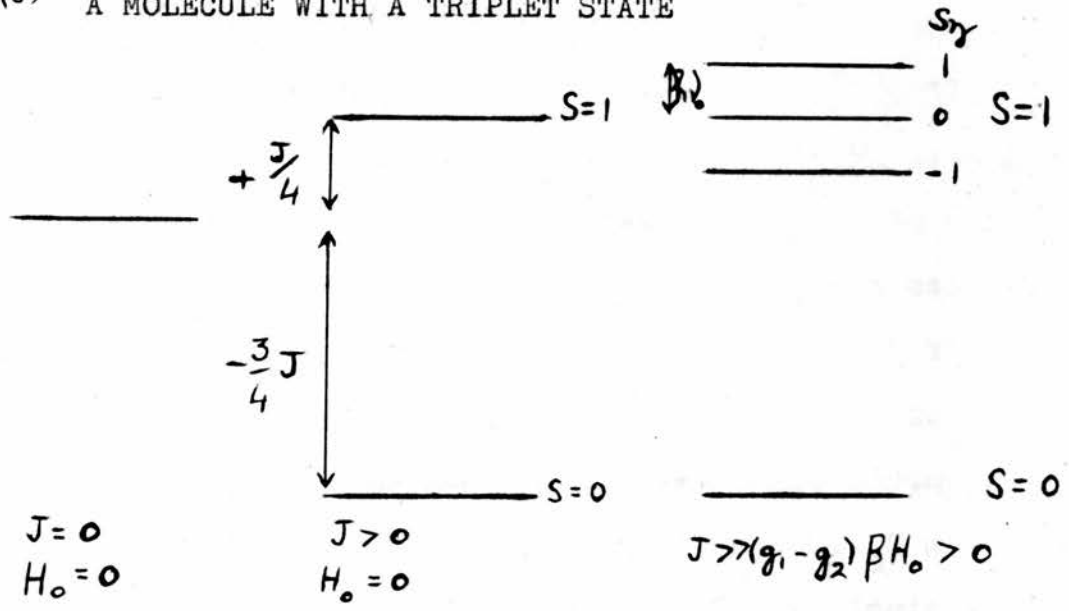

$$\mathcal{H}_e = J\,\underline{s}_1\cdot\underline{s}_2$$

$$= \tfrac{1}{2}J[S(S+1) - \tfrac{3}{2}] \qquad (2.24)$$

where $\underline{S} = \underline{s}_1 + \underline{s}_2$.

Including this in the isotropic spin-Hamiltonian $\mathcal{H}_e$, with no hyperfine effects

$$\mathcal{H}_e = g_1\beta\,\underline{H}\cdot\underline{s}_1 + g_2\beta\,\underline{H}\cdot\underline{s}_2 + J\,\underline{s}_1\cdot\underline{s}_2 \qquad (2.25)$$

$$= \tfrac{1}{2}(g_1+g_2)\beta\,\underline{H}\cdot\underline{S} + \tfrac{1}{2}J[S(S+1) - \tfrac{3}{2}]$$

$$+ \tfrac{1}{2}(g_1-g_2)\beta\,\underline{H}\cdot(\underline{s}_1 - \underline{s}_2) \qquad (2.25a)$$

g_1 and g_2 are the g-values of s_1 and s_2 respectively. Two cases can then be distinguished.

(1) If $J \ll (g_1 - g_2)\beta H$, there will be two separate lines characterised by g-values g_1 and g_2. In the particular case of J equal to zero, we call the molecule a biradical (see Fig. 1a).

(2) If $J \gg (g_1 - g_2)\beta H$, the energy levels will split into a lower singlet and a triplet separated by J (see Fig. 1b). Magnetic resonance transitions will be induced between the S_z levels of the triplet state so that there will be a single line with g-value $\tfrac{1}{2}(g_1 + g_2)$.

II.6.2 The Effect of Isotropic Intramolecular Exchange on Hyperfine Structure.

If there are hyperfine interactions present in a biradical molecule, then the resulting hyperfine structure can be modified depending on the magnitude of the intramolecular exchange. With the unpaired electron spins s_1 and s_2 coupled to the nuclear spins I_1 and I_2 respectively, the spin-Hamiltonian $\mathcal{H}_s$ of (2.25) will then be

$$\mathcal{H}_s = g\beta\underline{H}.\underline{s}_1 + A\underline{I}_1.\underline{s}_1 + g\beta\underline{H}.\underline{s}_2 + A\underline{I}_2.\underline{s}_2 + J\underline{s}_1.\underline{s}_2 \qquad (2.26)$$

$$= g\beta\underline{H}.\underline{S} + \tfrac{1}{2}A\underline{S}.(\underline{I}_1 + \underline{I}_2) + \tfrac{1}{2}J[S(S+1) - \tfrac{3}{2}]$$

$$+ \tfrac{1}{2}A(\underline{s}_1 - \underline{s}_2)(\underline{I}_1 - \underline{I}_2) \qquad (2.26a)$$

where the simplifications have been made that $g_1 = g_2 = g$ and that all the nuclei are equivalent.

Two types of hyperfine spectra are then possible. Either (1) if $J = 0$ and $g\beta H \gg A$, there will be two sets of hyperfine spectra superimposed with $(2I_1+1)$ and $(2I_2+1)$ components each of splitting $\frac{A}{h}$ mc/s, or

(2) if $J \gg A$, there will be $[2(I_1 + I_2) + 1]$ lines. with splitting $\frac{A}{2h}$ mc/s which does not depend on J and with relative intensities given by the number of ways of forming $(I_{1z} + I_{2z})$ Reitz and Weissman[24] have considered the particular case of $I_1 = I_2 = \frac{1}{2}$ in a biradical where case (1) gives a doublet and (2) a triplet. They also point out that for $A>J>0$, each of the doublets will split into a

triplet with splitting $\frac{J}{h}$ mc/s.

II.6.3 The Temperature Dependence of the E.S.R. Signal Intensity due to Intramolecular Exchange.

The integrated signal intensity is proportional to the difference in Boltzmann populations of the two levels involved in the e.s.r. transitions. As has been seen in (1.4) for a system with spin $\frac{1}{2}$ this signal intensity has a Curie temperature dependence of I/T provided $g\beta H \ll kT$. For a system whose e.s.r. levels belong to a triplet state which is J above a singlet state (see Fig. 1b), the temperature dependence of the integrated signal intensity (I.S.I.) is given by

$$\text{I.S.I.} \propto \frac{1}{T} \frac{1}{(e^{+\frac{J}{kT}} + 3)} \qquad (2.27)$$

II.7 Factors Influencing the Resolution of Hyperfine Structure.

Up to now, in this chapter, we have considered only the interactions in one molecule or a system of non-interacting molecules. If environmental effects on the molecule are taken into account, the widths of the component hyperfine lines are modified with the result that resolution of hyperfine structure is inhibited. Therefore, in order to obtain optimum resolution and hence maximum information about the radical system, these environmental effects have

to be minimised. They will be discussed in turn.

II.7.1 Nuclear-electron Spin Broadening.

In solid samples or viscous solutions the anisotropic hyperfine part of (2.15) does not average to zero but, due to the random orientations of the molecules, gives rise to line broadening. On averaging over all orientations of the magnetic field with respect to the line joining the unpaired electron to the nucleus, the line broadening ΔH is given by[25]

$$\Delta H \sim g_N \beta_N \sum_k \frac{1}{r_k^3} \quad \text{oe} \qquad (2.28)$$

where r_k is the distance in $\mathring{A}$ between the k^{th} nucleus and the unpaired electron, averaged over the wave function.

II.7.2 Electron-electron Spin Broadening.

The electron-electron spin interactions between the unpaired electrons on different radical molecules effect line broadening in two ways. The z-component of the unpaired spins on neighbouring radicals can cause a local field smearing at each dipole. Also, the rotating components (i.e. the x-component) of neighbouring unpaired spins cause a time-dependant magnetic field at each magnetic dipole. The frequency of this field is the Larmor resonance frequency, so it will be effective in inducing

transitions. This mechanism will reduce the spin-spin relaxation time T_2 - a measure of the time for the spins to achieve equilibrium among themselves. It will, therefore, reduce the lifetime of a spin in the upper Zeeman level and hence produce uncertainty broadening (see II.7.4). The resulting line broadening ΔH, for a system with total electron spin $\frac{1}{2}$, due to electron-electron spin interaction, is given by[25a]

$$\Delta H \sim \tfrac{2}{3} g \beta \sum_n \frac{1}{r_n} \text{ oe} \qquad (2.29)$$

where r_n is the distance in $\mathring{A}$ between electron spins averaged over their wave functions. Consequently, to reduce this type of broadening, the radicals are investigated in a dilute form.

II.7.3 Intermolecular Exchange Narrowing.

This is the exchange interaction of (2.23) which arises from the overlapping of the unpaired electron wave functions on neighbouring radicals.

If $\mathcal{H}_o$, $\mathcal{H}_e$, $\mathcal{H}_d$ are the operators for the main field splitting, the intramolecular exchange and the dipolar interactions of II.7.1, II.7.2, then the complete Hamiltonian $\mathcal{H}$ can be written

$$\mathcal{H} = \mathcal{H}_o + \mathcal{H}_e + \mathcal{H}_d \qquad (2.30)$$

It can be shown that

$$[\mathcal{H}_o, \mathcal{H}_e] = 0 \qquad (2.31)$$

$$[\mathcal{H}_e, S_x] = 0 \qquad (2.31a)$$

$$[\mathcal{H}_e, \mathcal{H}_d] \neq 0 \qquad (2.32)$$

and therefore from the Heisenberg equations of motion

$$i\hbar \dot{\mathcal{H}}_d = [\mathcal{H}, \mathcal{H}_d] = [\mathcal{H}_o, \mathcal{H}_d] + [\mathcal{H}_e, \mathcal{H}_d] \qquad (2.33)$$

From (2.31) and (2.31a) it is seen that the exchange has no direct affect on the radiation processes, which means it does not directly effect the line width. By relations (2.32) and (2.33) $\mathcal{H}_e$ can cause a time-dependence of the dipolar interactions and on time averaging, if J is large enough, a reduction of the dipolar broadening and hence a narrowing of the line. Anderson and Weiss have predicted[26] a Lorentzian line shape in the centre falling off more rapidly on the wings. This agrees well with observations from large concentrations of free radicals (see Fig. 38f). Indeed, so strong is this exchange in most solid samples that all Fermi interactions are narrowed out. The radicals then have to be studied in as dilute a form as possible to reduce the intermolecular exchange interaction and this is usually in solution to avoid the broadening from anisotropic hyperfine interactions (viz. 2.28). A well known example of this narrowing in solid

samples and resolution in solution[27] is given by diphenylpicrylhydrazyl $(C_6H_5)_2N_2C_6H_2(NO_2)_3$. Figs. 11 and 12 give the absorptions from this substance using the spectrometer described in Chapter III. The structure of five lines, whose relative intensities are in the ratio 1:2:3:2:1, results from almost equal coupling with two of the nitrogen atoms.

As has been stressed in this chapter, delocalisation of the unpaired electron throughout the molecule plays a major role in free radicals. This has been recently correlated with line narrowing[28], although whether it happens through exchange or motional effects is not clear. Increased delocalisation could mean increased overlap of neighbouring unpaired electrons and hence more exchange. Again, the delocalisation implies large migration of the unpaired electron which would produce dipolar averaging. The narrowing produced in this way should not, however, be removed on dilution. It seems likely, therefore, that intermolecular exchange is the major process in narrowing radical spectra.

II.7.4 Heisenberg Uncertainty Broadening.

The fundamental limitation on the line width is due to the Heisenberg Uncertainty Principle. If the lifetime

in the excited magnetic state is τ then the minimum attainable line width is $\Delta\nu$ where

$$\Delta\nu \sim \frac{\hbar}{\tau} \qquad (2.34)$$

The lifetime can be determined by its chemical stability or by the relaxation time T' defined by

$$\frac{1}{T'} = \frac{1}{T_1} + \frac{1}{T_2} \qquad (2.35)$$

where T_2 is the spin-spin relaxation time and T_1 is the spin-lattice relaxation time, which is a measure of the time the spin system takes to come to equilibrium with the lattice. The line width is then $\sim \hbar/T'$.

In solution, although there is no lattice, the spin system will be coupled to the thermal motions of the nuclei and these will effectively constitute the "lattice". The energy transfer between the spins and the "lattice" can take place through the spin-orbit coupling which is usually small because of orbital quenching or by exchange which is strongly coupled to the "lattice".

II.7.5 Hausser's Results.

Hausser's results[29] show that the resolution of hyperfine structure in solution depends on

(1) the temperature of the solvent,

(2) the solvent, and

(3) the absence of dissolved oxygen.

Thus he found that for a particular solvent, on decreasing the temperature, resolution is enhanced until an optimum value is reached. On further lowering, the hyperfine components broaden and the structure is smeared out. These results have been interpreted by Tuttle and Pake[30] who suggested that, at low temperatures, the broadening is due to anistropic hyperfine terms. This broadening will be reduced as the temperature is raised because molecular tumblings become faster and the anisotropic effects are averaged to zero. At still higher temperatures, remnant exchange will broaden the lines. The exchange occurs when two radicals molecules come together in solution for a finite time so that their unpaired electron clouds can overlap. The resultant spin coupling will interrupt the Larmor precession of the unpaired moments about the external magnetic field at the collision frequency and for the time of the overlap. When this frequency is greater than the hyperfine frequency, the hyperfine components will be broadened. The solvent dependence occurs through the viscosity which will determine the collision rate.

The effect of dissolved oxygen has not yet been explained, but Hausser has found[29] that in its absence hyperfine resolution is sometimes greatly enhanced.

II.7.6 Apparatus Broadening.

Over and above the molecular interactions which prevent resolution of lines, broadenings can be added by defects in the methods of recording the lines. These can arise from:

(a) Magnetic field inhomogeneities across the sample. No hyperfine splitting less than this inhomogeneity will be resolved.

(b) Power saturation of the sample. When the power incident on the sample is large, then the situation may arise where the thermal equilibrium of the spin system cannot be maintained by the relaxation processes. The population differences between the Zeeman levels is reduced and the absorption in the centre of the line, where the transition probability is greatest, decreases. This suppression of the peak changes the line shape and half-maximum signal width and prevents the observation of hyperfine components near the centre of the line.

(c) Modulation broadening. If either the magnetic field or the signal klystron is modulated at fc/s, then as well as the main signal, there are generated sidebands fc/s apart. If the main signal and some of the sidebands are passed by the receiving circuits, a line broadening will result due to the latter[31]. The minimum hyperfine

splitting which is resolvable is then fc/s.

Line distortion will also arise from the finite amplitude of the magnetic field modulation using the phase-sensitive detection scheme of (III.5). Thus, if this modulation amplitude is much greater than the hyperfine splitting, it can prevent resolution.

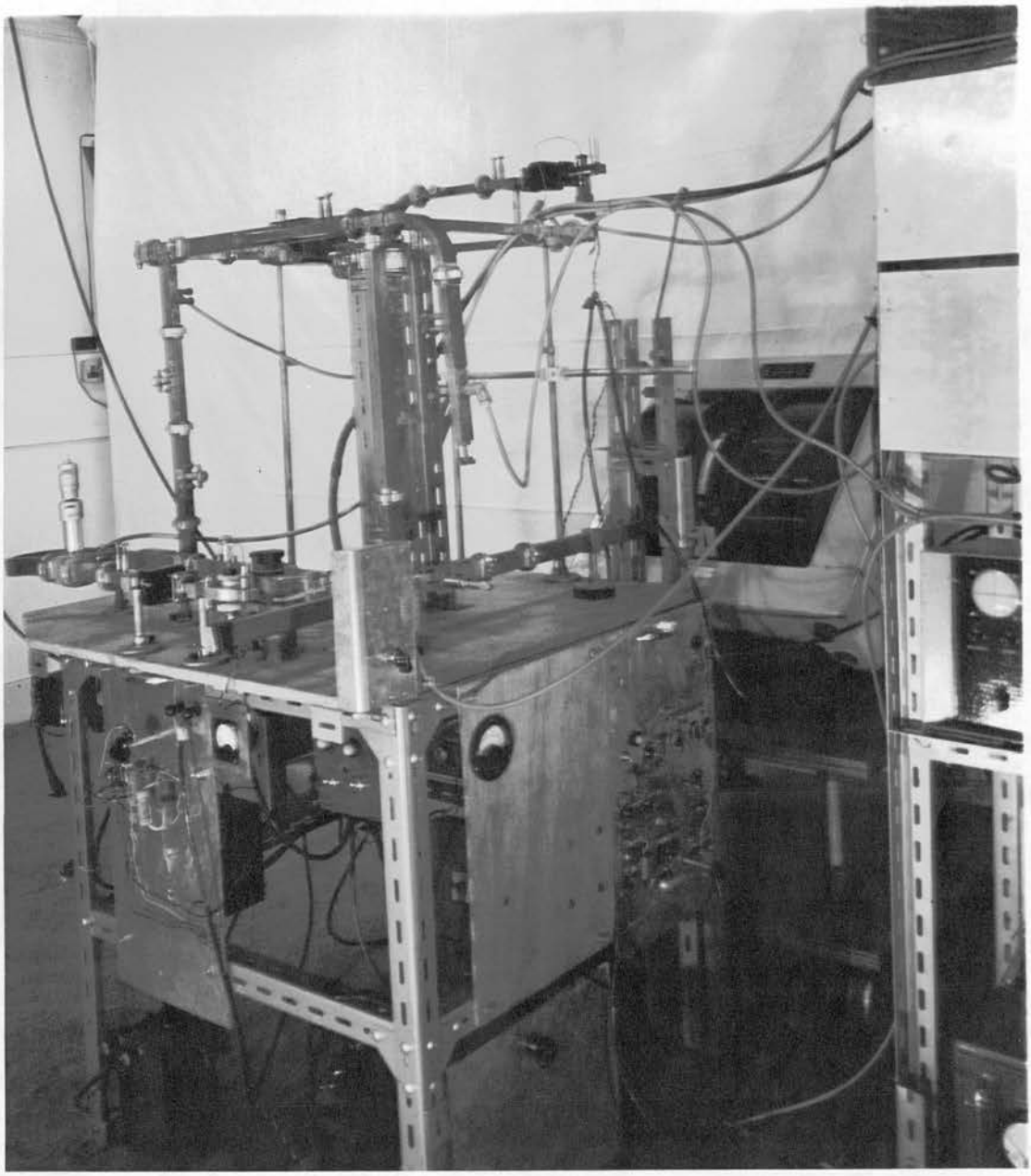

FIGURE 2 THE MICROWAVE SYSTEM AND THE MAGNET.

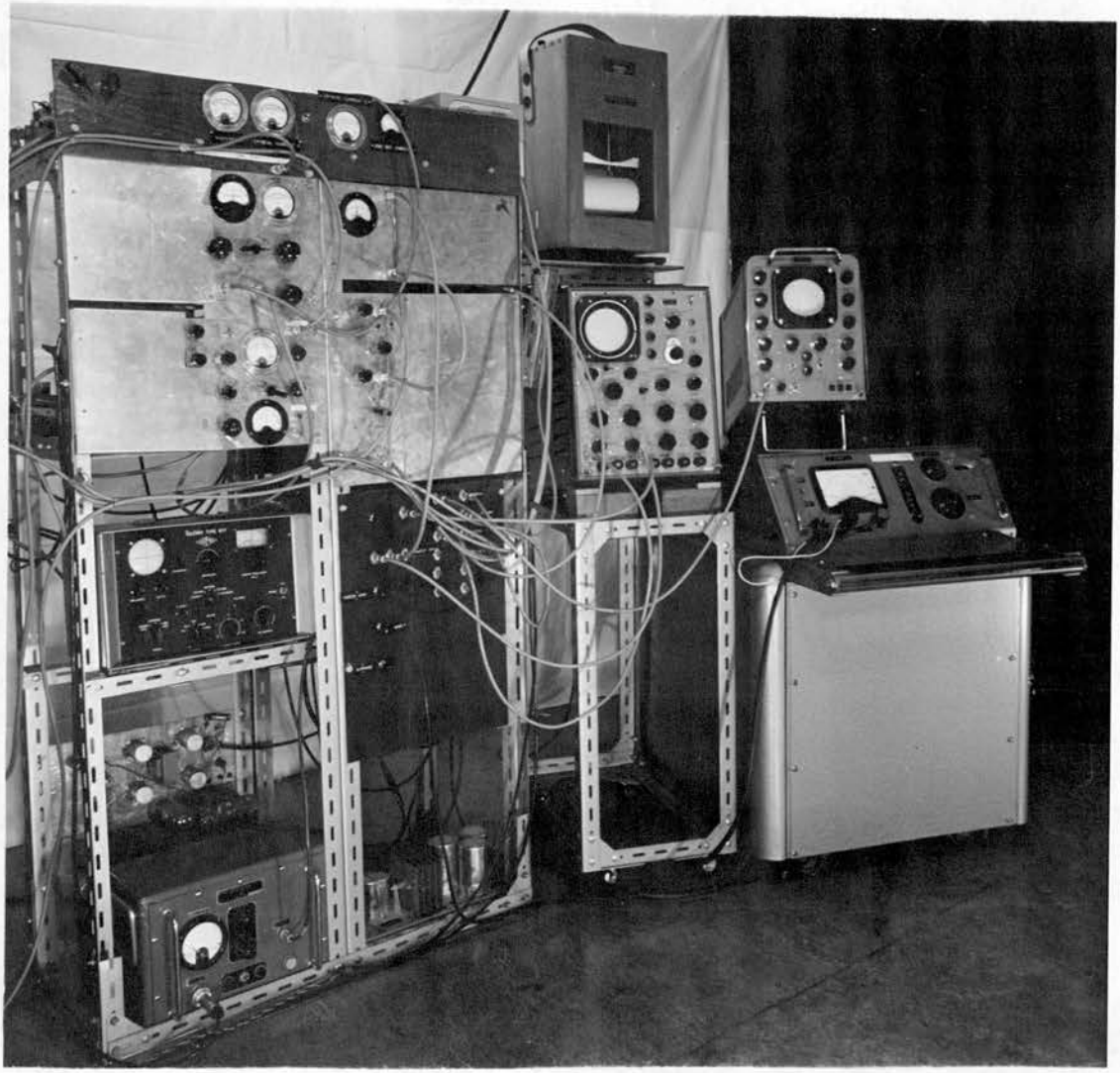

FIGURE 3. THE ELECTRONICS.

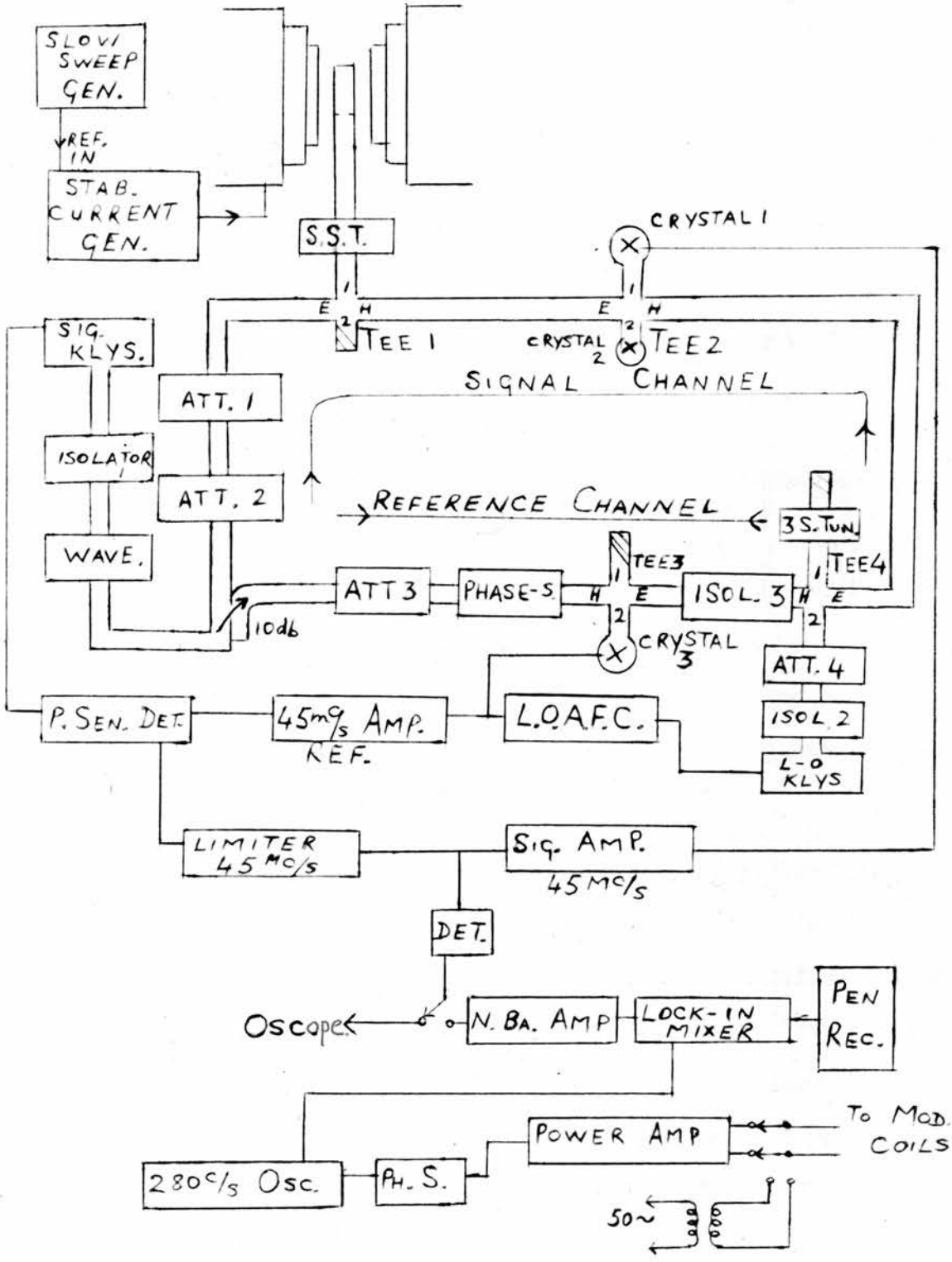

FIG. 4. A BLOCK DIAGRAM OF THE APPARATUS.

CHAPTER III

THE SPECTROMETER

This chapter describes the apparatus used to investigate the e.s.r. spectra at room temperature.

III.1 Introduction.

As was seen in the last chapter, e.s.r. studies of free radicals in solution and, in particular, of their hyperfine structure require radical concentrations to be as low as possible. However, the greatest dilution that can be used is limited by the sensitivity of the spectrometer.

A survey of the literature[27,31] shows that hyperfine components can be fairly well resolved in solutions at concentrations of ~ 10^{-3} moles/litre. This amounts to about 6.10^{14} radicals of linewidth 100 oe in a test sample of a few tenths of a cc., so that to obtain spectra from this demands a spectrometer of the highest sensitivity. Acoording to Feher[3] et al[4], this is a superheterodyne system.

The block diagram of the apparatus, the microwave

circuit and electronics is shown in Fig. 4. The whole spectrometer, except where specifically mentioned, was designed and built by the author. The general layout is similar to that of Hirshon and Fraenkel[4] and can be described as an x-band superheterodyne spectrometer with frequency stabilisation for both oscillators. An attractive feature of a spectrometer of this type lies in its frequency stabilisation schemes which add no modulation broadening of the type described in II.7.6c.

III.2 The Microwave Circuit.

x-band was chosen, partly for sensitivity requirements and partly for economic reasons. Thus up to x-band the minimum number of radicals that can be detected is proportional to $\nu_o^{-\frac{1}{2}}$ (see 1.17) provided that there is no r.f. saturation or dielectric losses. At higher frequencies this is not always the case, as there is a greater tendency towards r.f. saturation and dielectric losses. In addition, Q-band equipment is more expensive and demands higher tolerances. In the higher fields of the d.c. magnets, moreover, good homogeneity is more difficult to attain.

The microwave circuit used consists of a signal channel which provides power for the cavity containing the sample and a reference channel required for frequency stabilisation

of the klystrons. In the signal channel, use is made of the isolation properties of a magic-tee to form a microwave bridge. Thus at tee 1, with arm 2 matched and with a matched reflection cavity on arm 1, no signal is coupled from the signal klystron in the E arm into the H arm. A sliding-screw tuner is included between port 1 of tee 1 and the cavity for fine control in the balancing of this bridge. On e.s.r. absorption in the cavity, its Q will be lowered, its reflection coefficient changed and a signal proportional to the change in reflection coefficient which in turn is proportional to the power change in the cavity will be coupled to the crystals 1 and 2. Superheterodyne detection of this signal is used to avoid low frequency crystal noise. The intermediate frequency (I.F.) is produced by mixing with a local-oscillator klystron. Power from this local-oscillator is divided equally at tee 4, to pass along the signal and reference arms to tees 2 and 3 and provide mixing at crystals 1, 2 and 3. The signal voltages at these crystals are converted into I.F. voltages which are amplified by a suitably tuned I.F. amplifier. A 10 db. directional-coupler is employed to abstract signal power from the main channel into the reference channel and provide a reference voltage, independent of the reflection coefficient of the cavity, at crystal 3.

This as well as the phase-shifter, the three-screw tuner and isolator 3, all included in the reference channel as shown in Fig. 4, are necessary for the klystron frequency stabilisation schemes described in III.4. Attenuators are used to control the microwave power to various parts of the system. The use of the balanced magic-tee bridge in the signal channel means that:

(1) negligible zero-signal I.F. voltage is present in the signal amplifier, so that large gain can be used without saturating it, and

(2) there is a reduction of microwave noise. In a superheterodyne system with a straight waveguide run, microwave noise frequencies will be present due to signal klystron noise, local-oscillator noise and thermal noise. These noise voltages will beat with the zero-signal microwave voltage at the detecting crystal to produce noise frequencies that will fall within the passband of the rest of the receiver. The balanced bridge will reduce the zero-signal microwave voltage at the crystal and hence noise beats of this type. It will, however, not reduce beats between the local-oscillator and the microwave noise.

III.3 Microwave Components.

(a) Waveguide Mounting.

The waveguide system is fixed by a number of clamps

to a table with a wooden top and is oriented so that the cavity arm extends horizontally, narrow side up, into the magnetic field (see Fig. 2). The height of the table can be adjusted to ensure that the sample in the cavity is always at the centre of the magnetic field.

British waveguide 1 × 0.5" I.D. was used in the major part of the circuit because of the availability of some components in this size. The isolators, however, were commercially available only in waveguide size 16(1 × 0.5" O.D.) so that quarter-wave transformers had to be made. These were approximated to[33] by cutting away froma piece of waveguide 16 a narrow and a broad wall to a length equal to one quarter of a guide-wavelength (1 cm.). This was inserted into and soft-soldered to a piece of British waveguide. A pair of tuning screws for fine control of matching were mounted three eighths of a guide-wavelength apart on the broad side of the waveguide. TheV.S.W.R. of these using the screws were less than 1.05.

(b) Matched Terminations. (Fish-tail Loads).

These are of wood and were fashioned out in the laboratory. It was found that the lowest V.S.W.R. was obtainable from two pieces of tapered soft-pine clamped together in the shape of a fish-tail. Provided they were

longer than ten inches the V.S.W.R. was less than 1.02. If the length was less than this, a noticeable amount of microwave power was emitted from the end of the load. This had disastrous effects if this load was used in the bridge tee as anyone walking past it caused a reflection of power and an unbalancing of the bridge.

(c) Magic Tees.

Magic tees 1 and 2 were frabricated in the workshops from rectangular waveguide. The port and iris matching scheme was employed and the dimensions were taken from a standard design[34]. The E and H arms are longer than arms 1 and 2 and on the broad side of them are mounted tuning screws for additional control of matching. Tees 3 and 4 were available in the laboratory and since they did not have these screws, special waveguide sections were made up with them. When matched loads were attached,to arms 1 and 2 and with the screws out, the V.S.W.R. of the E and H arms of all the tees were less than 2.1. With the screws in their optimum position for matching, all the V.S.W.R. were less than 1.08.

(d) Cavities.

These are of two types, viz.

(i) the H_{012} rectangular reflection, and
(ii) the H_{011} cylindrical reflection.

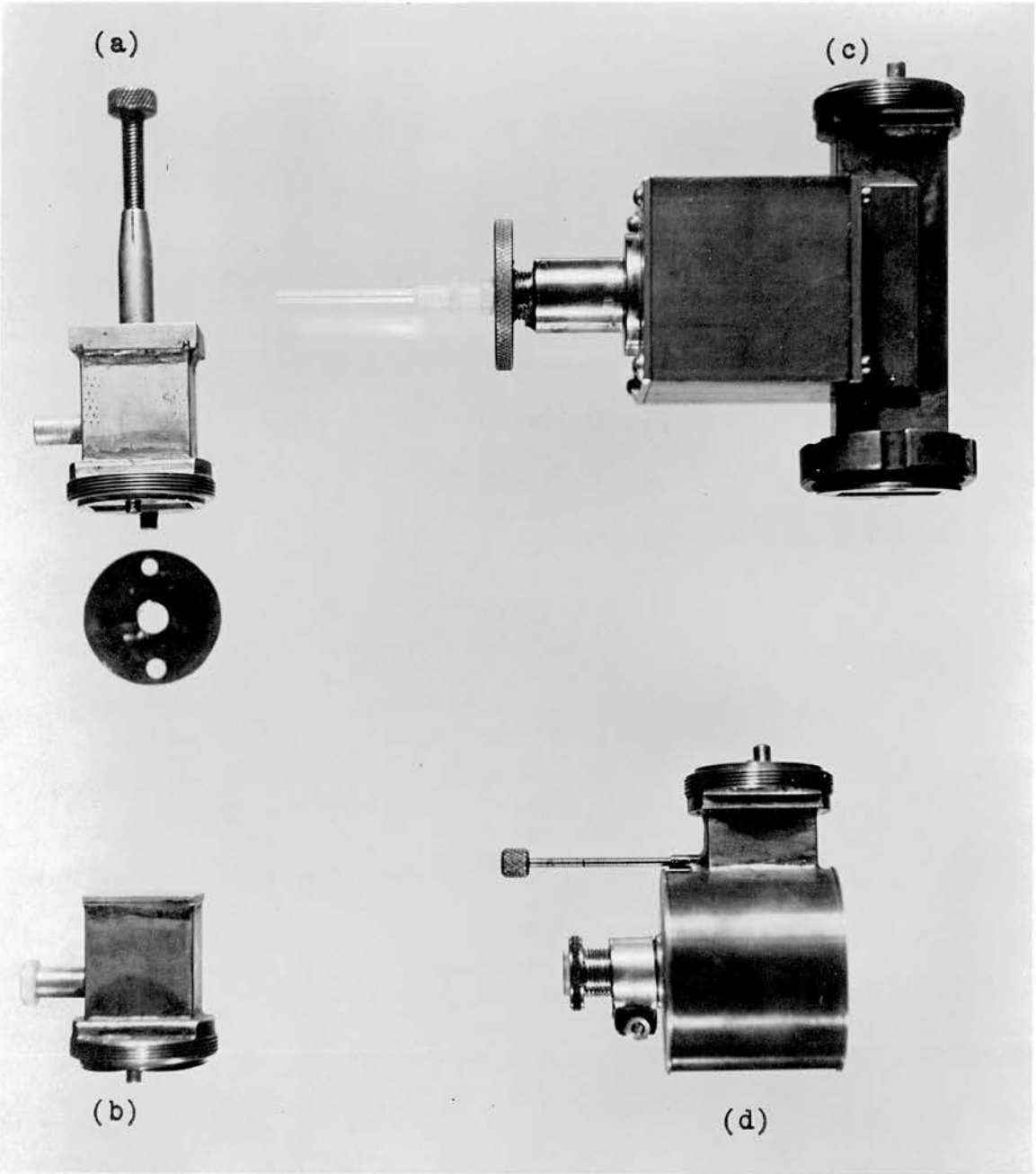

FIGURE 5 THE CAVITY RESONATORS.

(i) A tuneable rectangular H_{012} cavity (see (a) Fig. 5) was used in the initial experiments. This was made from a length of British waveguide (length = 3.95 cms.), to one end of which was soldered a brass plate. Tuning is accomplished by screwing a quartz rod through this end wall. The sample tube is inserted through a 2 cm. long bush, which is fitted at the centre of the wall. The tube is held in a perspex collar and extends over the maximum part of the r.f. magnetic field and the minimum part of the electric field. A standard male British coupler was soldered on the front end and a .003" thick silver-plated copper disc pressure clamped between this and a female coupler on the waveguide arm. An iris punched at the centre of this disc effects the coupling between the waveguide and the cavity. Several of these discs with different sizes of iris were made and by interchanging them, the coupling can be varied. This makes it possible to balance the bridge and match the cavity for maximum sensitivity when the solvents used vary greatly in dielectric losses. For an empty cavity the iris diameter required for match is 0.25". Samples with dielectric losses require larger coupling holes.

As work progressed, with lossy solvents, it was realised that the quartz rod might distort the cavity field

FIGURE 6. A CYLINDRICAL H_{011} CAVITY

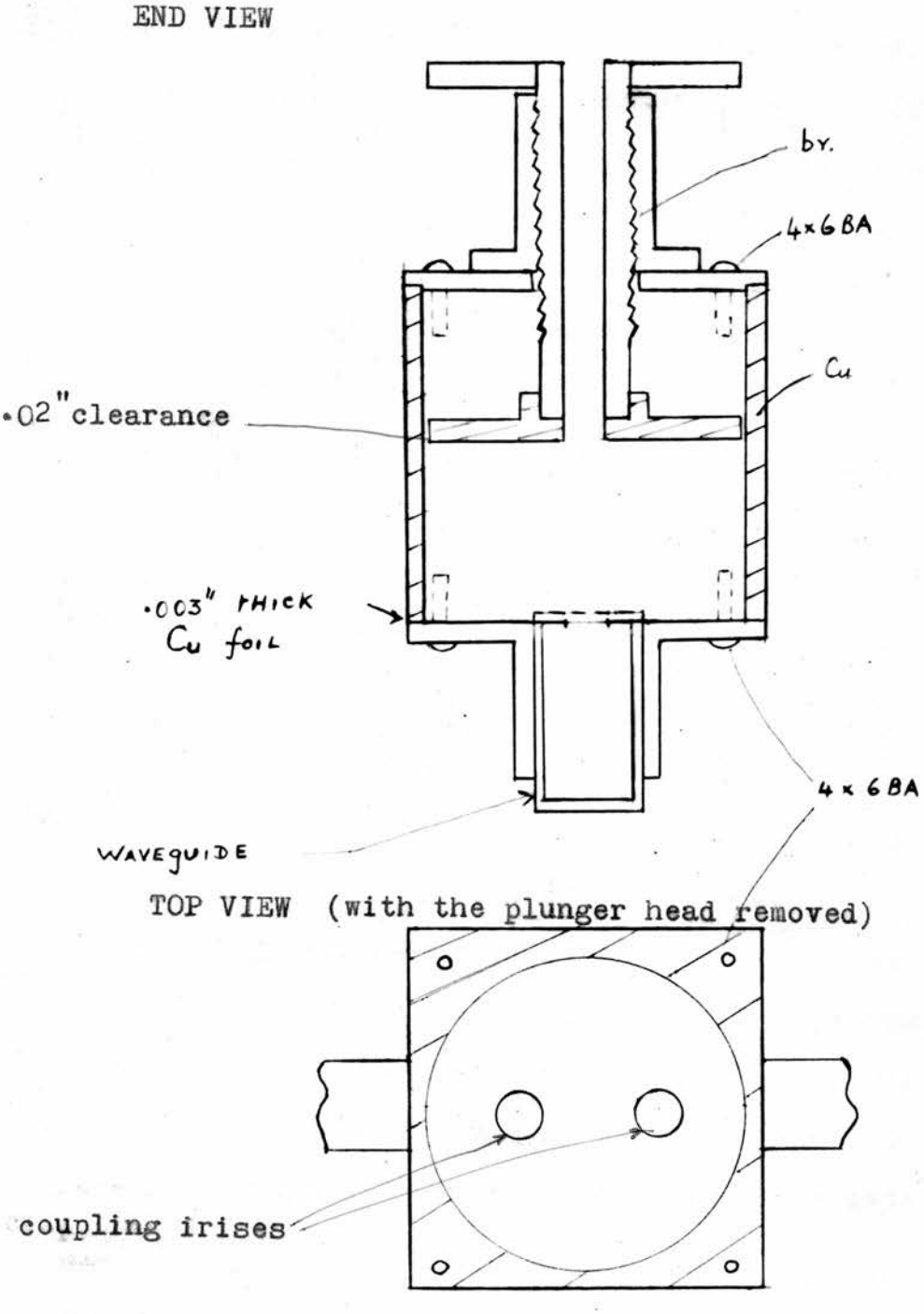

pattern so that the maximum r.f. magnetic field and the minimum electric field were not along the sample. This would result in a reduction of filling-factor and additional dielectric losses. To obviate this, a cavity similar to the above was constructed but was fixed tuned, i.e. no quartz rod (see (b) Fig. 5).

Length of cavity = 4.05 cms.

Loaded Q = 2,000.

Estimations of the Q's of all the cavities were made by measuring the separation of the half-signal points of the reflected signal on the oscilloscope, while sweeping the signal klystron. Wavemeter settings were used as frequency markers.

(ii) High Q Cavities: It has been seen in (1.14) that the spectrometer sensitivity is proportional to cavity Q. The only limitation, in principle, to the use of very high Q cavities is the frequency stability of the signal klystron. This, however, need not occur when working with lossy solvents, as the sample can always be increased to keep the cavity Q to a value that will not demand a frequency stability greater than that possessed by the signal klystron.

A high Q, H_{011} cylindrical cavity was therefore constructed as in Fig. 6 and Fig. 5 (c). This was turned

out of a square block of copper and had a non-contact tuning plunger mounted on one end. The thread for this tuning is 24 turns per inch. A 6 mm. diameter hole through the tuning head allows the sample to be inserted into the cavity. The cavity is mounted on a platform of two pieces of angled brass soldered to the broad side of a piece of waveguide. A square disc 0.003" thick copper foil is clamped between the bottom of the cavity and this platform. Coupling is achieved by two holes (0.25" diameter for empty cavity) spaced one half a guide-wavelength (2 cm.) apart along the waveguide axis. In this way, odd modes such as E_{111}, which is degenerate with H_{011} will not be excited in the cavity[35]. These would be present as spurious resonances and might even lead to damping of the required H_{011} mode. In addition, the dimensions were chosen from the mode-shape factor graphs[36] so that no higher modes might be excited. The specifications of the cavity are:

Length = 4.1 to 2.5 cms. tunable

Diameter = 4.5 cms.

Measured loaded Q = 8,000

Calculated loaded Q = 14,000
(from mode-shape factor graphs[36])

Weight = 894 grams.

Unfortunately, this cavity has its drawbacks when used in e.s.r. experiments, viz.

(a) It is more susceptible to mechanical disturbances than the rectangular types.

(b) Vibrations are set up when the magnetic modulation is on. This effect has been reported by several authors.[4,25] They conclude that the mechanical vibrations are set up in the walls of the cavity due to the interaction of the induced eddy currents with the d.c. magnetic field. These vibrations accentuate the effect of signal klystron frequency instabilities and, as they are field dependent, cause a base line drift on the pen-recorder (see Section III.9).

(c) Its use is inconvenient in that, interchanging with the rectangular cavity, the height of the table supporting the waveguide has to be adjusted so that the sample is in the middle of the magnetic field.

In an attempt to improve on (a), (b) and (c), another H_{011} cylindrical cavity was constructed (see (d) Fig. 5). This was turned out of a 2" diameter copper pipe. It weighs less and hence is easier to support (one holder clamped to the magnet trolley is used). Design specifications are:

Diameter = 4.8 cms.

Length = 3.2 to 2.1 cms. tunable.

Wall thickness = 1 mm.

Weight = 267 grms.

Measured loaded Q = 8,000.

The tuning plunger and head is of similar design to that in Fig. 6. Coupling is through a hole in the side wall to the middle of the end of a piece of rectangular waveguide. Variation of matching was tried with an extendable 6B.A. screw projecting through the narrow wall of the waveguide just in front of the plane of the coupling iris. This was found to provide only a small change in coupling.

Three spurious overcoupled modes are present which cannot be damped out by a lossy material (a piece of photographic negative) placed behind the plunger. Fortunately, they are separated from the H_{011} mode by more than 10 mc/s.

Summarising the performance of the spectrometer with these cavities, it was found that:

(1) using oscilloscope presentation the sensitivity is better with the H_{011} cylindrical cavities than with the H_{012} rectangular ones, and

(2) with phase-sensitive detection, the sensitivity was better with the light cylindrical cavity than with the heavy one. This, however, was no improvement on the sensitivity attainable when using the rectangular types.

The poor performance of the cylindrical cavities with phase-sensitive detection is probably due to their

larger weight and size, making them more liable to mechanical disturbances and causing a greater tendency for them to vibrate in the magnetic field. Consequently, when carrying out experiments which required high sensitivity, the rectangular fixed-tuned cavity was used.

(e) Klystrons.

Initially, two 723 A/B klystrons were used, but in spite of running them for a few hours in forced-air cooling, they were found to be too unstable in output frequency for sensitivity requirements. Recently an E.M.I. R5222 and E.E. K302 were substituted as signal and local oscillator respectively. These were found more stable. Ferrite isolators 1 and 2 are included after each klystron so that their full power can be utilised while frequency "pulling" by waveguide reflections is prevented. To reduce 100 c/s hum and mains voltage instabilities, electronically stabilised power supplies are used for both klystrons and their filaments are heated from a 6 v. battery which has its own charger. Even so, for maximum sensitivity, it is necessary to stabilise electronically the signal frequency and the intermediate frequency.

III.4 Frequency Stabilisation.

The criterion of stability for the signal frequency

is the bandwidth of the resonant cavity and for the I.F. the bandwidth of the signal I.F. amplifier. Both frequencies must remain well within these limits, if frequency instabilities are not to limit the sensitivity of the spectrometer.

When running free, the klystrons showed two main tendencies of frequency change:

(1) slow drifts due to environmental temperature changes, and

(2) 50 c/s and 100 c/s frequency modulation due to pick-up on the repeller.

When using a modulation frequency and phase-sensitive detection, it is necessary to remove frequency instabilities up to the modulation frequency[4](280 c/s). Therefore, for maximum sensitivity, these considerations dictated the minimum bandwidth requirements of the feedback loops as 0 to 300 c/s. Since the signal klystron frequency control depended on the I.F. remaining constant, it will be appropriate to describe the local-oscillator automatic frequency control first.

III.4.1 <u>The Local-Oscillator Automatic Frequency Control (L.O.A.F.C.)</u>.

(a) The intermediate frequency is kept constant at

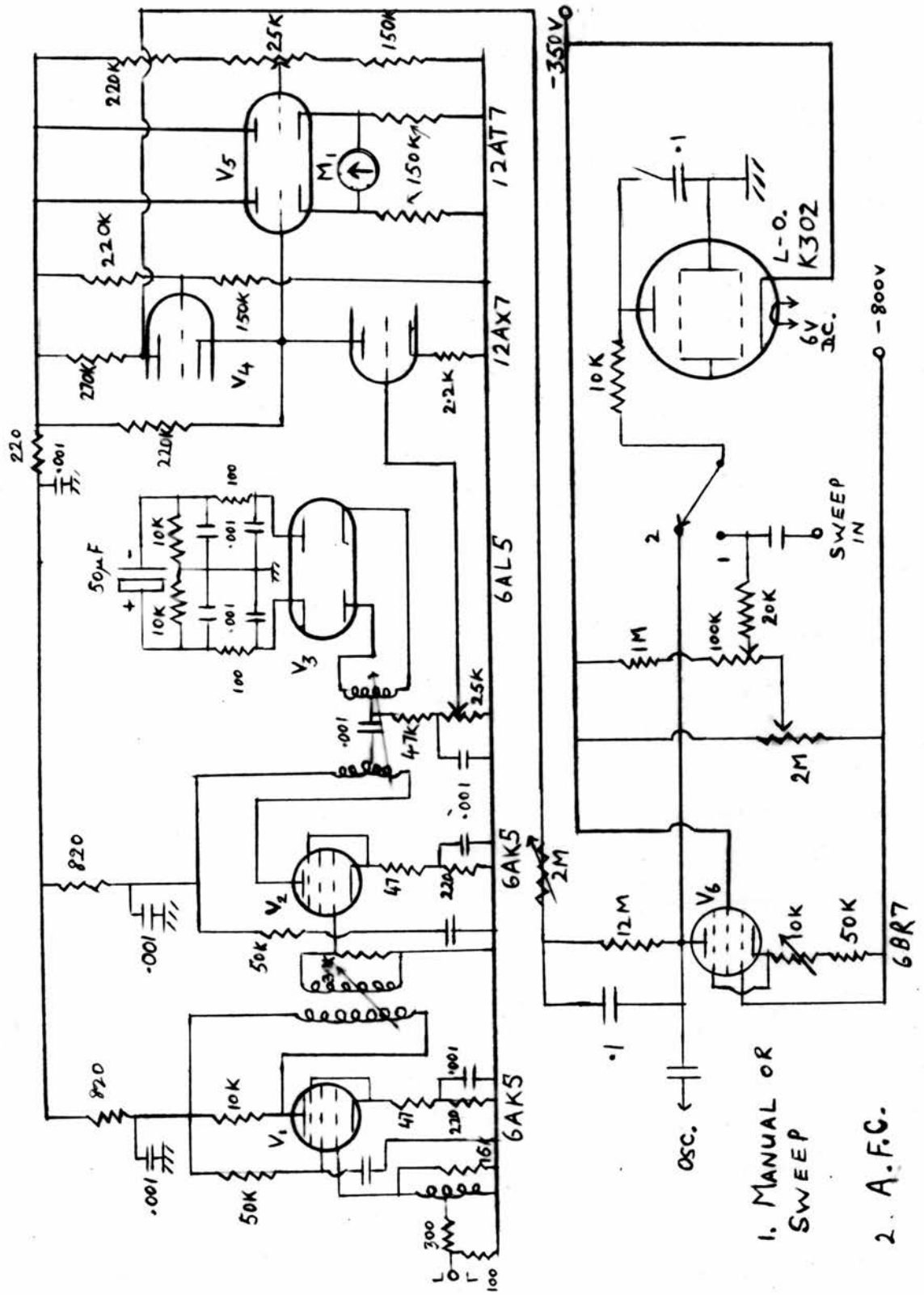

FIG. 7 THE LOCAL-OSCILLATOR AUTOMATIC FREQUENCY CONTROL CIRCUIT (L.O.A.F.C.).

45 mc/s by controlling the frequency of the local-oscillator electronically. Thus, if the frequency of either klystron changes, an error voltage is generated and is applied to the repeller of the local-oscillator. This error voltage is proportional to the frequency change Δf and is of such a polarity that it alters the local-oscillator frequency in the direction so that Δf will be reduced.

The design of the circuit that provides the error voltage is as in Fig. 7. The first two stages V_1, V_2 are conventional double-tuned I.F. stages centred on 45 mc/s. These are followed by a discriminator V_3, a.d.c. amplifier V_4 and a control circuit V_6, which applies the correcting voltage to the repeller.

The Discriminator.

The discriminator used here can be described as a ratio-detector[37] with a Foster-Seely input. The simple Foster-Seely discriminator (Fig. 8) is a phase-sensitive detector and as such requires two coherent I.F. signals, an error voltage and a reference voltage. The reference is brought from the primary via C_1 and is present across R. The error signal is across a resonant circuit, tuned to 45 mc/s. Frequency variations of the I.F. are converted by the reactance of the tuned circuit to phase variations of the error voltage with respect to the

FIG. 8 A SIMPLE FOSTER-SEELY DETECTOR.

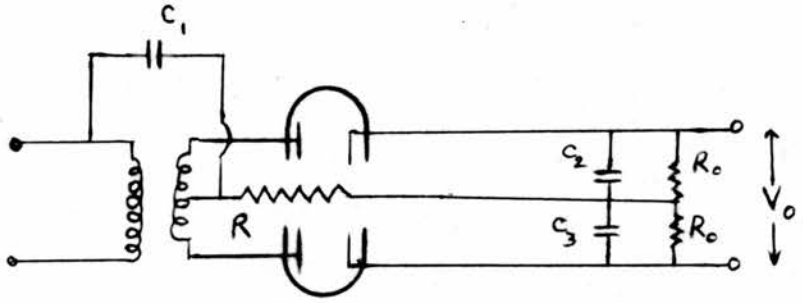

FIG. 9 A FOSTER-SEELY RATIO DETECTOR.

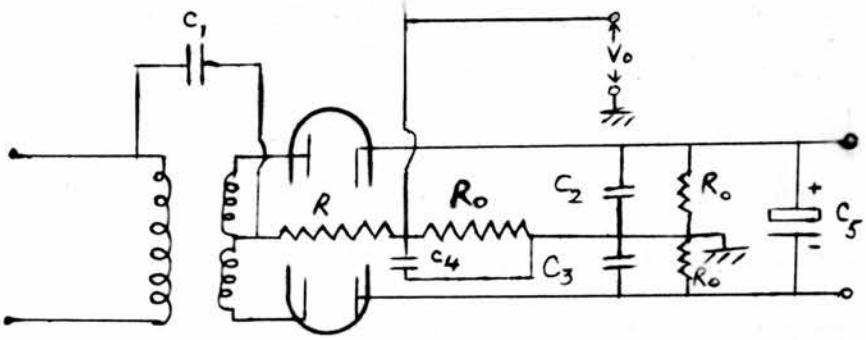

FIG. IO THE CONTROL STAGE AND EQUIVALENT CIRCUIT

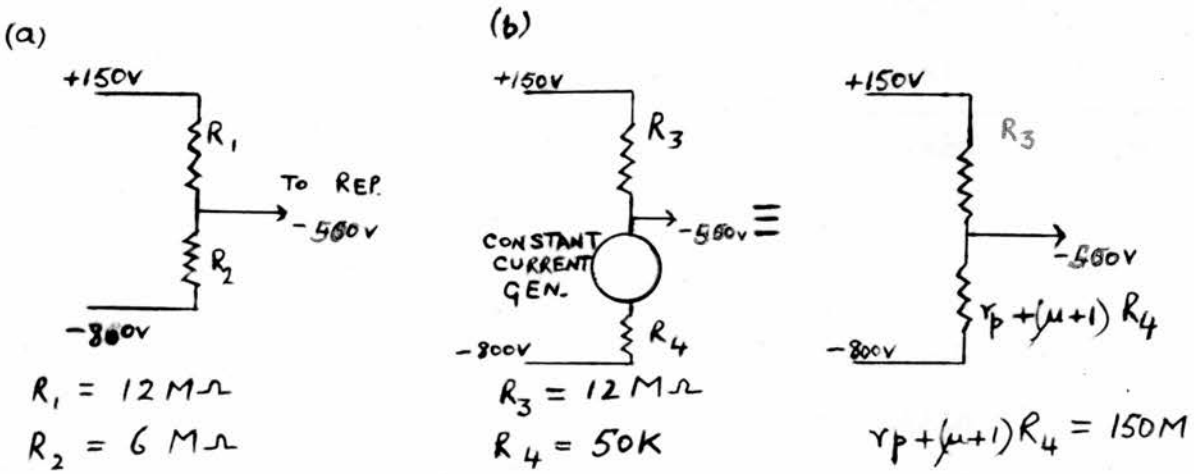

reference. Consequently, on adding these voltages vectorially and detecting, the difference of the resulting voltages across C_3 and C_2 is proportional to Δf and is taken off as V_o. Note that $\frac{1}{\omega C_2} >> R_o$ for audio frequency values of ω and $<< R_o$ for I.F. values of ω.

The ratio detector used here differs from the simple Foster-Seely, in that one of the diodes is reversed and an electrolytic capacitor is added as in Fig. 9. The sum of the voltages across C_2 and C_3 remains constant for a time $\sim$ discharging period of the electrolytic capacitor, irrespective of sudden changes in the I.F. amplitude. For this reason noise pulses will be suppressed in the output. Phase changes, accompanying changes in frequency, occur just as in the simple Foster-Seely circuit, but in this case to obtain the detected correcting voltage, the output is taken across C_4 (Fig. 9). In the discriminator built, the tuned coil was bifilar-wound to ensure that both halves were equally coupled to the primary so that a symmetrical S-shaped discriminator response would result.

The D.C. Amplifier.

The discriminator is followed by a cascode d.c. amplifier to increase the loop gain of the stabilisation network. A 220K ohm resistor, in parallel with the upper triode, increases the average current and transconductance of the

lower triode and hence the overall gain of this stage.

Measured gain = 60.

The Control Stage.

The d.c. level of the correcting signal has to be brought from the anode potential of the cascode amplifier (~ +150V) to the operating potential of the repeller of the local-oscillator (~ -500V). If a resistive potentiometer-dropping chain is used to achieve this, $\frac{2}{3}$ of the correcting voltage is "lost" across the upper resistor (Fig. 10a). Instead, a constant current device[38] is used to provide a high dynamic impedance in series with the large (12 MΩ) dropping resistor. When "viewed" from the anode, all impedances below the cathode appear multiplied by $(\mu + 1)$ where μ is the amplification factor. The equivalent circuit for this stage is shown in Fig. 10b. Thus to variations in voltage, the dropping chain appears as a 12MΩ resistor in series with 150MΩ so that now only $\frac{1}{12}$ of the correction voltage is "lost" across the 12MΩ resistor. The d.c. level of this stage can be varied ± 15 volts with potentiometers in the cathode and anode leads. The former provides the coarse control and the latter the fine.

Provision is made with a switching arrangement to operate the local oscillator repeller voltage:

(1) by manual control (position 1, Fig. 7)

(2) by sweeping with a saw-tooth voltage (position 1, Fig. 7)

(3) by automatic frequency control (position 2, Fig.7).

III.4.1(b) Setting-up Procedure for I.F. Stabilisation.

(i) Initial alignment of the ratio detector was carried out with the electrolytic capacitor disconnected. A frequency modulated signal from a wobbulator was injected onto the grid of the last I.F. stage and the output across C_2 (Fig. 9) observed on an oscilloscope. This gave the response curve of the tuned circuit which was tuned to 45 mc/s with the iron dust cores. The wobbulator signal was then applied to the input of the first amplifying stage and the I.F. stages tuned with the iron dust cores to give, at the output from the d.c. amplifier, an S-shaped curve with a bandwidth of 1 mc/s between peaks. On connecting the electrolytic capacitor the output stillshowed an S-shaped curve but modified slightly in height and width.

(ii) The following procedure is carried out to ensure correct operation of the L.O.A.F.C. The local oscillator is operated without stabilisation, and a sawtooth voltage obtained from the oscilloscope output is applied to the repeller of the signal klystron. As a result, the signal from crystal 3 is frequency-modulated and by varying the

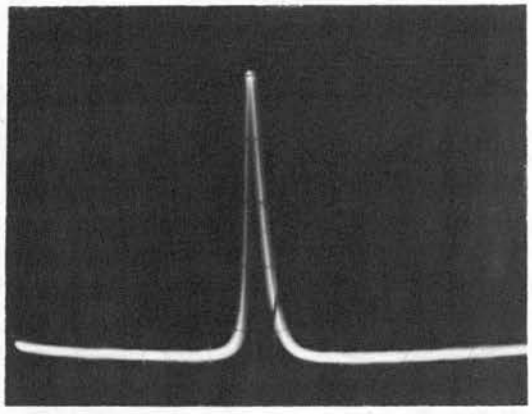

FIG. II
THE RESONANCE SIGNAL FROM 10^{17} SPINS OF POLYCRYSTALLINE D.P.P.H.

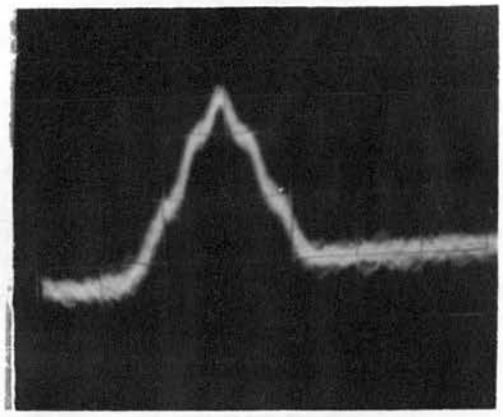

FIG. I2
THE HYPERFINE STRUCTURE FROM 10^{-3} MOLAR D.P.P.H. IN BENZENE.

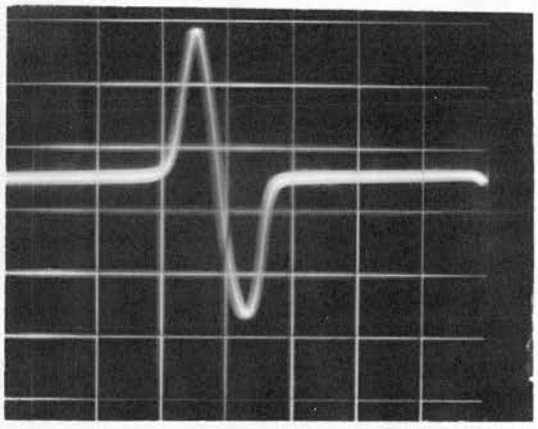

FIG. I3
THE OUTPUT FROM THE L.O.A.F.C. UNIT.

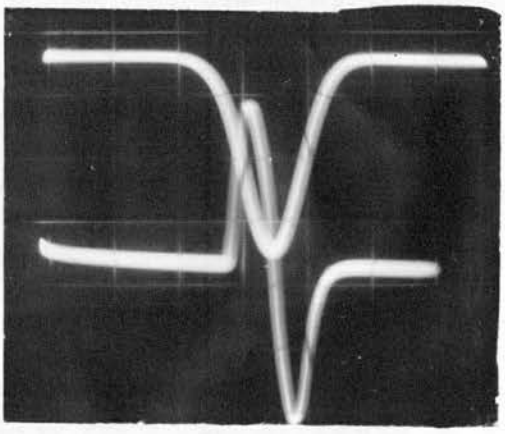

FIG. I4
THE OUTPUT FROM THE L.O.A.F.C. UNIT (lower trace) AND THE I.F. AMPLIFIER RESPONSE (low gain).

mechanical and electronic tuning of the local oscillator, it can be centred on 45 mc/s, as is indicated by the detected output from the signal amplifier. This amplifier has been previously aligned with the wobbulator. With the input of the L.O.A.F.C. unit connected to crystal 3 and by viewing the output on the same double-beam oscilloscope as used to obtain the sweep, a presentation of the S-shaped response v. I.F. is observed as Fig. 13. In this way, the spectrometer acts as its own wobbulator. Two types of output, differing in sign of slope can be obtained on having the local oscillator frequency either 45 mc/s above or below that of the signal klystron. Correct sideband operation[39] is obtained in only one of these settings. The criterion for this is that the slope of the discriminator curve v.I.F. at the output from the control stage be opposite in sign to the slope of the local oscillator repeller voltage v.I.F. Stabilisation of the I.F. will then be at the cross-over-frequency. With wrong sideband operation, the local oscillator can still be locked to the signal klystron, but not at the cross-over frequency of 45 mc/s. Locking will occur outside the peaks of the discriminator curve, or pull-in region, where the slope of the curve is suitable for stabilisation. The resulting I.F. will not be centred on the response of the signal amplifier so that the

spectrometer will be operated at reduced gain and less stability. The setting with the proper slope for correct sideband operation was originally found by trial.

It is possible to check that the cross-over-frequency coincides with the centre of the passband of the I.F. amplifiers. With the sweeping and viewing arrangements as above, an output is taken from crystal 1 to the signal amplifier and the detected output is displayed on the other beam of the oscilloscope. Fig. 14 is observed with the cavity tuned outside the mode of the signal klystron and the gain of the signal amplifier reduced to avoid saturating (in Fig. 14 the upper beam) the response curve. This shows that the L.O.A.F.C. unit and signal amplifier are correctly aligned. The reference amplifier can be substituted for the signal amplifier and its alignment also checked.

On switching off the sawtooth voltage, operating the signal klystron at the centre of its mode, and manual tuning of the repeller voltage, an S-shaped curve is traced out on the centre-reading meter M_1, shown in Fig. 7. This verifies the generation of an error voltage down to zero frequencies. It can also be used to indicate the sideband operated on.

To obtain automatic frequency operation the repeller is switched to position 2, Fig. 7, i.e. the output from the control stage. The d.c. level of this stage is adjusted until the pull-in region is reached. This is indicated by a reading on the second detector current meter of the signal amplifier. The improved constancy of this reading with the stabilisation on, shows that the L.O.A.F.C. is functioning.

With no deliberate limitation on the bandwidth of the stabilisation output, oscillations are set up in the feedback loop with a frequency of a few kc/s. The loop transmission does not then satisfy the Nyquist Criterion[40] for stability. These oscillations are completely removed by reducing the bandwidth to about 300 c/s, with a 0.1 μ.f. condenser from repeller to earth.

III.4.2 The Signal Klystron Frequency Stabilisation(S.K.F.S.).

The frequency of the signal klystron is kept constant by locking it to the resonating frequency of the cavity containing the free radical samples. The scheme used is similar to the Pound System[41], but differs in that the I.F. is produced by the local-oscillator.

The amplitude and phase of the microwave signal reflected from the cavity resonator depend on the difference

between the cavity and the signal klystron frequency. The signal is converted to an I.F. signal at crystal 1. After amplification, it is fed to a phase-sensitive detector where it is mixed with a coherent reference I.F. voltage whose amplitude and phase are independent of the reflection coefficient of the cavity. This reference voltage is obtained from an amplifier coupled to crystal 3. It will be shown in the following analysis, that the output from the phase-sensitive detector can be made proportional to the imaginary component of the cavity reflection coefficient. As such, it will be proportional to the deviation frequency and if it is applied with the proper polarity to the repeller of the signal klystron, it will act as a correcting voltage to the frequency.

III.4.2 (a) Analysis of the Signal Klystron Frequency Stabilisation.

The input impedance Z_c and the reflection coefficient Γ of a cavity, in the neighbourhood of the resonant frequency ω_o, can be written[42]

$$Z_c = \frac{\frac{1}{Q_e}}{\frac{1}{Q_o} + j\left(\frac{\omega_1}{\omega_o} - \frac{\omega_o}{\omega_1}\right)} \qquad (3.1)$$

and

$$\Gamma = \frac{Z_c - Z_o}{Z_c + Z_o} \qquad (3.2)$$

where Q_o is the unloaded Q, Q_e is the external Q, ω_i is the microwave frequency of the signal klystron and Z_o is the characteristic impedance of the waveguide.

For a matched cavity $Q_e = \frac{Q_o}{2}$. (3.1) then reduces to

$$Z_c = \frac{\frac{2}{Q_o}}{\frac{1}{Q_o} + j\left(\frac{\omega_i}{\omega_o} - \frac{\omega_o}{\omega_i}\right)} \qquad (3.3)$$

If $\delta\omega = \omega_1 - \omega_o$

$$\frac{\omega_i}{\omega_o} - \frac{\omega_o}{\omega_i} \rightarrow \frac{2\delta\omega}{\omega_o} \quad \text{as } \omega_i \rightarrow \omega_o \qquad (3.4)$$

The reflection coefficient can also be written as

$$\Gamma = \Gamma_r + i\,\Gamma_i = |\Gamma| \cos\varphi + i|\Gamma| \sin\varphi.$$

Substituting (3.3) in (3.2), it can be shown that for a matched cavity as $\delta\omega \rightarrow 0$

$$\Gamma_r \rightarrow 0$$

$$\text{and} \quad \Gamma_i \rightarrow \frac{\delta\omega}{\omega_o} Q_o \qquad (3.5)$$

The microwave voltage reflected from the cavity

$$= V_o/\sqrt{2}\ \Gamma \sin\omega_i t \qquad (3.6)$$

$$= V_o/\sqrt{2}\ |\Gamma| \sin(\omega_i t + \varphi)$$

where V_o is the amplitude of the voltage from the signal

klystron incident on tee 1.

The total voltage at the crystal 1

$$= V_o/2\ |\Gamma|\ \sin(\omega_1 t + \varphi) + \text{l-O voltage}$$

$$= V_o/2\ |\Gamma|\ \sin(\omega_1 t + \varphi) + V_2 \sin \omega_2 t$$

$$= e \qquad (3.7)$$

where V_2 is the amplitude of the l-O voltage at crystal 1 and ω_2 is the l-O frequency.

The crystal current i is given by the crystal characteristic

$$i = a + be + ce^2 \qquad (3.8)$$

The input voltage to the I.F. signal amplifier $V_{if} = Zi$ (3.9) where Z is the input impedance of the amplifier. This amplifier rejects all voltages except those whose frequency falls within its passband, viz. the voltages with frequency $(\omega_1 - \omega_2)$. Substituting (3.7) into (3.8) and hence into (3.9) the output voltage from the signal amplifier reduces to

$$AZ\ 2C\ |\Gamma|\ \frac{V_o V_1}{2} \cos\{(\omega_1 - \omega_2)t + \theta_1 + \varphi\} \qquad (3.10)$$

where A is the gain of the amplifier and θ_1 is the phase shift through the amplifier. This reduces to

$$T_1[\Gamma_R \cos\{(\omega_1 - \omega_2)t + \theta_1\} - \Gamma_i \sin\{\omega_1 - \omega_2)t + \theta_1\} \qquad (3.10a)$$

$$= V_{in}$$

where T is a constant = A Z C $V_o V_1$. (3.11)

V_{in} is the signal input to the phase-sensitive detector.

The total voltage at crystal 3

$$= V_2 \sin(\omega_1 t + \theta_2) + V_3 \sin(\omega_2 t + \theta_3)$$

where V_2 is the amplitude of the voltage at crystal 3 from the signal klystron, V_3 the amplitude of the voltage at crystal 3 from the ℓ-O and θ_2, θ_3 the corresponding phase angles.

The output from the reference amplifier is derived in the same way as (3.10) and has the form

$$T_2 \cos\{(\omega_1 - \omega_2)t + (\theta_2 - \theta_3 + \theta_4)\} \qquad (3.12)$$

$$= V_{ref}$$

where θ_4 is the phase shift through the reference amplifier, T_2 a constant which has a similar form to (3.11) and V_{ref} is the reference input to the phase-sensitive detector.

The phase-sensitive detector used here is a single ended pentode, with the signal voltage V_{in} of (3.10a) applied to the first grid and the reference voltage V_{ref} of (3.12) to the suppressor. The circuit details are given in III.4.2 (c)

The output voltage E_o, from the anode of this valve is given by

$$E_o = g_m (V_{g3}) R_\ell V_{in} \qquad (3.13)$$

where R_l is the anode load resistor, g_m the transconductance and V_{g_3} is the instantaneous suppressor voltage. In this type of mixer g_m can be written as a Taylor expansion[43]

$$g_m(V_{g_3}) = g_m V_{g_3}{}^{o} + \frac{\partial g_m}{\partial V_{g_3}} V_{ref} \qquad (3.14)$$

where $V_{g_3}{}^{o}$ is the suppressor d.c. voltage.

Substituting (3.14) into (3.13), putting in the expressions (3.10a) and (3.12) for V_{in} and V_{ref}, and averaging over a period much greater than $\frac{2\pi}{(\omega_1 - \omega_2)}$, the correction voltage $\bar{E}_o$ from the phase-sensitive detector is obtained. This averaging is accomplished in practice by a resistance-capacitor circuit where $RC \gg \frac{1}{(\omega_1 - \omega_2)}$, i.e.

$$\bar{E}_o = \frac{\int_0^{(\frac{2\pi}{\omega_1 - \omega_2})} E_o \, dt}{\int_0^{(\frac{2\pi}{\omega_1 - \omega_2})} dt} \qquad (3.15)$$

$$= \frac{(\omega_1 - \omega_2)}{2\pi} \int g_m(V_{g_3}) R_l \, V_{in} \, dt.$$

This reduces to

$$\bar{E}_o \quad T_1 T_2 \, R_l \frac{\partial g_m}{\partial V_{g_3}} [\sin \psi \, \Gamma_r - \cos \psi \, \Gamma_i] \qquad (3.15a)$$

where $\psi = \theta_1 + \theta_2 - \theta_3 + \theta_4$ and by making $\psi = 0$ or π.

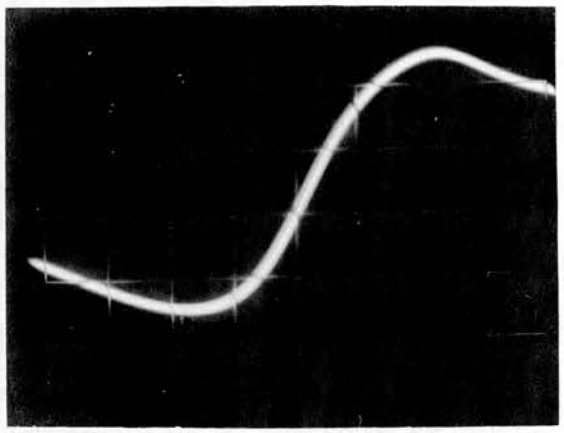

FIG. I5
THE DISCRIMINATOR CURVE FROM THE PHASE-SENSITIVE DETECTOR WITH LOW GAIN SETTING ON THE I.F. SIGNAL AMPLIFIER

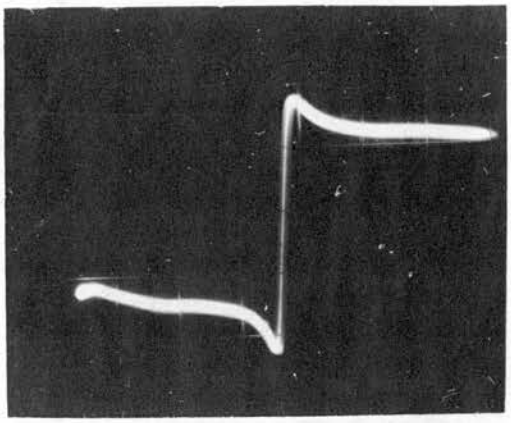

FIG. I6
THE DISCRIMINATOR CURVE AT HIGH GAIN SETTING.
(The scale of the X-axis is the same as that in FIG. I5)

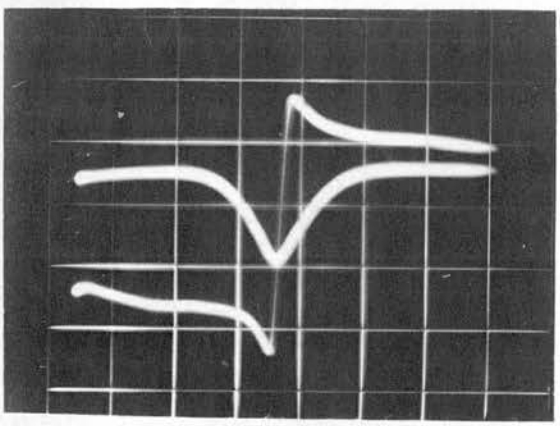

FIG. I7
THE DISCRIMINATOR CURVE AND THE CAVITY RESPONSE FROM THE I.F. SIGNAL AMPLIFIER.

$$\bar{E}_o = \pm \text{ constant } \Gamma_i \qquad (3.16)$$

From (3.5) we see that in the region of the cavity resonance frequency

$$\bar{E}_o \propto \delta\omega \qquad (3.16a)$$

III.4.2 (b) Discussion of Stabilisation Analysis.

Several points brought out by the above analysis are confirmed in practice by the experimental set up. It is seenthat, although the output from the signal amplifier is a function of the real and imaginary components of the cavity impedance (equation 3.10a), the output from the phase-sensitive detector can be made dependent on the imaginary component only, (see 3.16), providing $\psi = 0$ or π. To obtain these settings, a saw-tooth voltage sweeps the signal klystron about the cavity frequency, A.F.C. operation of the local oscillator is used and the phase-sensitive detector output is observed on the oscilloscope. The microwave phase-shifter is adjusted until this response is an S-shaped curve (Figs. 15 and 16). This occurs at two settings ($\psi = 0, \pi$) where the slopes of the curves have opposite signs. Only one of these settings can be used for stabilisation and this is the one that gives the necessary negative feedback. The particular slope was originally found by trial.

In addition, it is noted from the analysis that phase shifts in the I.F. amplifier are additive to the phase differences in the microwave carriers at crystal 1 and crystal 3. This was also verified, as the S-shaped discriminator curve can be produced by effecting phase shifts in the I.F. amplifier, i.e. changing θ_1 or θ_4. This is accomplished by slight adjustments of the I.F. tuning cores, but is not recommended in any routine alignment procedure as it might lead to drastic detuning of the I.F. strips. Setting up of the discriminating curve is always done, therefore, with the microwave phase-shifter.

In the initial construction of the microwave bridge, isolator 3 and the three-screw tuner were omitted. A spurious signal was then coupled along the reference arm, across the H to E arms of tees 3 and 4 to crystal 1. The input to the grid of the phase-sensitive detector was then not dependent solely on the cavity impedance. Inclusion of isolator 3 and the three-screw tuner as shown in Fig. 4 removes this completely. This is checked by cutting off the power to tee 1 with a metal window placed after attenuator 1 (Fig. 4), sweeping the signal klystron about the cavity frequency and monitoring the signal amplifier detected output. The three-screw tuner is adjusted to balance out any signal present.

III.4.2 (c) I.F. Circuit Details of the Signal Klystron Stabilisation.

All I.F. connections are made with 70Ω coaxial cable. The signal amplifier is a commercial Pye strip which has five EF50 double-tuned I.F. stages, a detector and a cathode follower output. This is followed by a low-pass variable filter. The gain is controlled by applying an external grid bias to the last three I.F. stages. This is preferred to lowering the screen voltages as the amplifier can then handle larger carrier levels before saturating. The 3 db. bandwidth of this amplifier is 4 mc/s.

A voltage for the S.K.F.S. is taken from the secondary of the last I.F. stage of the signal amplifier through a 3 ppf. capacitor so as not to load down this stage with the line resistance, and further amplified and limited by three EF 91 double-tuned stages. The screen-grids of these valves are operated at about +100 V to ensure a limited signal and hence a removal of the noise and 50 c/s amplitude modulation. A six-stage amplifier was modified so that the first three stages would serve as this limiter. Since it is of an open construction, great care had to be taken in the earthing and filtering of its power leads to prevent oscillation and pick-up in adjacent I.F. circuits. The output is coupled from the anode of the last stage with

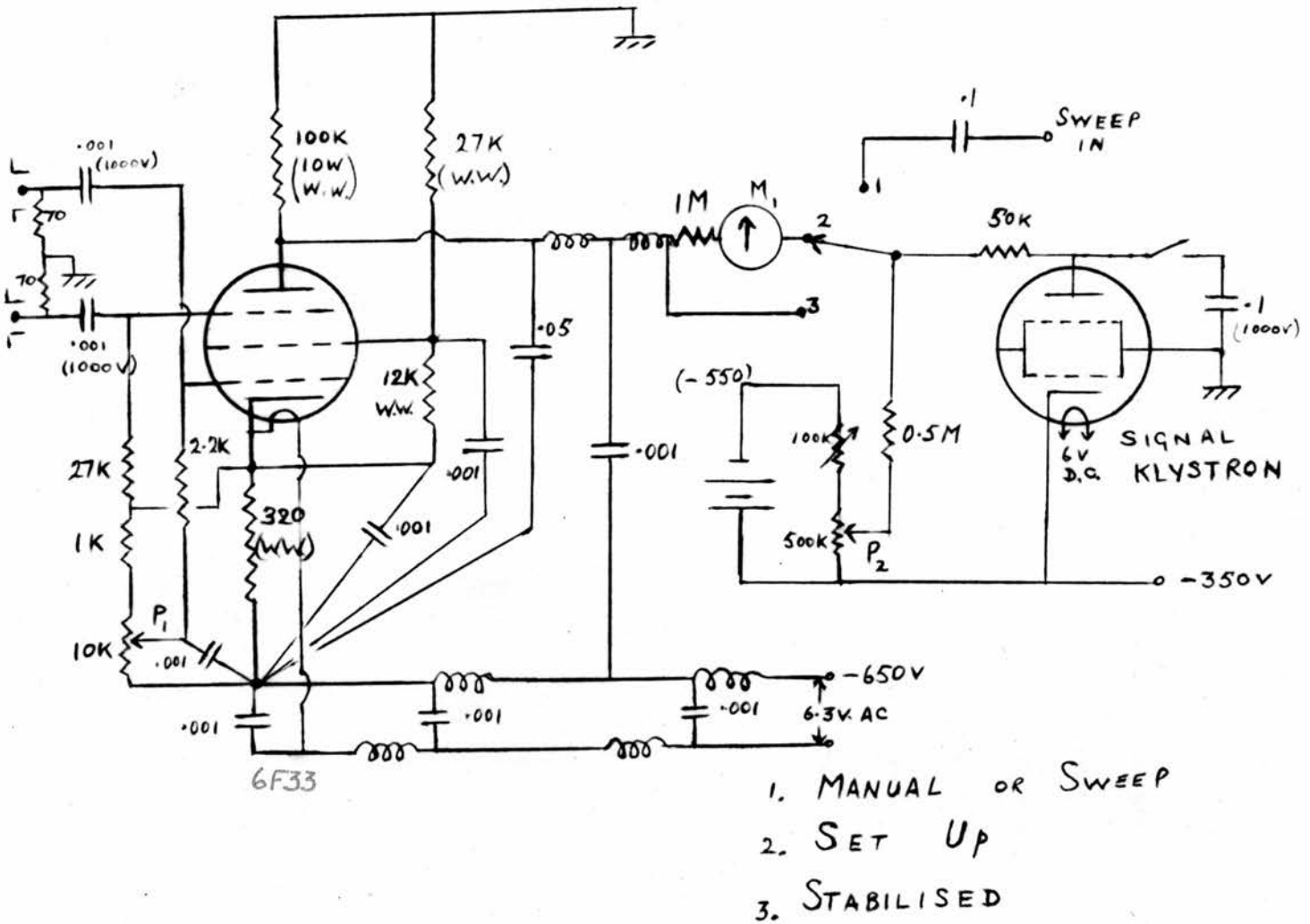

FIG. I8 THE PHASE-SENSITIVE DETECTOR AND THE SIGNAL KLYSTRON CONNECTIONS.

a secondary coil of suitable step-down ratio (~ 4:1) and is fed to the grid of the phase-sensitive detector.

The reference I.F. voltage from crystal 3 is amplified in the reference amplifier (another Pye strip), limited in a two-stage limiter[44] and fed to the suppressor of the phase-sensitive detector.

The Phase-sensitive Detector. (P.S.D.)

This is the single valve gating type shown in Fig. 18. A 6F33 was chosen because of its low suppressor cut-off voltage, which means that a reference I.F. voltage of several volts on the suppressor will be sufficient to change the anode current by several per cent and provide effective mixing, i.e. $\frac{\partial g_m}{\partial V_{g_3}}$ of (3.15a) is large. To avoid 45 mc/s on the repeller of the signal klystron, the H.T., filament and output leads are carefully filtered with I.F. chokes (4μH) and capacitors. The anode voltage, which has to be at the potential of the signal klystron repeller (~ -500 V) is controlled by varying the potentiometer P_1 (Fig. 18). Initially, it was attempted to operate this chassis and its power supply floating with respect to ground. Thus, the positive end of the supply was tied to chassis which was at the klystron cathode potential of -350 V. This, however, was not possible as the 50 c/s pick-up on the

chasses was large (0.5 v.R.M.S.). It was also attempted to ground these chasses and have the positive and negative ends of the supply floating. This also was not possible due to hum. The power supply now has an output of -700 V, with the positive end grounded. With the voltage drop (~ 500 V) across the anode load of the 6F33 controllable by P_1, the correct anode potential for stabilisation can be attained.

A switching arrangement allows either:

Position 1. Manual adjustment or sweeping of the repeller voltage.

Position 2. Setting up for stabilisation.

Position 3. Automatic frequency control.

With the switch in position 2, the reading on the meter M_1 (Fig. 18) indicates how the anode voltage differs from the operating voltage of the repeller.

The use of batteries for the manual control voltage is preferred to an electronic supply, for fear of supply failure (mainly due to fuses blowing) that would result in the repeller of the signal klystron becoming positive with respect to the cathode. For the same reason, the battery voltage is kept tied to the repeller through a 0.5 MΩ resistor even when operating on automatic frequency control.

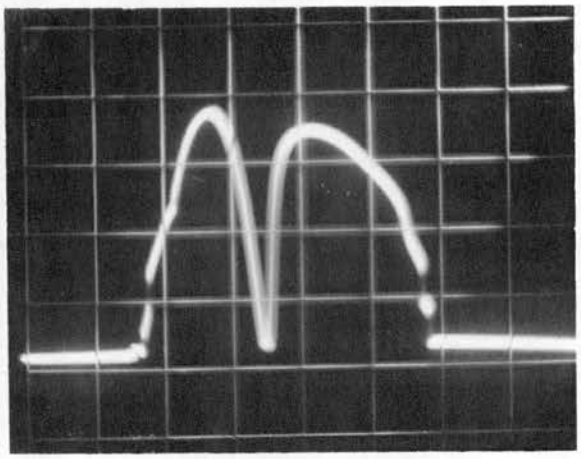

FIG. 19
THE CAVITY CENTRED ON THE KLYSTRON MODE.

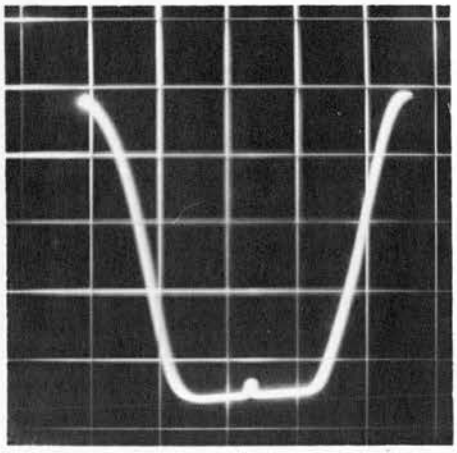

FIG. 20
THE I.F. AMPLIFIER RESPONSE WITH THE CAVITY POORLY MATCHED.

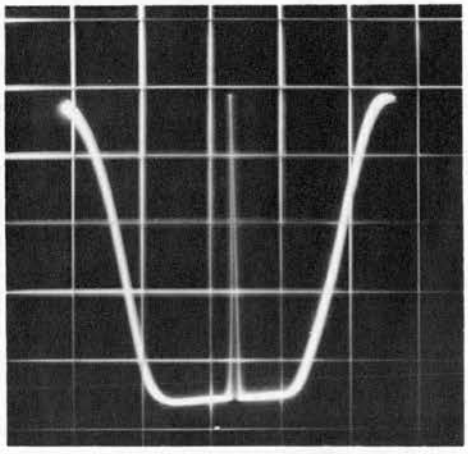

FIG. 21
THE I.F. AMPLIFIER RESPONSE WITH THE CAVITY ALMOST COMPLETELY MATCHED.

This resistor avoids shunting the anode load of the 6F33 by the low battery impedance. With this arrangement, there will be no discontinuities in switching to automatic frequency control and thus no transients will be set up which might tend to prevent locking.

III.4.3 Summary of the entire Setting-up Procedure of the Spectrometer.

The rectangular cavity with the sample inserted is roughly matched by choosing a diaphragm with the correct size of iris. With a sawtooth voltage applied to the signal klystron and the local-oscillator not oscillating, the output from crystal 3 is observed on a scope. The signal klystron is mechanically tuned until the cavity is centred on the middle of the klystron mode as shown in Fig. 19. The wavemeter is then tuned until its absorption dip coincides with that of the cavity.

The local oscillator is brought to the middle of the operating mode and mechanically tuned for an I.F. of 45 mc/s. This is indicated by a maximum I.F. amplifier response viewed on the oscilloscope. This waveform willbe similar to Fig. 20 for a roughly matched cavity. By varying the depth and position of the sliding-screw tuner, the cavity can be matched almost completely to give Fig. 21.

The S-shaped discriminator output from the L.O.A.F.C. is checked and the L.O.A.F.C. switched on, as described in Section III.4.1.

The signal klystron is swept about the cavity frequency and the output from the signal amplifier and phase-sensitive detector is observed simultaneously on a double-beam scope to ensure that the discriminator curve is that due to the cavity reactance. Fig. 17 is the resulting trace for the correct microwave phase-shifter setting. The upper trace is the discriminator curve and the lower is the cavity response from the signal amplifier.

The sweep is then switched off, the local oscillator retuned to the pull-in-region and the signal klystron tuned to the cavity frequency as indicated by the wavemeter, and a minimum on the second detector current meter of the signal amplifier. The signal klystron is then switched to position 2 (Fig. 18) and P_1 varied till the centre-reading meter M_1 is balanced. Automatic frequency control is then applied by switching to position 3. Throughout the entire switching process, the repeller voltage and intermediate frequency remain constant so that locking takes place smoothly.

The bandwidth of the feed-back loop is then reduced to 300 c/s to prevent oscillation and reduce the noise on

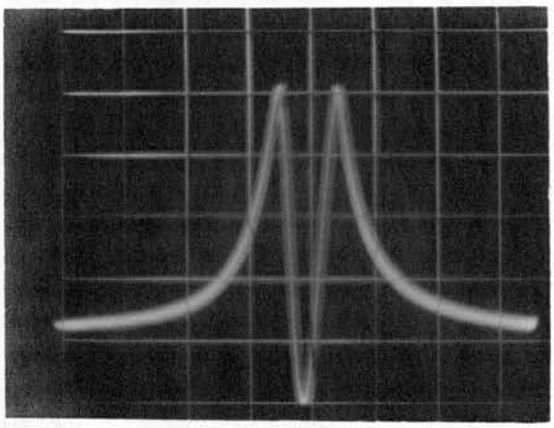

FIG. 22
A DISTORTED E.S.R. LINE DUE TO THE BRIDGE GOING FROM OVER TO UNDER COUPLING.

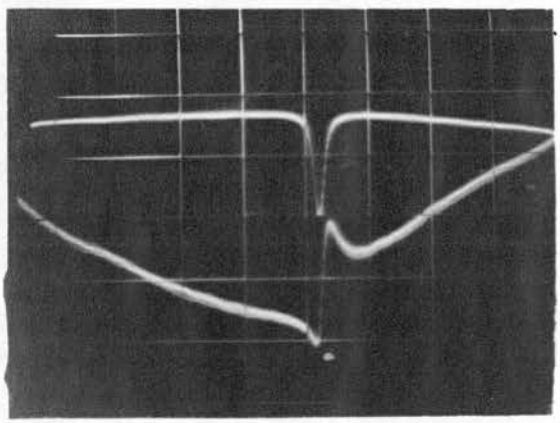

FIG. 23
E.S.R. ABSORPTION FROM THE I.F. SIGNAL AMPLIFIER (upper trace) AND DISPERSION FROM THE PHASE-SENSITIVE DETECTOR WITH THE STABILISATION LOOP OPEN.

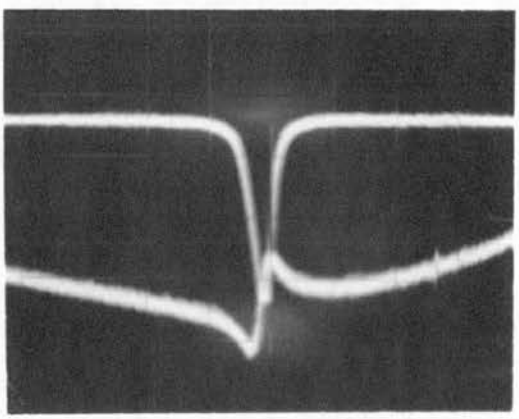

FIG. 24
E.S.R. ABSORPTION AND DISPERSION WITH THE LOOP CLOSED.

the repeller. The wavemeter reading and a minimum second detector meter reading indicate that the signal klystron is locked to the cavity.

Fine adjustments can be given to the local oscillator repeller voltage and sliding-screw tuner to reduce the noise from the signal amplifier observed on the scope. Sufficient unbalance of the waveguide bridge (tee 1, Fig. 4) has to remain to ensure that there is enough I.F. vdtage at crystal 1 to saturate the 3-stage limiter. It is also necessary, when the bridge is over-coupled, to make certain that it is not so close to match that an e.s.r. absorption takes it through match. This would involve a change of sign of the signal and hence a discontinuous change in slope of the e.s.r. line, of the type shown in Fig. 22.

III.4.4 Performance of the Stabilisation of the Signal Klystron

Since the frequency of the signal klystron is locked to the sample cavity, any perturbations in cavity frequency will be followed by the signal frequency. Thus, the dispersive component of paramagnetic susceptibility, which will change the phase of the reflection coefficient of the cavity (3.1) and effectively detune the cavity, will be corrected for. Only absorption can then be observed from the output of the signal amplifier. The reduction of

dispersion proved a way of measuring the stabilisation ratio.

If the signal klystron drifts df_o with respect to the frequency of the cavity when the feedback loop is open, the drift will be reduced to df with the loop closed. The general feedback equation holds, viz.

$$df = df_o - RGdf \qquad (3.17)$$

where G is the gain in volts/cycle with the loop open and R is the reflector sensitivity in cycles/volt. Define the stabilisation ratio

$$S = \frac{df_o}{df} \qquad (3.18)$$

so that from (3.17) $S = I + RG$ (3.18a)

To measure S, the klystron can be deliberately mistuned with a certain repeller voltage with the feedback loop open and closed. The frequency change in each case as measured with the wavemeter gave S greater than 100. This is not an accurate method. A more accurate method, proposed here by the author, is to measure the ratio of the size of the dispersion curves with the stabilisation loop open and closed. The exact procedure will now be described.

With the loop open and sweeping the magnetic field through the resonance value at 50 c/s, the sliding-screw tuner is adjusted so that only paramagnetic absorption

from a free radical sample is displayed on the scope. Due to the paramagnetic dispersion the microwave signal reflected from the cavity will vary in phase as though the cavity were frequency modulated at 100 c/s. The stabilisation circuit is sensitive to phase changes of the microwave carrier as it compares the phase of the microwave carrier at crystal 1 to the phase of the reference at crystal 3. The resulting output voltage generated at the phase-sensitive detector is proportional to the cavity detuning by the dispersion, similarly to (3.16a).

Fig. 23 shows the simultaneous display of the output of the signal amplifier (upper trace) and that of the phase-sensitive detector (lower trace) with the loop open, i.e. absorption and dispersion respectively.

After the stabilisation loop is closed, the signal klystron will follow the cavity and in so doing will be frequency modulated at 100 c/s in phase with the cavity detuning. Any instantaneous difference between the klystron and the cavity frequency, due to remaining dispersion, is a consequence of the finite gain of the feedback loop (see 3.18a). In Fig. 24 the upper trace is absorption and the lower trace, where the amplification is increased on that in Fig. 23, so that noise is visible, is the output from

the phase-sensitive detector (P.S.D.). This output which is due to the remaining dispersion will be proportional to df of (3.18). If the gain and bandwidth of the feedback loop are the same with the loop open and closed, then

$$S = \frac{df}{df_o}$$

$$= \frac{\text{the amplitude of the signal from the P.S.D. with loop open}}{\text{" " " " " " " " " " closed.}}$$

The value of S measured in this way is 800.

III.5 Presentation of the E.S.R. Spectra.

The spectra can be recorded in two ways:

5.1 Video Detection.

With a 50 c/s magnetic field modulation, the detected output is obtained from the signal amplifier and applied to the Y-plates of a scope. An external 50 c/s signal is applied to the X-plates and phased to centre the e.s.r. line. The back trace is eliminated by a 50 c/s Z modulation.

5.2 Phase-sensitive Detection.

The sensitivity of the spectrometer can be increased by reducing the output bandwidth (see 1.14). The sweep rate must also be reduced, however, so that the Fourier components, containing most of the information about the e.s.r. line, fall within the output bandwidth.

The magnetic field is modulated at 280 c/s to a depth less than, or equal to, the line width and simultaneously swept slowly with a linear sweep through the absorption line. The absorption is obtained as a 280 c/s signal from the I.F. amplifier. This is further amplified in a narrow-band-amplifier tuned to 280 c/s and detected in a phase-sensitive detector. This unit is described here (see Fig. 26) as in a lock-in-mixer, to avoid confusion with the phase-sensitive detector in the klystron stabilisation circuit. The spectra are displayed on a pen-recorder. The traces are proportional to the amplitude of the 280 c/s signal from the narrow-band-amplifier, which in turn, is proportional to the slope of absorption line, i.e. to the derivative of the absorption. The use of a phase-sensitive detection scheme, which employs a reference voltage, means that noise in the output is restricted to that falling within the output bandwidth, but centred on the modulating frequency. To avoid low frequency microphonics, therefore, the modulating frequency was chosen as 280 c/s rather than a lower value of, for example, 30 c/s.

In both recording schemes, line widths, hyperfine splittings and g-values, were estimated using radicals of known e.s.r. properties (e.g. solid D.P.P.H., D.P.P.H. in benzene and Wursters blue ion) as markers.

FIG. 25 THE NARROW- BAND AMPLIFIER.

(a) The Narrow-band Amplifier.

In coherent (i.e. phase-sensitive) detection it is only necessary to have the bandwidth of the narrow-band amplifier less than the modulation frequency, provided that noise and pick-up voltages do not saturate it.[4] To reduce this effect from harmonics of 50 c/s, the amplifier has a bandwidth of a few cycles centred on the modulation frequency of 280 c/s. The circuit designed to fulfil this is shown in Fig. 25. This utilises a difference amplifier V_1 cascaded by two triodes V_2,V_3 in parallel. V_2, the first of these triodes, amplifies the signal that is fed back to the second grid of the difference amplifier. This signal is frequency selective by using a twin-tee coupling network, and its phase is such that the overall amplifier characteristic is acceptive. With the twin-tee included as shown in Fig. 25 the high grid-cathode impedance does not load down the network and hence does not lower the circuit Q[45].

Measured mid-frequency gain = 450

Measured bandwidth = 6 c/s.

(b) The Lock-in-Mixer.

The lock-in-mixer (Fig. 26) is of the Schuster type[46]. The first stage V_1 is a concertina phase-splitter which provides the 280 c/s reference signal push-pull to the

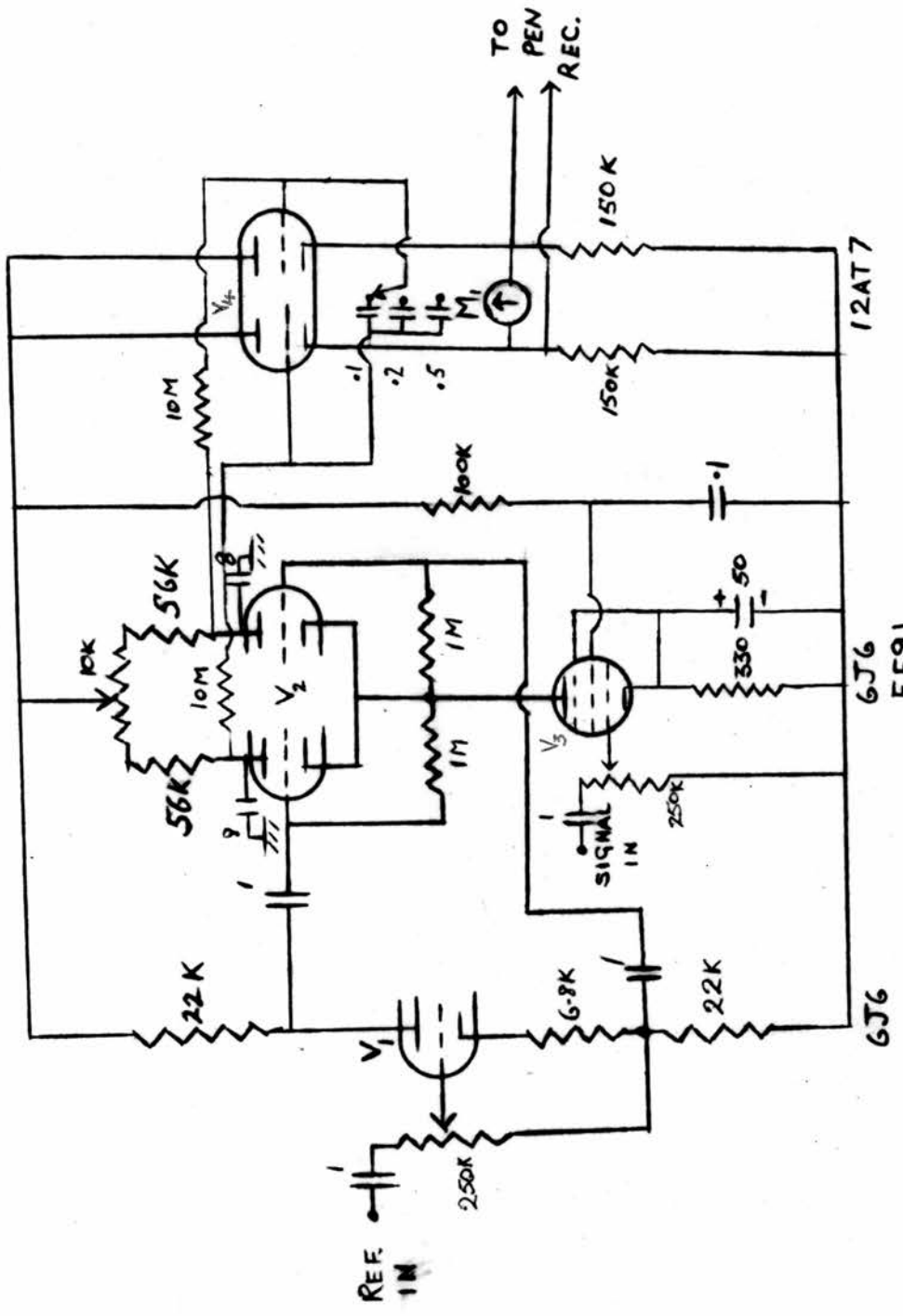

FIG. 26 THE LOCK-IN-MIXER (280 c/s)

gating-valve V_2 of the cascode mixer.

Correct phasing of the signal to reference voltage at this mixer can be carried out in two ways.

(a) With the reference voltage on the Y_1 beam and the signal from the narrow-band amplifier on the Y_2 beam of a double-beam scope, the magnetic field is varied to give a maximum signal voltage from a large paramagnetic sample, e.g. 10^{17} spins of D.P.P.H. The phase-shifter on the 280 c/s oscillator is varied so that signal and reference have a phase difference of π radians, or

(b) The magnetic field is adjusted to give a maximum output on the pen-recorder and then maximised by varying the phase-shifter.

A 10 k ohm potentiometer enables the output to be balanced with no resonance signal input. Balance is indicated on meter M_1 (Fig. 26). The capacitors used to determine the output bandwidth are a low-loss paperwound type and can be selected using a low-leakage switch, (leakage resistance > 200 MΩ). The pen-recorder, an Evershed and Vignoles, with a full-scale sensitivity of ± 0.5 m.a., is driven by V_4.

(c) <u>The 280 c/s Oscillator</u>.

This is of the Wien bridge variable frequency type[47] and is formed by the first two stages of Fig. 27. A

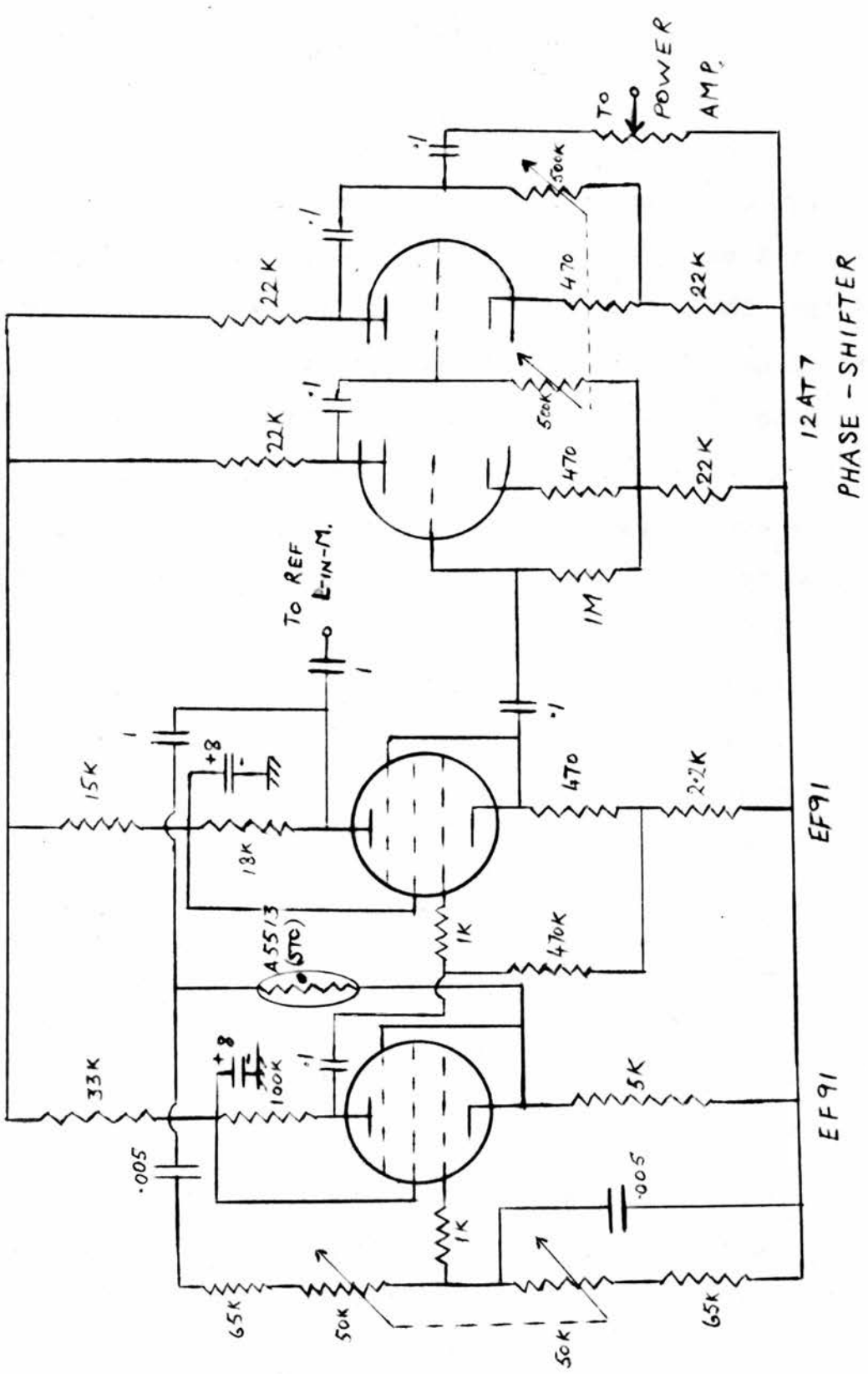

FIG. 27 THE 280 c/s WIEN BRIDGE OSCILLATOR.

thermistor of semiconducting material (Standard Telephone and Cables Co. A/5513) which has a negative temperature coefficient of resistance, is used as a limiter. This stabilises the output amplitude and, at the same time, keeps it free from harmonics. If the system is studied in the complex plane[47], it is found that a thermistor with a ngga-tive temperature coefficient of resistance has to be in the upper arm of the bridge as shown in Fig. 27. Care has to be taken to mount this thermistor in a region of constant temperature, as the equilibrium it attains is critically dependent on its temperature. For frequency stability, highly stable components are employed in the bridge network. Thus, silvered mica condensers, Radiospares "Hystab" resistors and wire-wound potentiometers are used.

Each day before recording e.s.r. spectra, the oscillator is tuned to the narrow-band amplifier. However, it is found that the long term stability (days) of the frequency is much better than 6 c/s (the bandwidth of the narrow-band amplifier).

Two outputs are taken from this oscillator; one (25 volts R.M.S.) to the reference of the lock-in-mixer, and the other to a conventional variable phase-shifter[25]. This is the phase-shifter used to adjust the phase differance between the 280 c/s reference and signal voltage to π

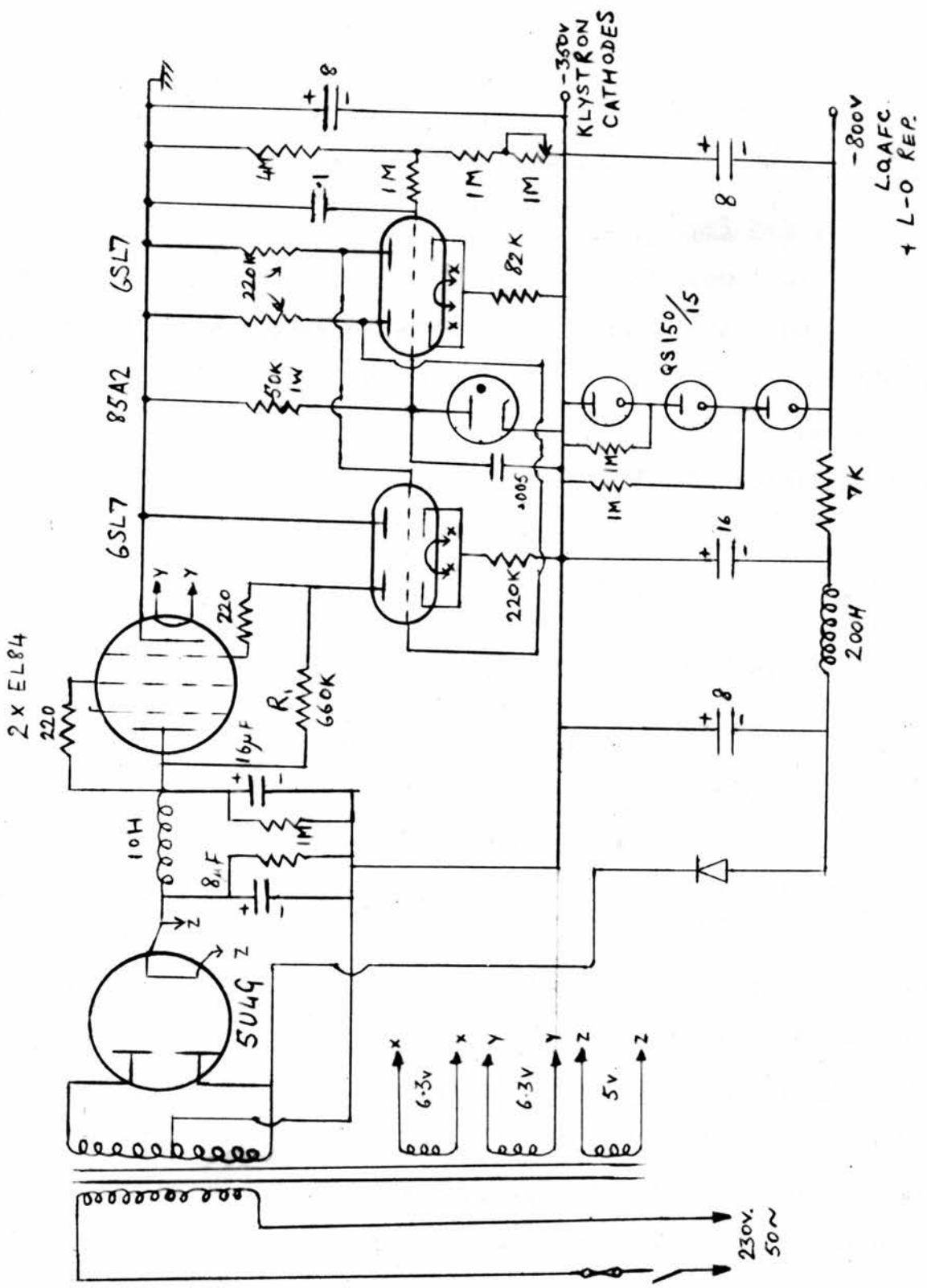

FIG. 28 POWER SUPPLY 2, FOR THE KLYSTRONS.

radians. The output from the phase-shifter is taken to the power amplifier which drives the modulation coils.

(d) The Power Amplifier.

It is a modified version of the Williamson high fidelity audio power amplifier[48]. No negative feedback is necessary at 280 c/s. The impedance of each of the modulation coils on the magnet is 2 K ohms. With a 2:1 matching transformer, the amplifier can develop 15 W in these field coils in parallel. This gives about 18 oe. peak-to-peak at the centre of the field gap.

III.6 Stabilised Power Supplies.

All electronic units are provided with electronically stabilised power supplies, which were designed and built by the author. The general design of these (Fig. 28) includes a transformer, rectifier, condenser-input filter followed by a negative-feedback electronic d.c. regulator. The d.c. amplifier, in the latter, consists of a balanced difference amplifier input, cascaded by a cathode-coupled difference amplifier. This was preferred to the Artree cascode[49] type, since in the latter, the current through the reference valve is dependent on the current through other valves. This is an undesirable feature, as variations in reference valve current mean changes in reference

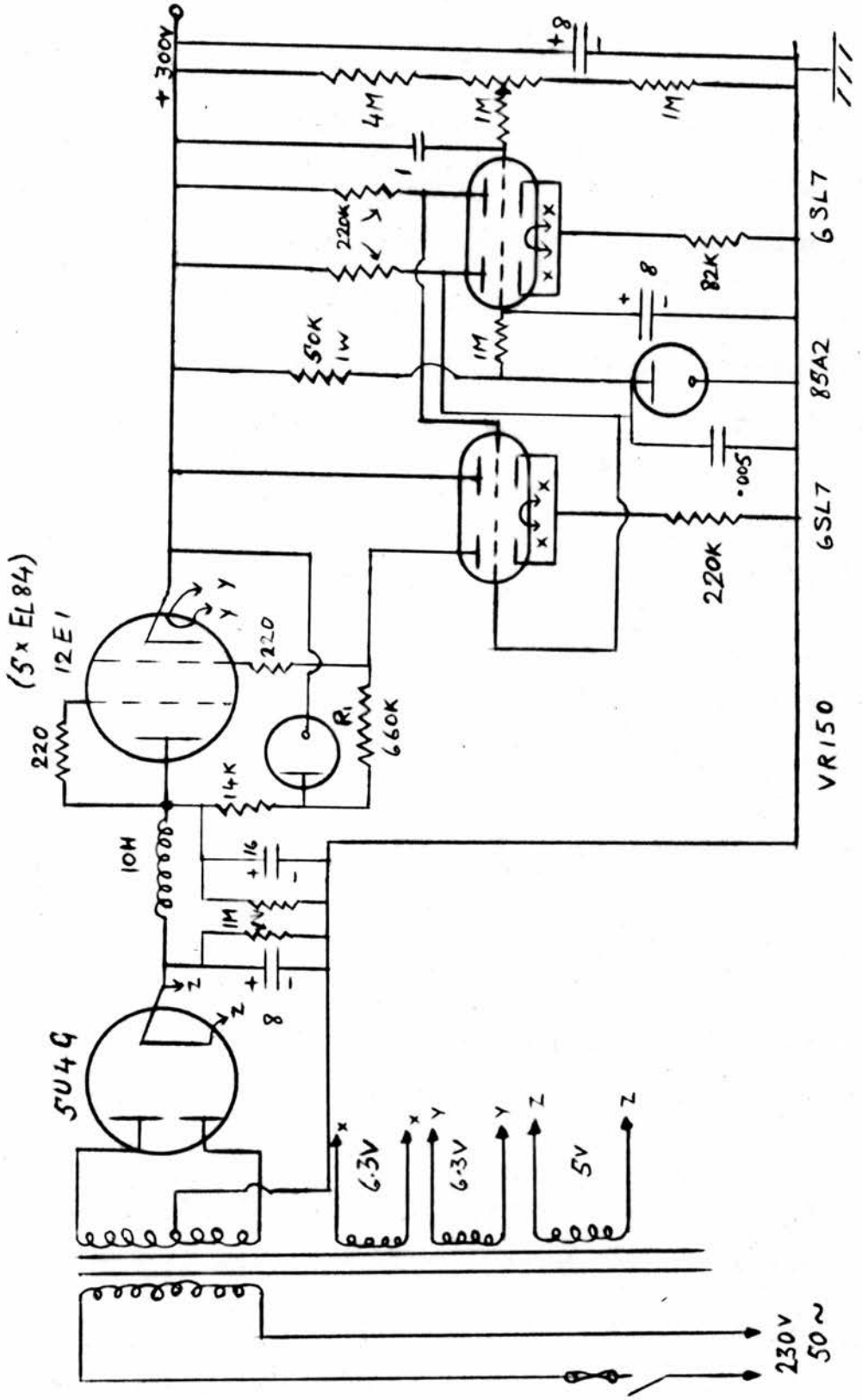

FIG. 29 POWER SUPPLY 4, FOR THE ELECTRONICS.

voltage, so that it will tend to limit output stability. The balanced input of the d.c. amplifier gives a first order balancing out of heater voltage variations.

In the supply for the klystrons, (Fig. 28), the H.T. end of the anode resistor R_1 of the last stage in the d.c. amplifier is connected to the unstabilised side of the control valve. This ensures an adequate gain of this stage when the grid to the cathode voltage of the control valve approached zero. However, in the power supplies for the electronics (Fig. 29) this lead is connected to a much more stabilised voltage (due to the VR 150 neon). This makes an improvement on the output resistance and regulation (see performance data), but gives no reduction in existing ripple. In fact, at this level, (~ 1 mv) ripple was probably due to pick-up in the wiring. A good discussion is given in reference 50.

A spike voltage (100 mv) was observed in the output of the -700 V supply. This was a damped oscillatory pulse of period ~100 μ sec. Its origin was traced to the mains transformer and by connecting a .03 μ F (2000 v.d.c.) capacitor across the secondary, it was reduced to 4 m.v.

Power Supply Specifications.

Power Supply 1, for the I.F. amplifiers, is operated

at +240 v. with a maximum load current of 200 m.a. The circuit is similar to Fig. 29 but does not have the V.R150 neon.

Power Supply 2 is for the cathodes of the klystrons and is operated at -350 v. with a maximum load of 100 m.a. The circuit, as shown in Fig. 28, includes a -750 v. output for the local oscillator stabilisation of Fig. 7.

Power Supply 3, for the phase-sensitive detector, is variable from -600 to -700 v. with a maximum load of 30 m.a. It is similar in design to Power Supply 2 but the components have a higher voltage rating.

Power Supplies 4 and 5, for the rest of the electronics, have an output of 300 v. with a maximum load of 200 m.a. The circuit diagram for Power Supply 4 is Fig. 29. The only modification in Fig. 29 for Power Supply 5 is that five EL84's replace the 12E1 control valve.

Performance of Power Supplies.

	Output Resistance	Ripple Content (R.M.S.)	Regulation for a 12% change in mains voltage
Power Supply 1:	2Ω	< 2 m.v.	200
Power Supply 2:	2Ω	< 2 m.v.	200
Power Supply 3:	-	< 5 m.v.	-
Power Supplies 4 and 5:	1.5Ω	< 2 m.v.	360

where the output resistance = $\frac{\text{the change in output voltage}}{\text{the change in output current}}$

$$\text{and the regulation} = \frac{\dfrac{\text{the change in R.M.S. mains voltage}}{\text{the R.M.S. mains voltage}}}{\dfrac{\text{the change in output voltage}}{\text{the output voltage}}} .$$

III.7 Construction and Mounting of the Electronics.

At the start of building the apparatus, attention was given to the construction and mounting of all the chasses for the electronic equipment. Accessibility and demountability were desired for all units as it is convenient to service them while mounted, although sometimes it is necessary to make adjustments, alignments etc. on a bench. For these reasons, the circuits were constructed on single panels of tinned iron or, when shielding was necessary, in boxes with removable lids. Except for the electronics involved in the modulation of the magnetic field, these units are mounted vertically on a rack, with the valves pointing inwards and the valve bases and circuit components on the side facing outwards. Power supplies, which need little adjustment once set to the required voltage, are mounted on the rear of the rack. The magnetic field modulation circuits are similarly mounted on the frame of the table supporting the waveguide.

III.8 The Magnet.

8.1 The Details. It was designed jointly by the St. Andrews E.S.R. Group and Newport Instruments Ltd. and was

constructed by the latter. The full yoke is of cast iron and the pole pieces and caps of mild steel. The main field coils are each wound with 3000 turns of rectangular cross-section, enamelled copper wire. This type of wire improves the cooling and filling factor of the coil. An additional set of coils is fixed to the d.c. coils for modulation purposes.

The magnet design details are:-

Outside length of yoke = 23" × 22.3/4"

Cross-section of yoke = 3.5" × 7"

Pole-piece diameter = 7"

Gap width = 2.5/16"

Weight of magnet and mount = 11 cwts.

Power dissipated in coils for 3,500 oe. = 260 W.

Resistance of coils in series (cold) = 12 Ω

With air cooling field range up to 6,000 oe.

Cross-section of rectangular wire = 0.05" × 0.015".

The Mount.

The yoke was supported at 45° in a cradle on a steel plate, and can be rotated about a vertical axis over a ball race. To facilitate movement to two other sets of apparatus, the magnet was mounted on a trolley that can travel over a set of rails.

FIG. 30 THE INHOMOGENEITY PLOT OF THE MAGNETIC FIELD.

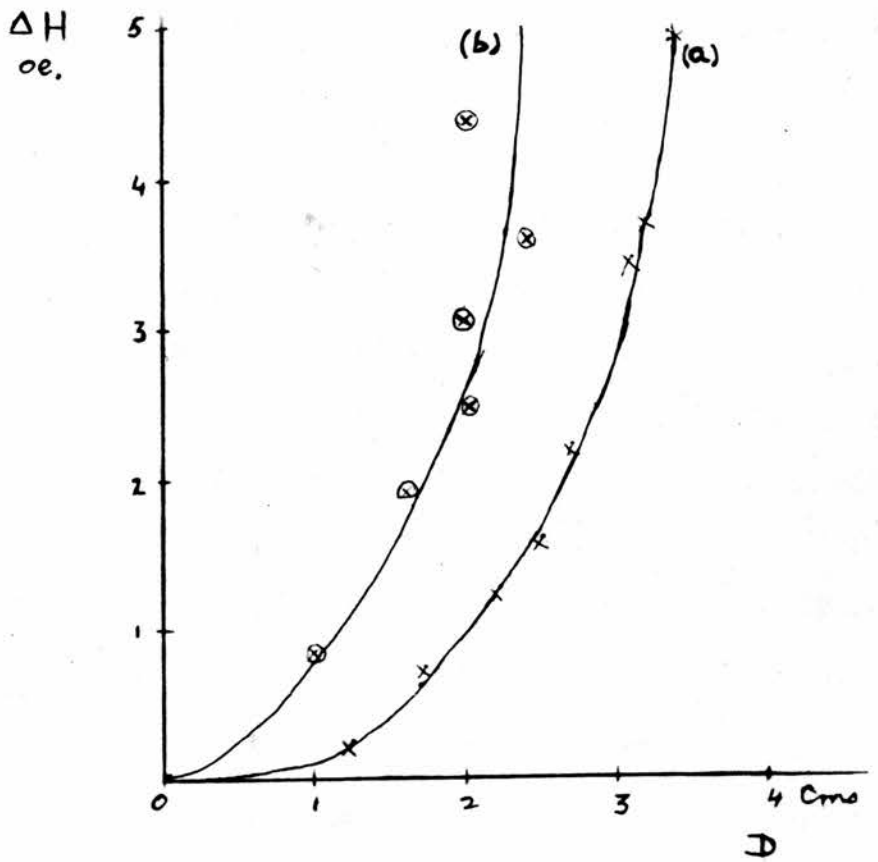

ΔH is the difference in the field from that at the centre.
D is the distance from the centre.

Alignment and Homogeneity.

The sections were assembled in the laboratory and the pole-caps were aligned parallel to within 0.0004". The pole-caps are optically flat so that the spatial homogeneity, for the fixed field gap, depends on the parallelism of the faces. This homogeneity was determined using a proton resonance head[51], constructed by Mr I. Firth. Accuracy of field measurements could be made to 0.25 oe. The field differences, ΔH, from that at the centre, along a vertical axis, are shown in Fig. 30(a). Thus with a sample length of one inch, the total field inhomogeneity across it, when it is placed at the centre of the pole-caps, is 0.25 oe. The inhomogeneity plot along a horizontal axis, parallel to the pole-faces was found to be the same as Fig. 30(a) within the experimental accuracy ($\pm$ 0.25 oe.). The field difference across the gap, at the centre, was 2.25 oe., i.e. 0.4 oe./cm.

When these measurements were being made, a factor contributing to field inhomogeneities was discovered. As will be mentioned in the next section, the first method used to scan the magnetic field with a slow sweep was to apply a voltage sweep to one of the modulation coils and the 280 c/s voltage to the other. The magnetic flux from

the former, due to its non-Helmholtz nature, increased the inhomogeneity as shown in Fig. 30(b) by more than a factor two. This curve was obtained with a d.c. current of 300 m.a. through the modulation coil.

Magnet Power Supply.

Originally, a stack of twelve 12 v. 40 A.H. lead-acid batteries were used as the power supply. These batteries were charged from their own rectifier and could be used under trickle-charged conditions. After about eighteen months service, they began to deteriorate both in stability and capacity. Thus, even after five hours warming up powered by the rectifier, on using the batteries, the magnetic field drift was as large as 2 oe./min. Under trickle-charging operation of the batteries, this was reduced to 0.5 oe./min. They have now been replaced by a commercial constant current generator, the Newport Instrument Type B, Mark II whose specifications are:-

Time constant of mains stabilising transformer = 0.02secs.

Current stability = ± 1 in 10^4 for $\pm$ 4% mains charge.

Ripple field = 0.5 oe.

Controllable current range = 0 to 8 A.

III.8.2 Magnetic Field Modulation.

Depending on the presentation required, (see Section

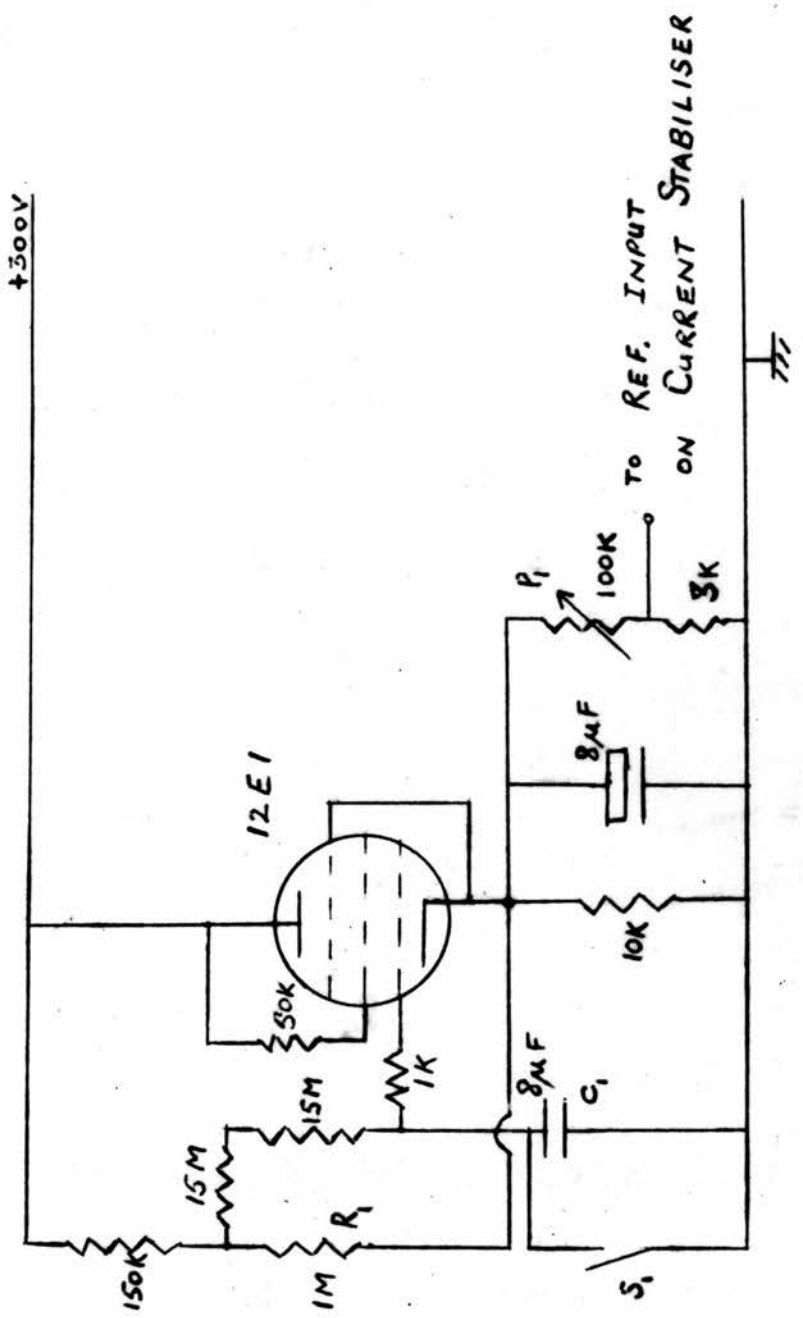

FIG. 31 THE BOOTSTRAP SLOW-SWEEP GENERATOR.

III.5) the modulation coils are driven by a 50 c/s voltage from a transformer, or by 280 c/s from the power amplifier.

Trouble was found in attempting to apply a satisfactory slow linear magnetic field sweep. When the battery stack was used to power the main coils, the field was swept by passing an additional current through one of the modulation coils. This was obtained from a motor-driven rheostat connected across another set of batteries. This method was abandoned when the added spatial inhomogeneity effect was measured. It was replaced by a method of passing the additional current through the main coils. A 12 Ω resistor was required in series with the main coils and main battery stack, to isolate the sweep voltage from the low impedance of the batteries. However, this sweep proved very non-linear. At present, the magnetic field sweep is produced by applying a slow linear swept voltage to the reference input of the stabilised current generator. This voltage is produced by the bootstrap generator.

III.2(a) Bootstrap Slow Sweep Generator (Fig. 31).

Use is made of the time constant of the charging of the capacitor by a d.c. applied voltage. The voltage across the condenser C_1 is exponential with time, but by letting it charge to only a small fraction of the applied

voltage, and by employing some degree of positive feedback, i.e. bootstrapping[52] the grid to the cathode with resistor R_1, it is possible to achieve reasonable linearity in output voltage. The extent of the sweep is limited by the valve bottoming when it is driven into the positive grid region. The sweep is switched on and off manually with switch S_1. Rate of sweep is determined mainly be the value of the time constant for the charging circuit of C and by the setting of the 100 KΩ potentiometer P_1. The latter also controls the sweep extent.

III.9 The Sensitivity of the Spectrometer.

The sensitivity of the spectrometer for a given set of operating conditions was measured using standard samples containing estimated amounts of free radicals. The first standards were made up by mixing D.P.P.H. to known dilutions with solid calcium carbonate. Even although these mixtures were shaken for hours with an electrical shaker, their uniformity was poor. Thus, all samples which should have contained 5×10^{16} spins and less, gave no observable e.s.r. signals, (i.e. were less than 5×10^{14}). The second method used was to prepare solutions of D.P.P.H. in benzene to known concentrations and, with a syringe, inject amounts into a hole of measured dimensions drilled in a perspex

capsule. The benzene was allowed to evaporate (1 day) and then the sample was capped. On monitoring the detected output from the I.F. signal amplifier on the scope and optimising the signal-to-noise amplitude ratio S/N by fine adjustments of the sliding-screw tuner and the local oscillator repeller voltage (see Section III.4.3), the following results were obtained with the standard samples.

TABLE I.

Estimated Number of Spins	S/N(after a few days)	S/N(after 3 month
10^{17}	300:1	300:1
2.10^{16}	50:1	6:1
5.10^{15}	12:1	1:1
9.10^{14}	7:1	0
2.10^{14}	2:1	0

The recording conditions used were those stated in Section 1.5, i.e. klystron power 50 m.w., the output bandwidth Δf = 10 kc/s and the unloaded cavity Q = 4,000.

The filling factor for each sample was kept the same byhaving all in the same part of the r.f. field. The measurements given in the second column were made a few days after the samples were prepared. They show the authenticity of the estimation of the number of radicals to

be within a factor of two. Moreover, solid samples of D.P.P.H. (10^{17} spins) were weighed out and their S/N values (300:1) were consistent with the standard samples. Thus, with the above operating conditions, the sensitivity could be quoted as saying 10^{14} spins of D.P.P.H. (i.e. 2.10^{-10} moles) gave a signal whose amplitude equalled that of the noise.

It was noted that some of these standard samples deteriorated with time. After three months, the measurements were repeated and those in the third column found. This is similar to that observed by Feher[4].

$N_{min.-th}$, the theoretical value of $N_{min.}$, for the spectrometer is $\sqrt{2}$ X the expression (1.16), because of the power loss along arm 2 of tee 2 (see Fig. 4). Thus from the sensitivity measurements

$$\frac{N_{min.-obs.}}{N_{min.-th.}} = 30 \qquad (3.19)$$

The sensitivity of a spectrometer can be expressed in terms of a noise figure[53] F where, due to noise from the amplification and detection circuits, the noise power at the output of the microwave detector is $FkT\Delta f$. Viz.

$$\frac{N_{min.-obs.}}{N_{min.-th.}} = F^{\frac{1}{2}} \qquad (3.20)$$

For a superheterodyne receiver[54]

$$F = L(t_c + t_\ell + F_A - 1) \qquad (3.21)$$

where L is the crystal conversion loss at 45 mc/s and t_c is the noise temperature of the crystal[55] at 45 mc/s. Both are a function of microwave power and operating in the crystal current region of 0.5 m.a. F is minimised[55]. This minimum is broad, as crystal currents up to 2 m.a. have been used with no observable reduction in signal-to-noise ratio.

For the CS3A and CS3B silicon crystals (B.T.H.) used, the conversion loss is 8 db. and the noise temperature is about 2. t_ℓ is the noise temperature taking account of the noise from the local oscillator. Published data give values about 2. F_A is the noise figure of the I.F. amplifier, and for the "Pye-strip" is 30. This was measured using a Marconi IOS/16149 noise-diode generator.

Substituting these values into equation (3.21)

$$F = 200$$

and therefore from (3.20)

$$\frac{N_{min.-obs.}}{N_{min.-th.}} \text{ should be I4.}$$

Within the experimental accuracy of the sensitivity

determinations this agrees well with (3.19); so that expression (3.21), and the values used in it, takes full account of the noise limiting the oscilloscope detection. To improve F appreciably F_A must be reduced to

$$\sim t_c + t_\ell - 1 = 3$$

which is an amplifier of the highest quality with a grounded-cathode grounded-grid input stage[56]. One of these amplifiers has recently been used as a signal pre-amplifier, but the lowest noise figure attainable was eleven. From (3.21) and (3.19) this should have improved the sensitivity by 1.5. No improvement was detected. The inclusion of a balanced mixer[57], to eliminate local oscillator noise, will reduce F appreciably only when F_A is reduced to ~ 3.

With phase-sensitive detection, the sensitivity is better than that with the oscilloscope and for an output time constant of two seconds the signal-to-noise ratio for 2×10^{14} spins of D.P.P.H. is 30:1. Evaluating $N_{min.-th}$ for this bandwidth of 2 secs. from (1.14) gives

$$\frac{N_{min.-obs.}}{N_{min.-th.}} = 90 \qquad (3.22)$$

Comparing (3.19) and (3.22) the added "noise" in the recorder detection is mainly due to:

(a) Microphonics, i.e. acoustical and mechanical

disturbances.

(b) Base-line drifts.

(a) Microphonics enter the system via the microwaves. The part of the waveguide most sensitive to disturbances is that involved in the balancing of tee 1, namely the elements in arms 1 and 2. Of these, at 25 mw. incident power on the rectangular cavity, the sliding-screw tuner is the most susceptible.

(b) With small bandwidths and wide line, requiring recording times larger than ten minutes the base-line drifts limit the sensitivity. These are of two types, a field-dependent drift and one due to the variations in the temperature of the room. The former is due to cavity vibrations caused by eddy currents interacting with d.c. field. The latter, which sometimes occurred is caused by temperature drifts of the cavity arm. If the temperature and hence the frequency of the cavity drift slowly, even although the signal klystron is locked to it, the drift will show up as a base-line variation because of the frequency sensitivity of the sliding-screw tuner. Considering these drifts and the instabilities described in (a), the sliding-screw tuner used in this work (BR 1400 Microwave Instruments Ltd.) is unsatisfactory. It would, therefore, improve the sensitivity to use a bridge-balancing element that is less sensitive to frequency.

FIGURE 32 THE SUBSTANCES USED

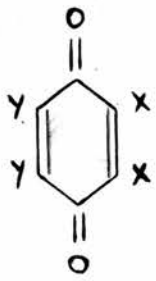

X = Y = Cl CHLORANIL

= Br BROMANIL

= I IODANIL

X = CN
Y = Cl } DICYANODICHLORO -P-QUINONE

Z = H P-PHENYLENEDIAMINE

Z = CH_3 TETRAMETHYL P-PHENYLENEDIAMINE

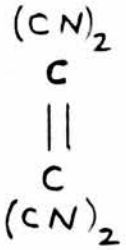

TETRACYANOETHYLENE.

CHAPTER IV.

THE EXPERIMENTS AND RESULTS

IV.1 Molecular Complexes.

There exist many cases of complex formation between electrically neutral closed shell molecules[58]. Most of them have a 1:1 stoichiometric composition and show intense optical absorption bands - the so-called charge-transfer bands - which are characteristic of the molecule as a whole and which are not found in either separate moiety. Largely due to contributions from Brackmann[59], Weiss[60], Dewar[61] and Mulliken[58], the presently held theory attributes the complex formation to either a partial or a full transfer of one electron from one molecule (the donor) to the other (the acceptor). Mulliken has written a series of papers[58] clarifying these ideas of charge-transfer with a quantum mechanical description of the molecular complex. Thus, for a 1:1 complex AD the wave function for the ground state ψ_n is a singlet and can be written to a first order as

$$\psi_n = a\,\psi_{AD} + b\,\psi_{A^-D^+} \qquad (4.1)$$

with $a \gg b$

where ψ_{AD} is the singlet wave function for the "no bond" structure AD held together by Van der Waals forces, and $\psi_{A^-D^+}$ is the singlet wave function for the dative structure A^-D^+ that is formed on transferring an electron from the donor D to the acceptor A. ψ_{AD} and $\psi_{A^-D^+}$ possess the same symmetry. As $a \gg b$, the ground state will be mainly the no-bond structure, but its energy will be lowered, i.e. its stability increased, through interaction with $\psi_{A^-D^+}$ as in equation (4.1).

There will be an excited state ψ_e where

$$\psi_e = c\,\psi_{A^-D^+} + d\,\psi_{AD} \qquad (4.2)$$

but $c \gg d$ so that this state is predominantly ionic. Mulliken considers this state only as a singlet and attributes the charge-transfer band as due to the transition $\psi_n \rightarrow \psi_e$. The absolute values of charge-transfer intensities estimated from this theory agree to within the correct order of magnitude with the experimental results. This theory can also explain the geometrical configurations of some complexes. The determining factor, apart from steric effects, being a maximum value of the resonance integral $\int \psi_{AD}\, H\, \psi_{A^-D^+}\, d\tau$, where H is the total Hamiltonian.

Mulliken does not, however, consider the possibility of paramagnetism of the ionic state. This would not be of

importance to the properties of a complex whose ground state is given by (4.1) as the ionic level would be about 10 e.v. (i.e. >> kT) above it. According to Bijl, Kainer and Rose-Innes[6], (henceforth referred to as B.K.R.) the ionic state can be the ground state provided the donor and acceptor tendencies of the constituent molecules are great enough. This is so if D has a low ionisation potential and A a large electron affinity. The magnetic state levels will then either be (see Fig. 1)

(1) Two doublets if the intermolecular exchange between the unpaired electrons is zero, i.e. the complex is a bi-radical, or

(2) A lower singlet separated from an upper triplet by the exchange integral.

(3) A lower triplet and upper singlet.

The charge-transfer optical transitions can still take place between the singlet in the ionic state and that of AD and are still characteristic of the complex as a whole. Such ionic complexes seemed to be formed from NNN'N' tetramethyl-p-phenylenediamine (TMPD or Wurster's base) as the donor and ortho and para halogenated quinones as the acceptors.

B.K.R. investigated the e.s.r. properties of these complexes in the solid state, but could offer no conclusive

proof of the molecular structure of the free radicals present. The e.s.r. programme intended by the author was to follow up their work by studying these complexes in various solvents at room temperature with the aim of obtaining two types of hyperfine structure. These are (a) the hyperfine structure of the two spectra from the dissociated ions A^- and D^+ and (b) the hyperfine structure from the complex molecule A^-D^+. Observation of both (a) and (b) in the same or in different solvents would prove the existence of biradical molecular complexes. Moreover, the modifications in the spectrum of (b) to either of those in (a) would give information about the chemical bonding between the donor and acceptor. Sections IV.3 and IV.4 describe the experiments carried out and the conclusions arrived at. Section IV.2 describes some additional experiments on polycrystalline samples.

IV.2 Solid Biradical Molecular Complexes of Tetramethyl p-phenylene diamine (TMPD) with Tetrahalogenated Quinones.

On bringing together a solution of TMPD (Wurster's base) in benzene and chloranil in benzene, a dark precipitate immediately forms. Isolating, washing and drying this, the resulting solid is found to be paramagnetic. Similarly prepared complexes are formed from TMPD and bromanil, and

TMPD and iodanil.

These preparations were carried out in a sample tube in a cavity while monitoring the e.s.r. signal on an oscilloscope. The sample tube initially contained only the solution of TMPD in benzene, which was diamagnetic. On addition of the chloranil in benzene - also diamagnetic - the e.s.r. signal was found to appear instantaneously with the formation of the precipitate.

The e.s.r. properties of these solid complexes can be summarised as follows.

TABLE 2.

Compound	Line Width*	g-value*	Radical Content
TMPD.chloranil	11 oe	2.0023	0.5 %
TMPD.bromanil	24 oe	2.000	5 %
TMPD.iodanil	30 oe	2.0016	50 %

* The measurements of B.K.R.

The percentage radical content at room temperature was measured by comparing the signal-to-noise ratios from samples of the complexes with those from standard samples of D.P.P.H. The oscilloscope presentation was used and the measurements were made on the complexes and standards in turn, carrying out the method described in (III.9). In obtaining the

ratio of the integrated e.s.r. intensities, the appropriate ratio of the line width to that of D.P.P.H. was taken into account. The figure in the third column was accurate to within a factor of two.

Under the high resolution of phase-sensitive detection, the resonance lines from polycrystalline samples of all three complexes showed a single structure similar to a Lorentzian exchange narrowed line. This conflicts with the findings of Matsunaga[62] who reports distinct asymmetry of the spectrum from the TMPD.chloranil complex.

B.K.R. carried out temperature dependence measurements of the e.s.r. signal intensity for TMPD.chloranil and found that down to 6°K, it followed a Curie law, (i.e. $\frac{1}{T}$). This implied from (2.27) that the singlet-triplet splitting (equal to J, the intermolecular exchange coupling of the unpaired electron spins in the complex) is much less than 4 cm^{-1}. Furthermore, this temperature dependence does not give any indication as to whether the ground state is a singlet, triplet or doublet. If a triplet state is involved in the e.s.r. transitions of the molecular complexes, then these compounds should show, at a fixed microwave frequency, resonance lines when the value of the d.c. magnetic field is half that for the normal transition given by (1.1). These lines would arise from the $\Delta S_z = \pm 2$

transition and would indicate the presence of two spins per complex molecule coupled through intramolecular exchange (see Fig. 1). Transitions of this type are usually forbidden when evaluating the transition probability of (1.12), but can be weakly allowed through dipolar perturbation in the triplet state[63]. Polycrystalline samples of TMPD.chloranil and TMPD.bromanil were investigated for such a resonance. None was observed. It could be said from these experiments that if a triplet state does exist in these compounds, then the transition probability at half-field resonance is less than one thousandth of that at normal resonance. This could be due either to the lines being very broad or to the mechanism which allows such transitions being very weak. It is possible that the half-field resonance lines are anisotropic, i.e. have characteristics that depend on the angle between the molecular axis and the direction of the splitting field. In polycrystalline samples, where the molecules will have random orientations with respect to the applied magnetic field, such anisotropies will produce line broadening.

It was pointed out by B.K.R. that the e.s.r. absorption strengths (i.e. the number of molecules in a paramagnetic state) increased with increasing redox potential of the acceptor in benzene (this is a measure of the electron

affinity in solution). This is compatible with the idea that large donor-acceptor tendency means small overlap of the M.O.s of the odd electrons in A^- and D^+ and from(2.23) a corresponding small value of J, the singlet-triplet splitting. Thus, measurements carried out at a temperature which is not much greater than the largest value of J for the complexes of Table 2 should show e.s.r. absorption strengths that depend on the donor-acceptor tendencies. From the value of the free radical content of TMPD.chloranil in Table 2, however, (2.27)implies that for this complex at room temperature, J is larger than kT (i.e. 450 cms^{-1}) which conflicts with B.K.R.'s prediction of J from the temperature dependence measurements. As a consequence, the radical content in the third column of Table 2 cannot be explained as due to a Boltzmann statistical distribution over a number of energy levels. It is possible, however, that the solid complexes are chemically impure. Thus, although the initial reactants A and D and the solvents used are chemically pure, there may be present other reactions over and above the univalent redox reaction, which give rise to non-radical products. Such side reactions have been suggested by B.K.R. as (1) a double electron transfer from the donor to the acceptor, (2) a double hydrogen atom transfer from the TMPD to the quinones.

These reactions and possibly also the univalent redox reactions will have equilibria which depend on the temperature and the particular solvent used. Hence, the radical content in the solid should depend on these conditions at the instant of formation. It is interesting to note, therefore, that on preparing TMPD.bromanil from hot benzene the radical content was only one twentieth of that prepared from cold benzene. Also, the radical content in TMPD.bromanil precipitated from cyclohexane was three times that from benzene.

IV.3 The E.S.R. Spectra of the Ionic Complexes in Solution.

3.1 Polar Solvents.

The ionic compounds of Table 2 dissolved in polar solvents to give a reddish-wine colour. All the solvents were Analytical Reagent Grade (AnalaR, British Drug Houses Ltd.) and were used as obtained without further purification. Once, AnalaR ethanol, which had been distilled several times, was used as the sample solvent. The e.s.r. spectra of the complexes in this solvent were the same as in the Reagent Grade ethanol. The spectra were recorded with phase-sensitive detection, as the signal-to-noise ratios on the oscilloscope at the concentrations used, were only 3:1. About one tenth of a cc. of solution in

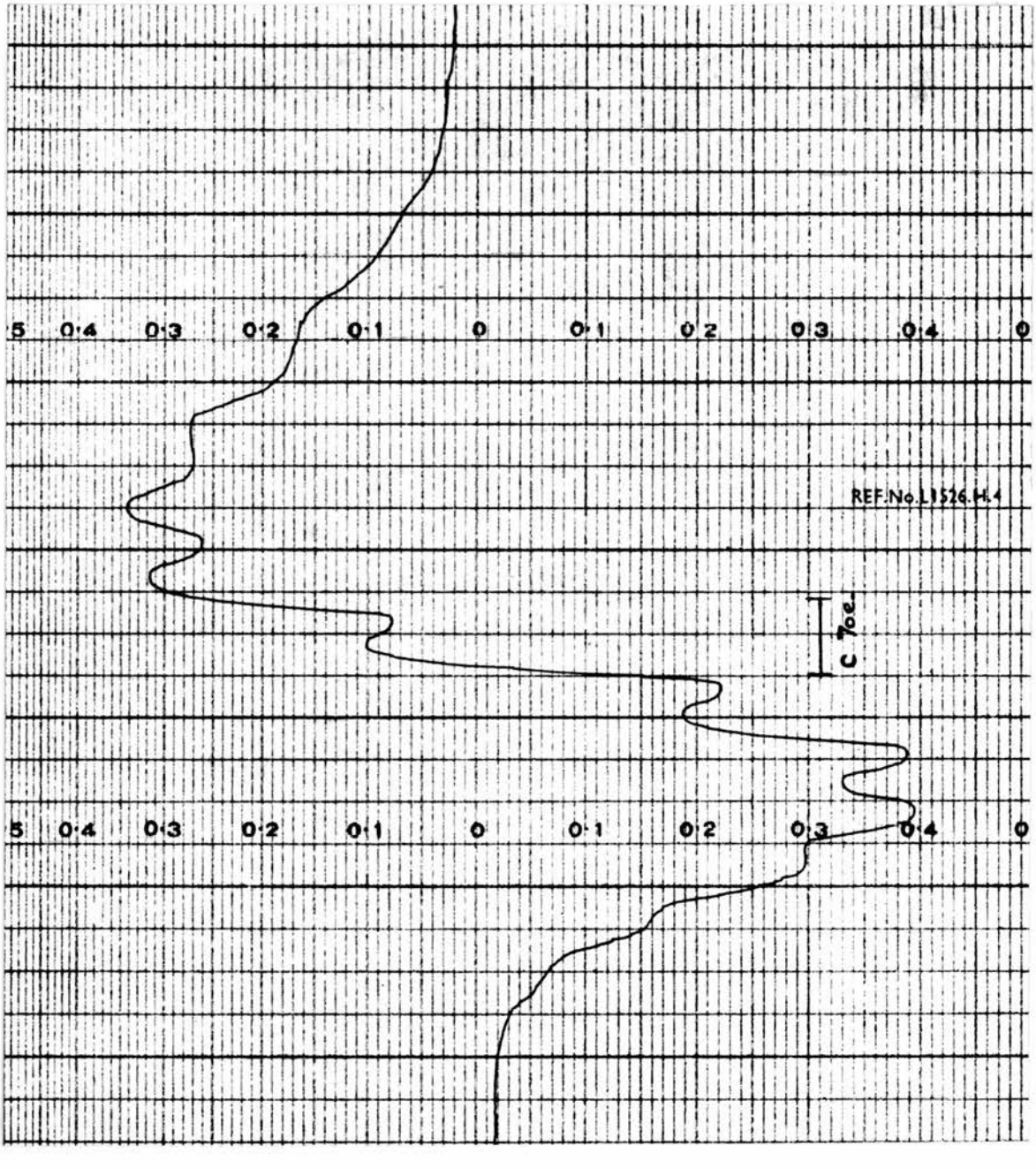

FIG. 33 THE DERIVATIVE OF THE E.S.R. ABSORPTION SPECTRUM FROM THE COMPLEX TMPD.CHLORANIL IN ETHANOL.

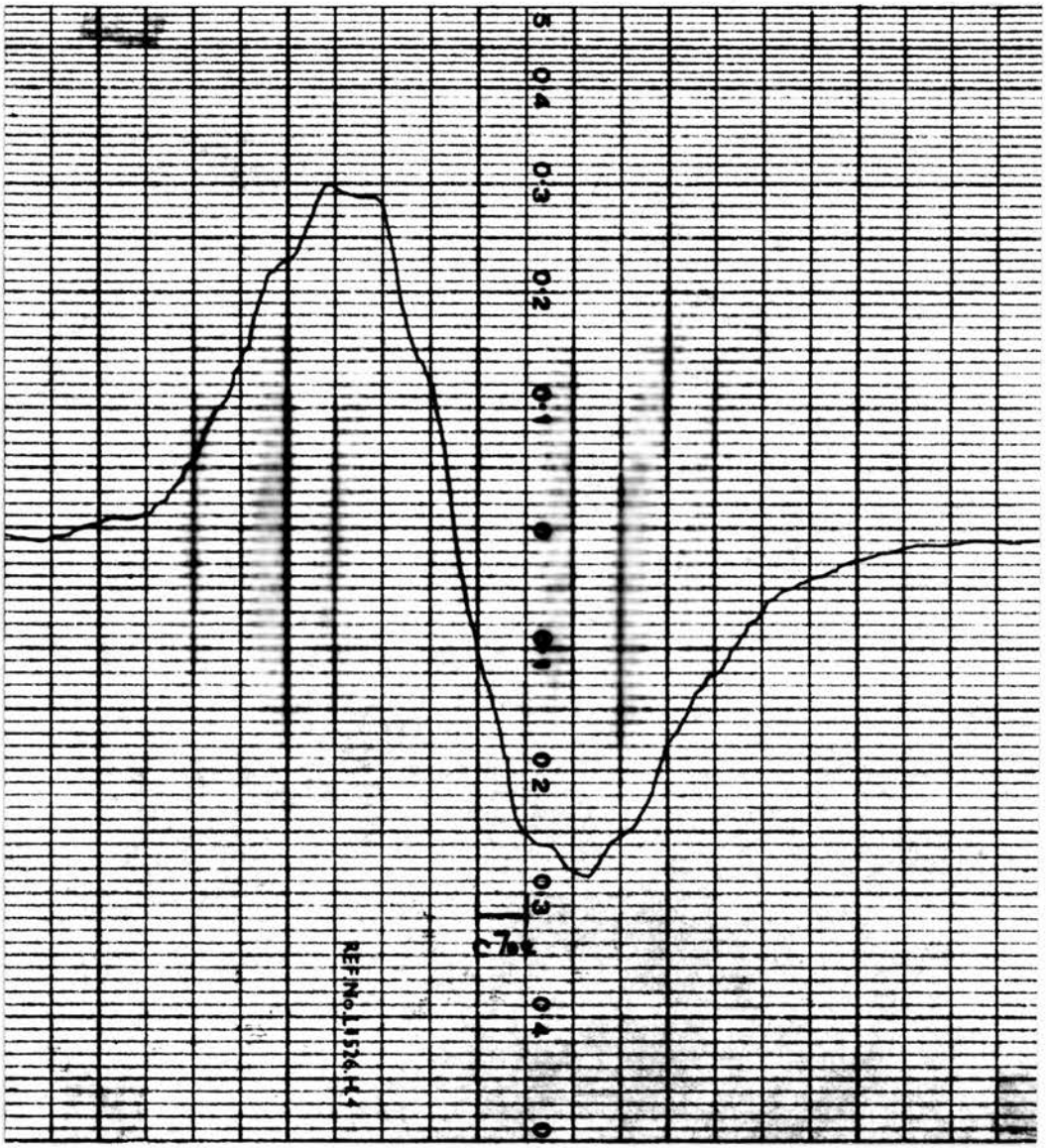

FIG. 34 THE DERIVATIVE OF THE E.S.R. ABSORPTION SPECTRUM FROM THE COMPLEX TMPD.BROMANIL IN ETHANOL.

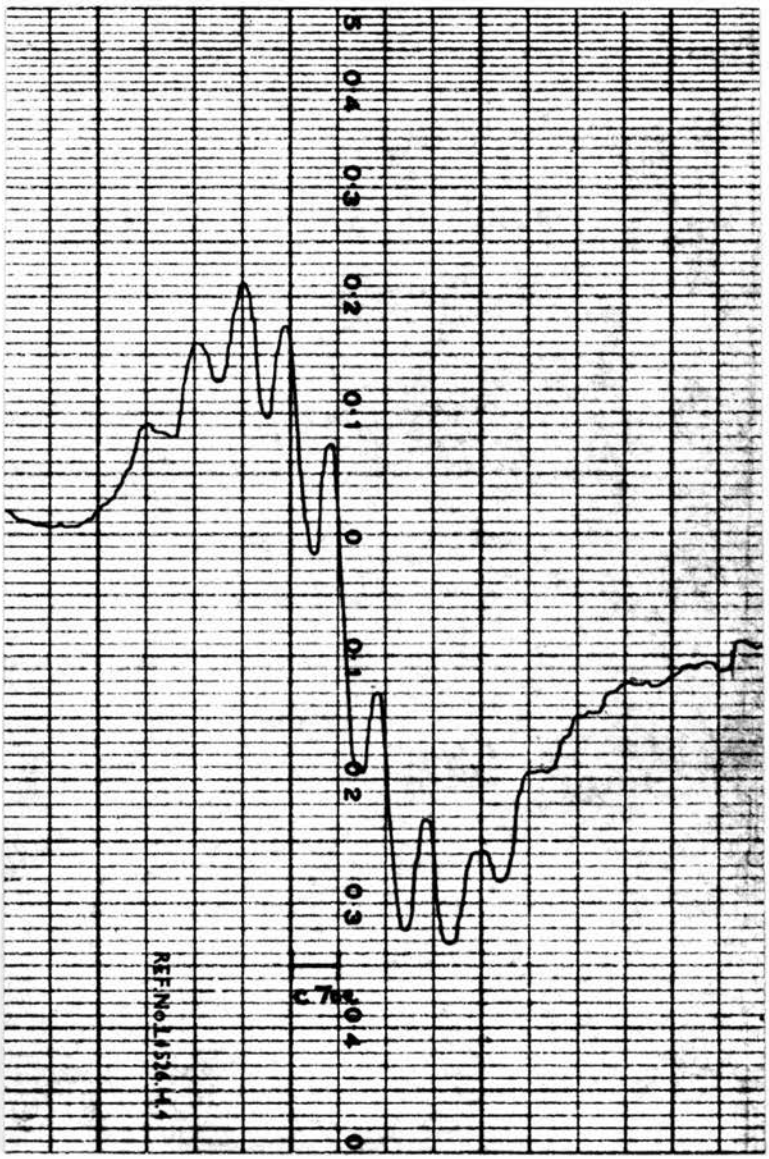

FIG. 35 THE DERIVATIVE OF THE E.S.R. ABSORPTION SPECTRUM FROM THE COMPLEX TMPD.IODANIL IN ETHANOL.

a glass tube of inside diameter 2 mm. was used as the sample. The features of the spectra that were observed in each case will be discussed in the following paragraphs. The interpretations of these spectra are made in IV.3.4.

TMPD.chloranil.

On increasing dilution in ethanol, the line broadened and several hyperfine lines were resolved. Fig. 33 is such a structure in ethanol at a radical concentration, estimated from the signal-to-noise ratio, of 5×10^{-3} moles/litre. This shows the partial resolution of eleven lines of splitting 7 ± 0.5 oe. It is typical of the spectra observed in methanol, n-propanol, isopropyl alcohol and chloroform. Further dilution was limited by the spectrometer sensitivity.

TMPD.bromanil.

Down to the minimum observable concentration ($\sim 10^{-3}$ moles/litre) in ethanol, propanol and chloroform no improvement of the resolution was made on Fig. 34 where the solvent was ethanol. Here some structure can just be discerned.

TMPD.iodanil.

Resolution of the hyperfine structure in the alcohols was about the same as TMPD.chloranil at the same concentrations. The number of lines (eleven), the splittings and

overall width were also the same. After about thirty minutes, the sample changed colour from wine to reddish-brown, but with no accompanying effect on the e.s.r. spectra. These remained unchanged as in Fig. 35 for at least twelve hours. This colour change may be due to the presence of free iodine.

3.2 The Effect of Dissolved Oxygen.

Prompted by the findings of Hausser (see II.7.5), a solution of TMPD.chloranil in ethanol was prepared and an attempt made to remove the dissolved oxygen from the ethanol. The ethanol was boiled in a flask over a sand-bath. The tap on this flask was then closed, the flask allowed to cool and then opened under an atmosphere of nitrogen in a dry-box. The solution of the complex was made up in this atmosphere and glass tubes with ground glass stoppers used as sample holders. No improvement on the resolution of Fig. 33 was noted. It seems, therefore, that at the concentrations used here, the dissolved oxygen is not inhibiting the resolution.

3.3 The Effect of Power Saturation.

The incident microwave power to the cavity was reduced by a factor four. For solutions of all the complexes it resulted in a smaller e.s.r. signal and no improvement in the

hyperfine resolution. This indicated that the lines were not being saturated with 25 m.w. of microwave power.

3.4 Interpretation of the Spectra.

As the above spectra were only partially resolved, it was not possible to account for them with any particular relevant radical structure by applying the formula given in II.4. Instead, they were compared with the spectra of a known radical, the Wurster's blue ion ($TMPD^+$). Wurster's perchlorate was dissolved in ethanol to concentrations of $\sim 3 \times 10^{-3}$ moles/litre and the spectra of $TMPD^+$ obtained, as Wurster's perchlorate is known to dissociate in solution into this radical ion and the non-radical perchlorate ion, i.e.

$$TMPD.Clo_4 \rightarrow TMPD^+ + Clo_4^- \qquad (4.4)$$

Weissman first reported[32] thirteen triplets of splitting 7.4 oe. between the centre of each triplet and 2.1 oe. between members of each triplet. The twelve methyl protons are equivalent and give rise to thirteen lines which are further split by interactions with the ring protons. The best resolution to date, of this radical ion has been carried out by Hausser[29], who has observed all the lines (325) expected from interactions with the twelve methyl protons, four ring protons and two nitrogen atoms. The coupling constants are 6.8, 2.1 and 0.6 oe. respectively.

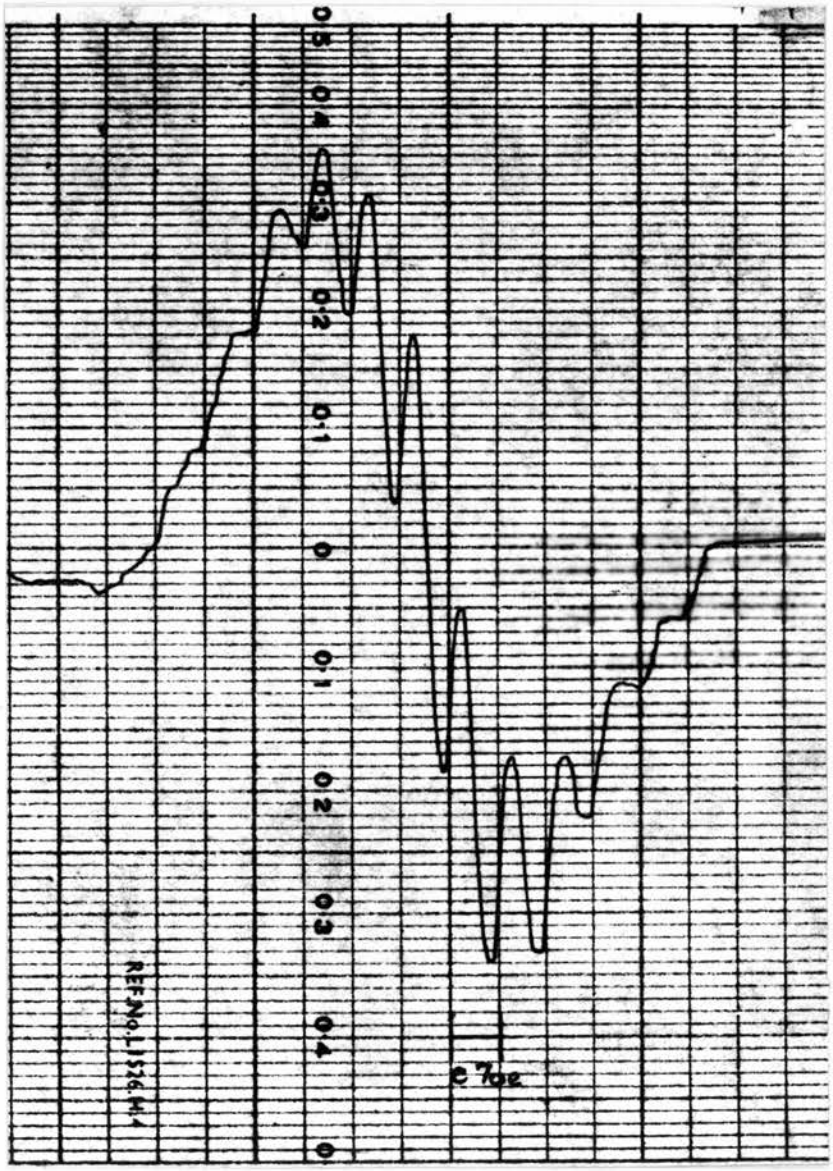

FIG. 36 THE DERIVATIVE OF THE E.S.R. ABSORPTION SPECTRUM FROM WURSTER'S BLUE PERCHLORATE IN ETHANOL.

To attain this degree of resolution, Hausser found it necessary to remove all the absorbed molecular oxygen and use concentrations of 5×10^{-4} moles/litre. The best resolved spectra of $TMPD^{+}$ using the spectrometer described in Chapter III was that of Fig. 36 showing eleven partially resolved lines.

The effect of the removal of the dissolved oxygen was investigated using the method of preparation of samples described in IV.3.2. At the concentrations used no additional lines were resolved so that it was not the dissolved oxygen that limited further resolution. The sample was also checked to see that the e.s.r. lines were not being saturated. Since, in the cases of the ionic complexes and Wurster's perchlorate in sdution, the resolution of the e.s.r. spectra improved with increasing dilution, it seems that the resolution of Figs. 33, 34, 35 and 36 is limited by exchange interaction which is due to the solutions being too concentrated. This concentration was required for a good signal-to-noise ratio from the spectrometer. Increased sensitivity is therefore necessary for higher resolution. The difference between the sensitivity here and that attainable by Hausser, as indicated by his spectra of $TMPD^{+}$, is not surprising when the recording times used in each case are considered. The maximum time used here was ten

minutes whereas Hausser reports[64] times of eight to ten hours.

A comparison of the spectra of Figs. 33, 35 and 36 shows that they are the same as regards hyperfine splitting and the number of partially resolved components. In fact, the known splitting of $TMPD^+$ was used as a marker to determine the splittings in Figs. 33 and 35, by employing the same sweep rate in each case. This similarity suggests that in the polar solvents the complexes TMPD.chloranil and TMPD.iodanil are not present wholly as complex molecules, but dissociate into separate solvated ions A^-, D^+ and that Figs. 33 and 35 are the spectra of D^+ (i.e. $TMPD^+$).

$$\text{i.e. } A^-D^+ \rightarrow A^- + D^+ \qquad (4.5)$$

However, if all three species of (4.5) are present, then three different spectra would be expected. These are
(1) the spectra and its characteristic hyperfine structure associated with the Wurster's blue radical ion, $TMPD^+$,
(2) the narrow, single line spectrum which would arise from the chloranil negative ion. This anion has no hyperfine structure as the splittings produced by the chlorine nuclear moments are too small to be resolved[64a], and
(3) a spectrum from A^-D^+ different from (1) or (2) due to the intramolecular exchange coupling between the two unpaired

electrons in the biradical.

No spectra corresponding to either (2) or (3) have been observed. From the e.s.r. results of Figs. 33 and 35 alone, it could be that the spectrum of D^+ and A^-D^+ are so similar that they cannot be distinguished. This would imply that J is very small. However, Foster's[65] measurements of the optical absorption spectra of all these complexes in polar solvents show no charge-transfer bands so that the existence of A^-D^+ in these solvents is not indicated. On the other hand, Foster can identify bands associated with the $TMPD^+$ radical ion which is consistent with the e.s.r. data of Figs. 33 and 35. Weaker additional bands are also preeent which disappear after a few minutes. These may account for the anion as being chemically unstable and with insufficient lifetime to be observed by e.s.r.

It is difficult to account for the poor resolution of the e.s.r. spectrum in the case of the TMPD.bromanil. More work at greater dilution, demanding higher sensitivities, will have to be done to discover if this effect is significant.

3.5 Solvent Activity.

If the ionic complex dissociates as (4.5) then the extent of the dissociation would be expected to depend on

the solvent used. The more polar the solvent, the greater would be the dissociation. Kosower has introduced[66] the Z-value as an empirical measure of solvent polarity and ionising power. He found that the position of the charge-transfer band of the 1ethyl-4-carbomethoxypyridinium iodide complex in solution is very sensitive to the particular solvent used. The Z-value of a solvent was defined as the transition energy in kilocals./mole. of this charge-transfer band. Using this complex as a standard, Kosower could directly measure the Z-values ranging from 79.6 for ethanol to 63.2 for chloroform.

In an ionic complex, the apparent absorption coefficient of the charge-transfer band gives a measure of the extent of association of the complex as ion-pairs rather than solvated ions in solution. Kosower showed that for the 1-ethyl-4-carbomethoxypyridinium iodide complex, this absorption coefficient is approximately linear with Z-value. In alcohols, this complex is largely dissociated into ions, whereas in chloroform it is in the form of ion-pairs. In contrast, the results of IV.3.1 show that TMPD.chloranil has the same form in methanol (Z = 83.6), ethanol (Z = 79.6), isopropyl alcohol (Z = 76.3), n-propanol (Z = 78.3) and chloroform (Z = 63.2). Similarly, the spectrum of TMPD.bromanil was the same in chloroform as

in ethanol.

Less polar solvents, e.g. benzene, where Foster[65] has observed charge-transfer bands, from TMPD.chloranil, dissolve the complex so sparingly that no e.s.r. has been observed from the solutions.

Conclusions of Section IV.3.

It appears from the e.s.r. experiments and Foster's optical absorption measurements, that the complexes TMPD. chloranil and TMPD.iodanil dissociate completely into solvated radical ions in alcoholic solvents and that TMPD. chloranil also dissociates in AnalaR chloroform. The e.s.r. experiments were unsatisfactory in that (a) no spectra associated with the complex molecule A^-D^+ has been observed, and (b) there is no indication in the e.s.r. spectra of the presence of the anions A^-. As has been mentioned, the negative ion of chloranil does not show any hyperfine lines because of the small nuclear momant of the chlorine nucleus. The iodanil negative ion would probably also not give any observable hyperfine structure since the iodine nucleus with a spin 5/2 would give a splitting about 1/5 of that from a proton with the same spin density. Therefore, even if these anions were stable, it would be difficult to identify them positively

by their single line e.s.r. spectra. A search was therefore carried out, both in the literature and through the author's own invesitations, to find an acceptor which would give a more stable radical anion with a characteristic hyperfine strudure. Such negative radical ions are formed from the electron acceptors, tetracyanoethylene and dicyanodichloro-p-quinone, although it should be mentioned here that the hyperfine structure obtained from a solution of the latter with sodium iodide was not conclusively that of the dicyanodichloro-p-quinnne radical anion, but this will be discussed in Section IV.6.2. The e.s.r. properties of solutions of these acceptor compounds with substances which are known donors, were examined and are described in Sections IV.5 and IV.6.3.

IV.4 Tetracyanoethylene.

Tetracyanoethylene (TCNE) is known to be a good electron acceptor[67]. In this system the accepted unpaired electron occupies a molecular orbital of the π system. Tetracyanoethylene is therefore known in the Mulliken terminology as a π acceptor or π acid. The radical ion $TCNE^-$ is easily formed in reactions with sodium and sodium iodide in tetrahydrofuran and acetonitrile[66]. The reactions, which are univalent redox reactions, are

FIG. 37 THE HYPERFINE STRUCTURE OF THE TETRACYANOETHYLENE NEGATIVE ION IN TETRAHYDROFURAN.

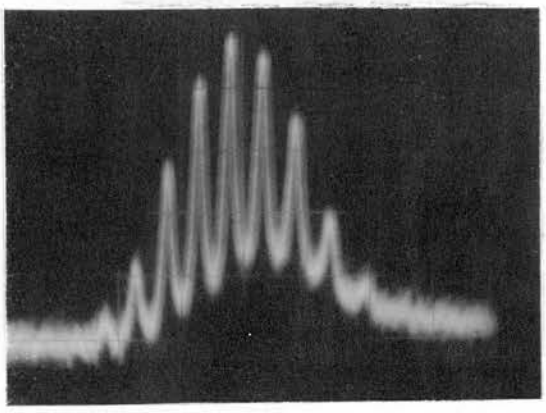

(a) THE VIDEO PRESENTATION.

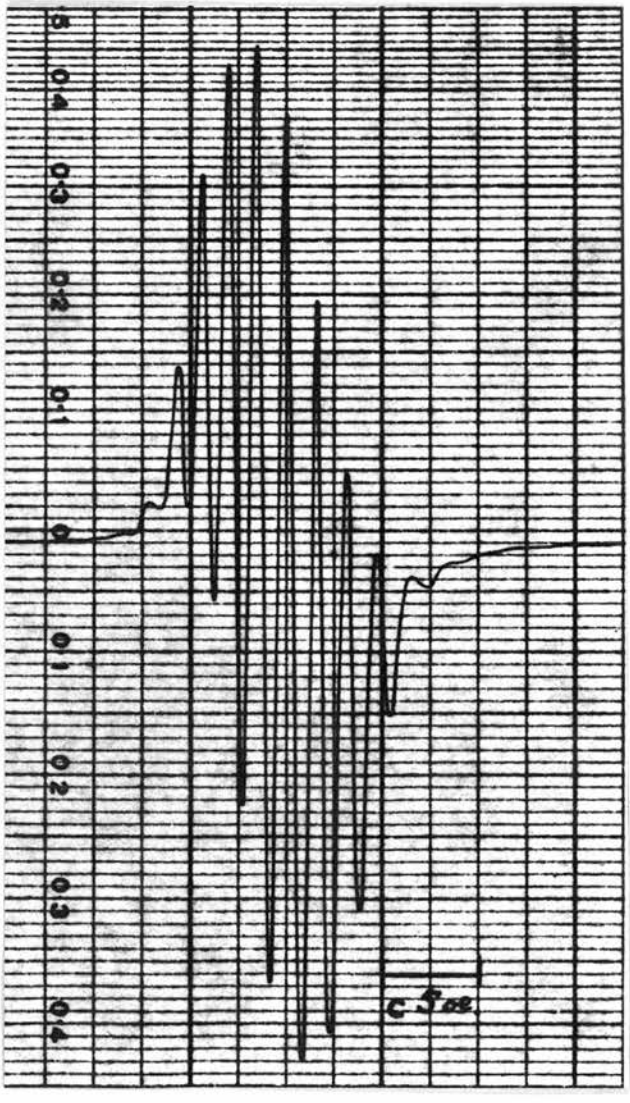

(b) THE DERIVATIVE OF THE ABSORPTION.

$$Na + TCNE \rightarrow Na^+ + TCNE^- \quad (4.6)$$

and $$NaI + TCNE \rightarrow Na^+ + I^\cdot + TCNE^- \quad (4.7)$$

It was found here that $TCNE^-$ can also be formed with sodium in ethanol, methanol and propanol as is indicated by its characteristic hyperfine spectra to be discussed below. The radical ion is not stable in these solutions, however, and the e.s.r. signal disappears after about twenty minutes. This could be due to the fact that in addition to (4.6) there is a vigorous reaction of sodium with the alcohols. For example, with methanol, sodium forms sodium methoxide CH_3ONa with the evolution of hydrogen

$$\text{i.e. } 2CH_3OH + 2Na \rightarrow 2CH_3ONa + H_2 \quad (4.8)$$

In the reaction (4.7) in tetrahydrofuran, a dark red colour formed almost immediately and on examining a sample of this for e.s.r., it was found to exhibit a narrow intense line. On diluting, the well resolved spectrum of nine lines associated with $TCNE^-$ was obtained on the oscilloscope (Fig. 37a).

The measured splittings were $1.5 \pm .2$ oe. The widths of the individual lines were 0.25 oe. which was about that expected from the magnetic field inhomogeneities (see Section III.8). Nine hyperfine lines with intensities in the ratio 1:4:10:16:19:16:10:4:1 are expected from equal

coupling with the four nitrogen atoms with nuclear spin one. The slight asymmetry in the hyperfine pattern in Fig. 37a is caused by the apparatus. In Fig. 37b, the pen-recording of the same spectra, the lines are symmetrical about the centre line. Increasing the bandwidth of the video stage at the output of the signal amplifier to 4 mc/s does not improve the symmetry of Fig. 37a. This asymmetry must, therefore, be due to the limited bandwidth (300 c/s) of the signal klystron stabilisation loop.

Under the high resolution of the phase-sensitive detection, additional lines are detectable on the wings of the nine line spectrum. These are shown in Fig. 37b, but are below the noise in Fig. 37a. Phillips has reported[67] eleven lines and has concluded that the extra two are from 4.4% of the $TCNE^-$ radicals containing a $C^{13}N$ group. The outer two lines are therefore due to splitting from the C^{13} nucleus which has spin $\frac{1}{2}$ and a coupling constant $A_{C^{13}} = 6A_{N^{14}} = 9.4$ oe. This then can explain the extra outer lines in the spectrum of Fig. 37b.

Calculations[67] using L.C.A.O. molecular orbital theories give the unpaired electron densities at each nitrogen atom as 0.11. This implies that if Q_{CN} is the isotropic splitting due to the nitrogen nucleus for an unpaired electron totally on the nitrogen atom of a cyano

group then $Q_{CN} = 15$ oe. (4.9)

Atherton and Weissman[68] have observed splittings of the lines of naphthalene negative ion which can be associated with some odd electron density at the sodium nucleus. This means that there is overlap between the M.O. of the naphthalene negative ion and that of the sodium ion, i.e. there is an ion-pair formation. No such splittings by the sodium nucleus have been observed in the $TCNE^{-}$ spectra in the solvents tetrahydrofuran, acetonitrile and the alcohols, so that no ion-pair formation was indicated.

In investigating the reaction (4.6) in tetrahydrofuran, a sequence of spectra was observed as the reaction progressed. The time dependence of the appearance of this sequence of spectra varied with the initial concentrations of the reactants used. To illustrate the changes in spectra, a particular case will be described.

Tetrahydrofuran was purified by refluxing it over sodium for several hours. The tetrahydrofuran, purified in this way, is henceforth referred to as clean tetrahydrofuran. A single piece of sodium was added to a solution of tetracyanoethylene in clean tetrahydrofuran which had a concentration of $\sim 4 \times 10^{-2}$ moles/litre. Samples were separated from this reaction (4.6) every half-hour and

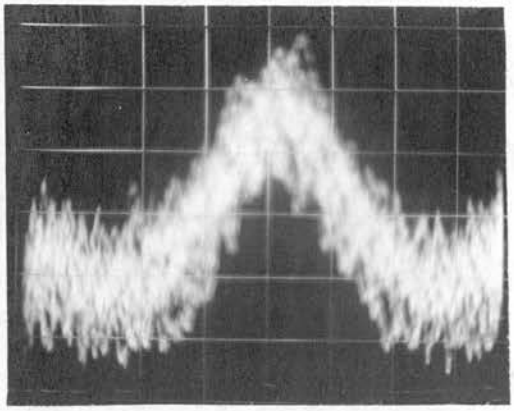

(a)

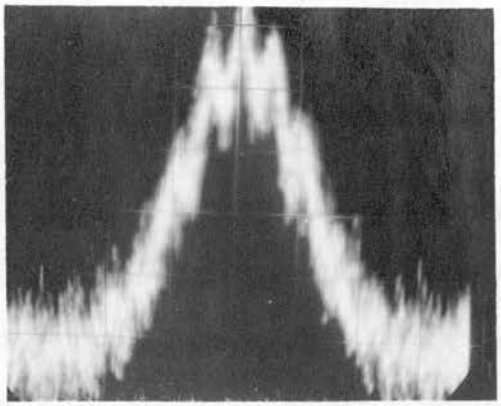

(b)

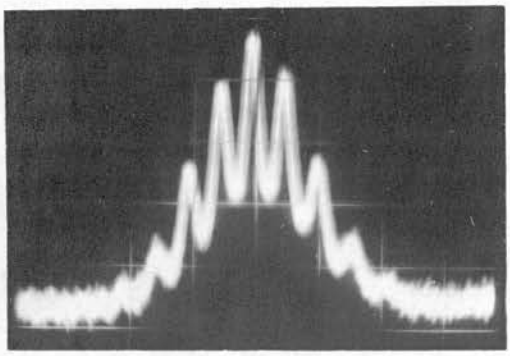

(c)

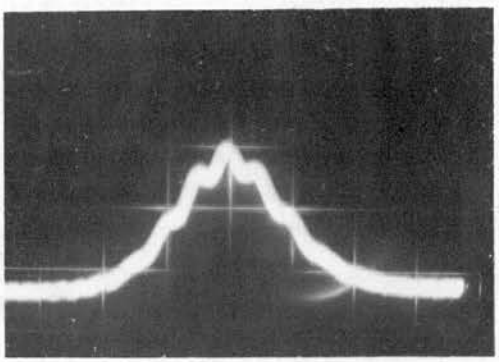

(d)

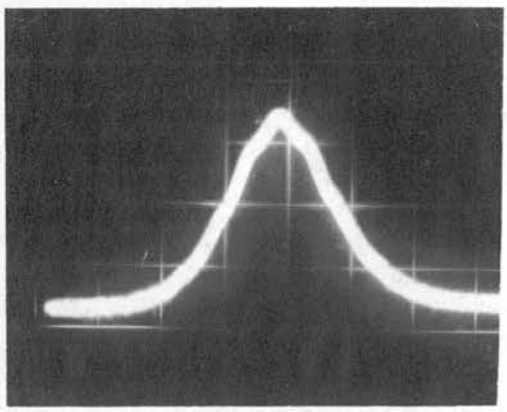

(e)

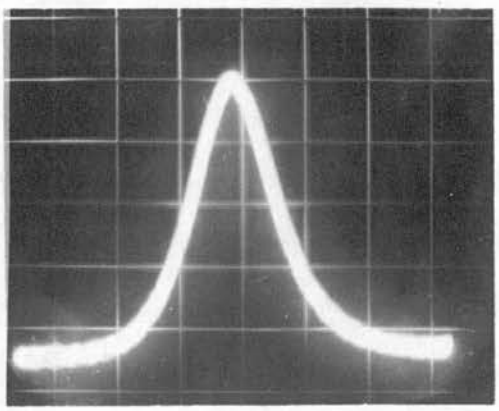

(f)

FIG. 38 THE SERIES OF SPECTRA OBSERVED FROM SODIUM AND TETRACYANOETHYLENE IN TETRAHYDROFURAN.

their spectra monitored on the oscilloscope for twenty minutes. Samples up to 7½ hours after the reaction had been initiated all showed a single e.s.r. line. On diluting these, no hyperfine structure was observed down to concentrations where the signal merged with the noise. The radical content, as indicated by the e.s.r. signal intensity, increased with time, (increasing by about a factor three over several hours). A sample taken eight hours after the reaction had begun, initially showed a single line (Fig. 38a). Five minutes later, hyperfine structure became resolved as in Fig. 38b. In ten minutes, the spectrum was almost completely resolved (Fig. 38c) and at the same time, the signal intensity increased. With further increase of signal, after fifteen minutes, the line began to narrow (Fig. 38d), the hyperfine peaks merge until only a single line remained (Fig. 38f).

Another sample taken from the reaction vessel, now 8½ hours after the reaction had been initiated, showed a line which was narrowing. This meant that the reaction was proceeding in the same way in the reaction vessel as in the sample tube. To check this, the reaction was carried out with about the same concentration of TCNE in the sample tube and monitored continuously on the oscilloscope. In this case, the same sequence of spectra as depicted in Fig. 38

was observed although in less time, i.e. two hours. The speed of the reaction can probably be accounted for by a larger effective surface area of sodium.

Investigations were then carried out to find out whether the spectra of Fig. 38 are due to different radicals or to the effects of the processes determining the linewidths.

To a sample showing a well-resolved hyperfine structure was added about an equal volume of a concentrated solution of tetracyanoethylene in clean tetrahydrofuran. The sample was shaken up and the spectra re-examined. It was found that the hyperfine structure disappeared and a single line of slightly less intensity, due to the dilution of the radicals, was observed. This was now repeated with a sample showing a well-resolved hyperfine structure, but this time the tetracyanoethlene solution was added while the sample remained in the cavity and the oscilloscope was monitored continuously. After a few minutes, as mixing took place, the hyperfine components broadened until only a single line remained. From these two experiments, it can be inferred that in the early stages of the reaction (4.6) the spectra were broadened (as in Fig. 38a,b) and the resolution of hyperfine structure inhibited by the electron transfer process.

$$TCNE + TCNE^{-} \rightarrow TCNE^{-} + TCNE \qquad (4.10)$$

This mechanism has been investigated in the case of naphthalene by Ward and Weissman[69]. They give the broadening ΔH_{et} to the half-maximum linewidth from this electron transfer process as

$$\Delta H_{et} = \frac{[T]\,k}{2\pi \times 2.83 \times 10^{6}} \text{ oe.} \qquad (4.11)$$

provided that ΔH_{et} is much less than the splitting between adjacent lines. [T], in the case of the reaction (4.10), is the concentration of neutral tetracyanoethylene and k is the rate constant of the process (4.10).

Measurements of ΔH_{et} on addition of a 2.10^{-2} molar solution of tetracyanoethylene in clean tetrahydrofuran gave an order of magnitude estimate of k as 10^{8} to 5.10^{8} litre moles^{-1} sec^{-1}. A more exact value in the literature[66] is 2×10^{8} litre moles^{-1} sec^{-1}.

The narrow intense line of Fig. 38f was then investigated to discover the mechanism determining its linewidth. A sample of $TCNE^{-}$ showing this narrow line was diluted to about one tenth of the concentration and the characteristic nine line spectra of $TCNE^{-}$ was observed. From the Lorentzian shape, the large intensity and the reproducibility of the hyperfine spectrum on dilution, it can be inferred that the narrow intense line was due to large intermolecular

exchange interaction which was a consequence of large concentrations of radicals. It was possible to detect that the hyperfine peaks move toward the centre of the line, as the exchange interaction increases (compare Fig. 36c and 36e, noting that the X but not the Y scales are the same). This effect is predicted by Anderson[26].

Summarising, all the spectra of Fig. 38 observed in the reaction of (4.6) in tetrahydrofuran can be accounted for by the tetracyanoethylene radical ion and the processes determining its linewidth. In the early stages of the reaction, where the concentration of TCNE is large, (4.11) fixes the linewidth. As the reaction (4.6) proceeds, more radicals are formed and the concentration of TCNE is reduced. This results in less broadening and a stage is finally reached in the reaction where the broadening ΔH_{et} of (4.11) ceases to prevent resolution of the hyperfine structure. Further increase of radical concentration gives line narrowing through intermolecular exchange. To explain why the spectrum of a sample separated from the reaction vessel changed with time, it is suggested that the sodium breaks up and particles of it are present in the sample tube so that the reaction (4.6) can proceed there.

The rate of radical production increased sharply as the hyperfine spectra became resolved. This is indicated by

the integrated signal intensity which increases by a factor three over several hours, but by about thirty over the twenty minutes the spectra of Fig. 38 were recorded. This is probably also due to the sodium breaking up and providing a larger effective concentration.

An overall conclusion of these experiments is that it is necessary to have the concentrations of TCNE and $TCNE^-$ suitable to observe the isotropic hyperfine structure.

IV.5 Reactions of Tetracyanoethylene with Donor Molecules.

5.1 NNN'N' Tetramethyl-p-Phenylenediamine (TMPD)

When solutions of TMPD and TCNE in clean tetrahydrofuran were mixed, a reddish wine colour immediately appeared. If the concentrations of TMPD and TCNE were large enough, a precipitate was also formed. The solid obtained on filtering and drying this solution was almost black and was paramagnetic, showing an intense e.s.r. line of about 20 oe. wide. This solid dissolved in tetrahydrofuran to give a reddish wine colour and the same e.s.r. properties as the original wine solution. These paramagnetic properties will now be discussed.

In concentrated solutions the line was about 20 oe. wide. On dilution, it broadened until hyperfine components could be resolved. Fig. 39 is an example of the best

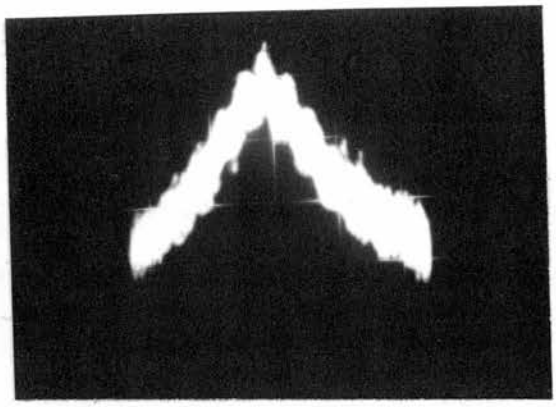

(a) THE VIDEO PRESENTATION

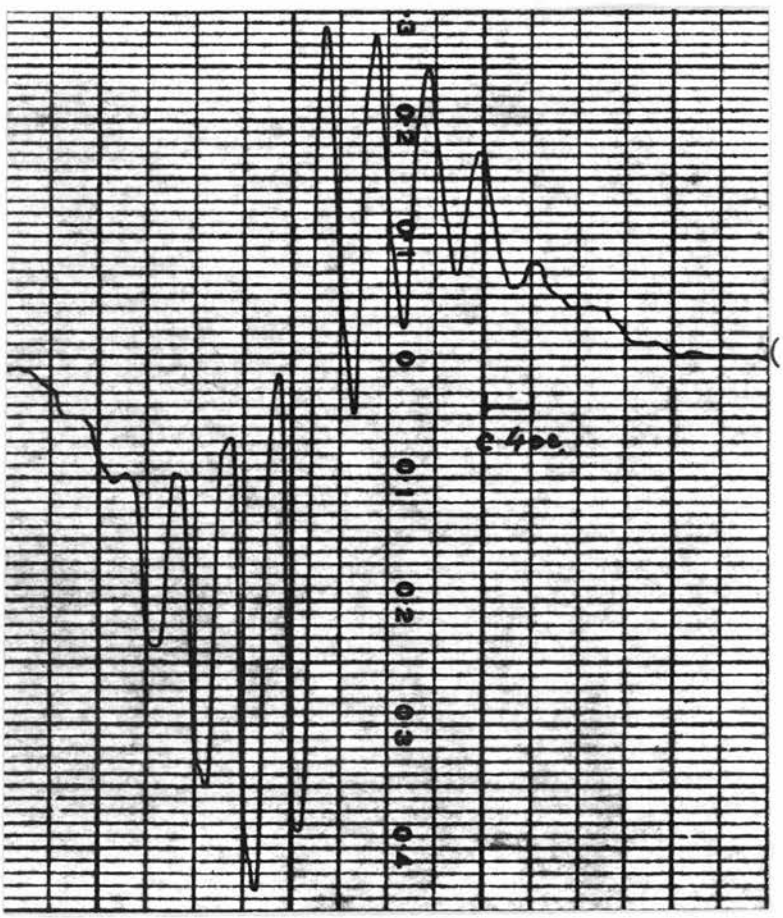

(b) THE DERIVATIVE OF THE ABSORPTION.

FIG. 39 THE E.S.R. ABSORPTION FROM WURSTER'S BASE (TMPD) AND TETRACYANOETHYLENE IN TETRAHYDROFURAN.

resolved spectra obtained. Thirteen lines of splitting 4 ± 1 oe. are detectable in Fig. 39b. This spectrum cannot then be explained by $TMPD^+$ which has splittings 6.8 oe. (see Fig. 36) or by $TCNE^-$ which has splittings 1.5 oe. (see Fig. 37). We have seen in IV.2 that TMPD can act as an electron donor and in IV.4 that TCNE is a strong acceptor. There is presumably, therefore, a tendency for these substances to form a complex that will involve the transfer of an electron from TMPD to TCNE. Such a complex is the 1:1 compound $TMPD^+.TCNE^-$. There is the possibility that overlap of the M.O.'s of the two ions will also contribute to the stability of the complex. This would mean that the intramolecular exchange J was not zero so that it would cause the hyperfine structure from the complex to be different from that obtained from either separate radical ion, i.e. $TMPD^+$ or $TCNE^-$ (see II.6.2). The observed paramagnetism, in the solid and in solution, supports the existence of the biradical molecular complex $TMPD^+.TCNE^-$ and it is suggested that the spectrum of Fig. 39 is a partial resolution of the isotropic hyperfine structure characteristic of this complex. The chemistry of tetracyanoethylene has recently been extensively studied[70]. It is, however, difficult to account for the free radicals that are indicated by the e.s.r. studies without the formation of the

charge-transfer complex $TMPD^{+}.TCNE^{-}$.

On the addition of impure tetrahydrofuran - this had been kept over sodium for several weeks but had become cloudy due to the effects of absorbed moisture and oxygen - to the solution of the complex in clean tetrahydrofuran, there was a colour change from reddish wine to reddish brown. Examining the e.s.r. of this resulting solution the spectrum of Fig. 39 had disappeared and the distinctive nine line spectrum of $TCNE^{-}$ was observed. This effect suggests that the impurities in the tetrahydrofuran attack the complex to release $TCNE^{-}$. No other spectrum superimposed on that of $TCNE^{-}$ was observed. If $TMPD^{+}$ had also been present as a result of the dissociation of the 1:1 complex $TMPD^{+}.TCNE^{-}$ then its spectrum, even although five times broader and hence five times weaker than that of $TCNE^{-}$, should have been detectable above the noise. $TMPD^{+}$ must therefore be also removed from the solution. The complex can react with the impurities in the tetrahydrofuran in at least two possible ways.

(i) It can be attacked by sodium hydroxide. Any $TMPD^{+}$ that is present in solution as a result could also be attacked by the sodium hydroxide and reduced to TMPD. Viz.,

$$4\ NaOH + 4\ TMPD^{+} \rightarrow 4\ TMPD + 4\ Na^{+} + 2\ H_2O + O_2 \qquad (4.12)$$

This reaction is clearly visible with Wurster's blue perchlorate in ethanol, where on addition of the sodium hydroxide, the characteristic blue colour and paramagnetism of $TMPD^+$ disappears.

(ii) It can react with the peroxides that will be in the tetrahydrofuran due to its oxidation by the air. These are

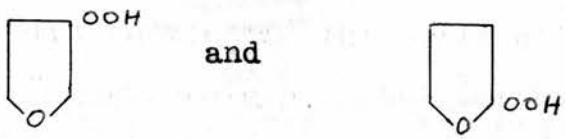

These effects were checked. Tetrahydrofuran was kept over solid sodium hydroxide for several hours. This was added to the complex in solution and again the spectra of Fig. 39 disappeared and that of $TCNE^-$ appeared. Sodium hydroxide therefore seems effective in breaking up the complex and removing the $TMPD^+$ from the solution. The sodium hydroxide added will also react with any excess TCNE to produce $TCNE^-$ as a result of the reaction

$$4\ NaOH + 4\ TCNE \rightarrow 4\ Na^+ + 4\ TCNE^- + 2\ H_2O + O_2 \quad (4.13)$$

This was verified by examining the brown solution of sodium hydroxide and concentrated TCNE in tetrahydrofuran for paramagnetism. After several hours only a very weak

signal was observed. The rate of radical production through the reaction (4.13) must therefore be slow. Even so, to avoid any production of $TCNE^-$ as a result of (4.13) all excess TCNE was removed from the solution of the complex. This was done by adding excess TMPD before the sodium hydroxide. However, on addition of the latter, an intense nine line hyperfine structure which indicated the presence of $TCNE^-$ was again observed. This could only have been released as a result of the complex breaking up through its reaction with sodium hydroxide.

The effect of the presence of the peroxides was investigated by allowing a sample of tetrahydrofuran to remain open to the air for a few days. No change in the hyperfine structure of the complex was observed on adding this solution to that of the complex.

Conclusion.

The existence and nature of the spectrum of Fig. 39 seems to indicate the presence of a complex which in tetrahydrofuran is neither of the separate ions $TCNE^-$ or $TMPD^+$. Moreover, the appearance of the spectrum of $TCNE^-$ on the addition of sodium hydroxide suggests that the complex formation occurs through a univalent redox reaction between TMPD as a donor and TCNE as an acceptor. As the spectrum of

Fig. 39 is only partially resolved, no assignation of coupling constants can be made to the atoms in the complex and no exact value of J (the intramolecular exchange) can be obtained.

5.2 P-Phenylenediamine.

A solution of TCNE in tetrahydrofuran added to that of p-phenylenediamine gives a red colour, but no e.s.r. was observed. P-phenylenediamine is not so strong a reducing agent as TMPD and hence would be less likely to form a charge-transfer complex with TCNE.

IV.6 Dicyanodichloro-p-Quinone (DDQ).

DDQ has a larger redox potential[71] (c 1.0v) than chloranil (0.742v). It should, therefore, be a better electron acceptor and analogous to TCNE in (4.6) and (4.7) should form DDQ^- radical ions with sodium and sodium iodide in solution.

DDQ was purified by dissolving it in benzene, filtering and reprecipitating with petrol. As a criterion of the chemical purity, samples of this DDQ melted over a temperature range of 201 to 203°C. The solution of this DDQ and sodium in clean tetrahydrofuran was red and it showed a very weak e.s.r. signal. The rate of radical production was slow since even after eight hours the signal was still

very weak. At no stage was any hyperfine structure observed. The results with sodium and TCNE in Section IV.5 suggest that the resolution of the hyperfine structure of DDQ^- is inhibited by the electron transfer process

$$DDQ + DDQ^- \rightarrow DDQ^- + DDQ \qquad (4.14)$$

The reaction of DDQ with anhydrous sodium iodide in clean tetrahydrofuran gave a green colour (dilute solutions were yellow) and the e.s.r. of this solution was a weak single line. The addition of 10% ethanol to this solution gave a distinct colour change to clear red and an enhancement of the e.s.r. intensity by about a factor ten. The line was initially a single line, probably due to the process (4.14). As it was observed on the oscilloscope, in ten minutes, the broadening was reduced and a hyperfine structure was observed, as is shown in Fig. 40. This will be discussed in the next section. The addition of the polar solvent ethanol seems to favour radical production. If these radicals are also ions, e.g. DDQ^-, this would be expected as a result of solvation effects stabilising the ion.

6.1 The Hyperfine Structure given by a Solution of DDQ and Sodium Iodide in Tetrahydrofuran.

The five hyperfine components visible above the noise in Fig. 40a would be expected from equal coupling with the

FIG.40. THE E.S.R. ABSORPTION FROM SODIUM IODIDE AND DICHLORODICYANO P- QUINONE IN TETRAHYDROFURAN

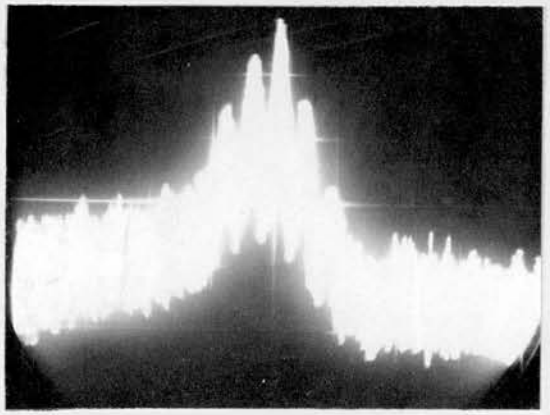

(a) THE VIDEO PRESENTATION

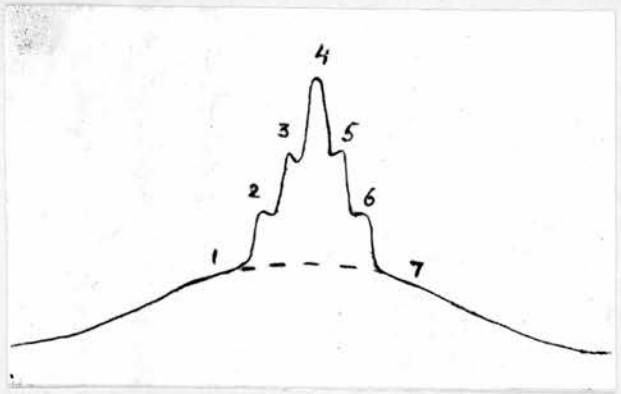

(c) A RECONSTRUCTION OF THE ABSORPTION

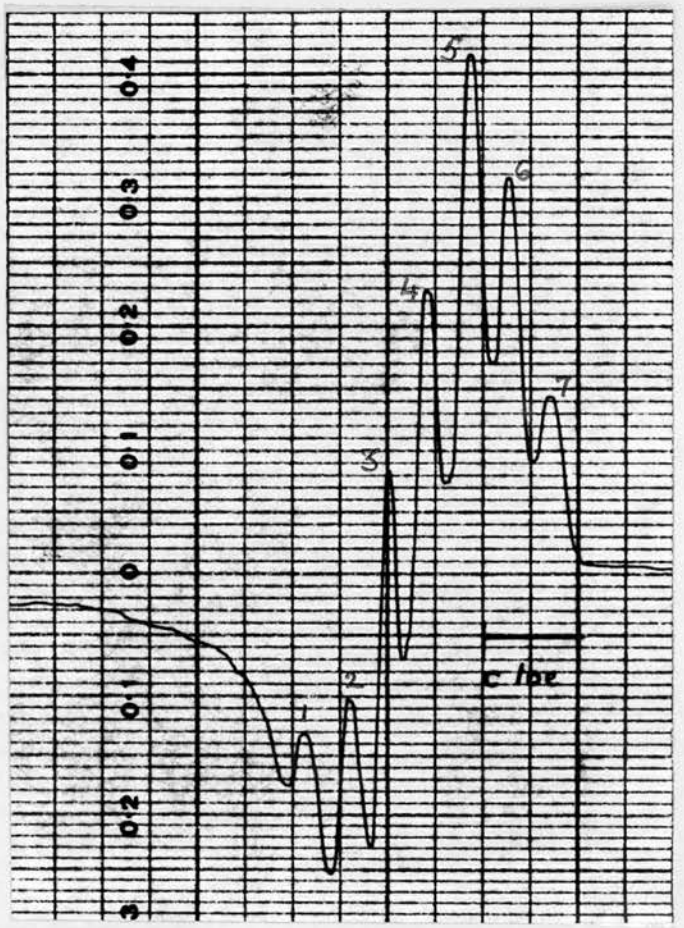

(b) THE DERIVATIVE OF THE ABSORPTION

two nitrogen nuclei of the cyano groups attached to the carbon ring atoms. Moreover, the ratios of the intensities of the hyperfine peaks corresponds roughly to the 1:2:3:2:1 expected from two equivalent N^{14} nuclei. With the higher sensitivity of the phase-sensitive detection, however, two additional lines were recorded. These are indicated as lines 1 and 7 in Fig. 40b. From this spectra we see that all the splittings are approximately equal to 0.45 $\pm$ 2 oe. If the coupling with one nitrogen nucleus is twice that with the other, seven lines would arise. This would mean from the McConnell relation (2.19) for the cyano groups that there is twice as much odd electron density on the one nitrogen atom as on the other. It is difficult to see how this could happen as the symmetry about the broken line

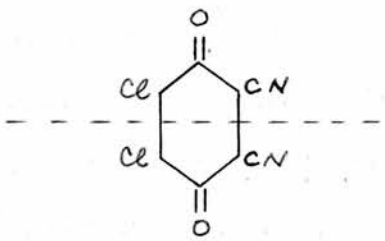

points to the equivalence of the nitrogen atoms. In addition, intensity ratios 1:1:2:1:2:1:1 would be expected from two nitrogen atoms with this coupling (e.g. see the spectra of carbazyl[72]). This is certainly not so in

Fig. 40a where the central peak is the largest.

Chlorine nuclei have a spin 3/2. Thus two equivalent chlorine nuclei would give rise to seven lines as $(2I + 1) = 7$. With the presence of the highly electrophilic cyano groups in DDQ^- there will be less odd electron density on the chlorine of DDQ^- than on the chlorine of the negative ion from chloranil. It would seem surprising, therefore, that the chlorine nuclei in DDQ^- should give splittings while those in chloranil negative ion do not.

The following alternative explanations are therefore suggested for the spectrum of Fig. 40b.

(i) The seven "lines" are due to a superposition of a five line spectrum from DDQ^- (lines 2 to 6 in Fig. 40b) on a broad line from some other radical. "Lines" 1 and 7 therefore indicate only changes of slope from the narrow to the broad line spectrum. The symmetry of "lines" 1 and 7 about the centre of the pattern means that both spectra have very close g-values. Fig. 40c is a reconstruction of such a superposition of spectra. If this is true, the splitting associated with the lines 2, 3, 4, 5 and 6 is a measure of the odd electron density on the nitrogen atoms of DDQ^-. Using the value of Q_{CN} = 15 oe. in (4.9), substituted into (2.19) gives the relation between the odd electron density ζ on the nitrogen

atoms and the isotropic hyperfine splitting a produced by the nitrogen nuclei. The splitting value of 0.45 oe. therefore means an odd electron density of 0.03 on the nitrogen atoms.

(ii) The other suggestion is that the seven lines all belong to the hyperfine pattern of an unidentified free radical.

6.2 Reactions of Dicyanodichloror-p-Quinone with Donors.

(a) Tetramethyl-p-phenylenediamine (TMPD).

Mixed solutions of TMPD and DDQ in benzene show an intense red colour. This solution is paramagnetic with an intense, narrow e.s.r. line of g-value 2.002 ± 0005.

(b) P_phenylenediamine.

A single intense e.s.r. line with a g-value approximately equal to the free electron value was observed from the red solution of p-phenylenediamine and DDQ.

The paramagnetism of the solutions in (a) and (b) indicates the presence of free radicals. As DDQ is a good electron acceptor, it is likely that these radicals are biradical molecular complexes.

IV.7 Final Conclusions and Recommendations.

Section IV.3 shows that in polar solvents some of

the donor-acceptor complexes dissociate into separate ions. As this work was concerned with identifying the radicals through their hyperfine structure, the resolution attained in Figs. 33, 34 and 35 for these ions is disappointing. For complete resolution of these spectra, all the mechanisms which determine the linewidth and inhibit the resolution of the spectra will have to be investigated at increased dilution. To attempt this, the sensitivity of the spectrometer will certainly have to be improved so that the steps suggested in Section III.9 for this improvement should be carried out.

Although one of the original ideas was to obtain the hyperfine structure of the e.s.r. spectra of the complexes A^-D^+, in the case of Wurster's base and the tetrahalogenated quinones, no such spectra could be recorded. Thus, in non-polar solvents the complex did not dissolve sufficiently to give an e.s.r. signal, while in polar solvents the complex dissociated into radical ions. Yet there does appear to be a donor-acceptor complex which in tetrahydrofuran is present as the complex molecule $TMPD^+.TCNE^-$. Again, however, the resolution is disappointing and no interpretations of the distribution of the odd electron densities or the magnitude of the intramolecular exchange between the unpaired electrons were possible from the spectrum

shown in Fig. 39. It will be necessary to discover the mechanisms preventing further resolution of the hyperfine spectrum from this system. Such a mechanism as the electron transfer process (4.10) between a negative radical ion and its neutral molecule may also play a part here in inhibiting the resolution of the isotropic hyperfine structure.

The free radicals of Section IV.6.3 (Wurster's base and DDQ, P_phenylenediamine and DDQ) should also be studied in dilute solutions to obtain the isotropic hyperfine structure which might indicate the form in which they are present in solution.

In conclusion, it can be said that all the experimental e.s.r. results and the interpretations arrived at in this thesis are consistent with the fundamental idea of a 1:1 biradical molecular complex formed through a one electron transfer from a donor to an acceptor molecule.

APPENDIX A

PRINCIPAL MICROWAVE COMPONENTS

Component	Type
Klystrons: K302 type	English Electric Valve Co.
R5222 type	E.M.I. Ltd.
Directional Coupler, 10 db.	Microwave Instruments Ltd. BR/1700
Attenuators	BR/670
Phase-Shifter	BR/2320
Sliding-screw Tuner	BR/1400
Isolators 1 and 2	32/4010
Isolator 3	Philips PP4420X

REFERENCES

1. L. Pauling and G.W. Wheland, J.Chem.Phys., 1, 362 (1933).
2. L. Schiff, "Quantum Mechanics", McGraw-Hill, 1955.
3. J.M. Hirshon and G.K. Fraenkel, Rev.Sci.Instr., 26, 35 (1955).
4. G. Feher, The Bell System Technical Journal, 36, 449 (1957)
5. G.E. Pake, "Solid State Physics", Vol.2, 1 (1956).
6. D. Bijl, H. Kainer and A.C. Rose-Innes, 30, 765 (1959)
7. M. Born and J. Oppenheimer, Ann.Physik, 84, 457 (1927).
8. C.A. Coulson, "Valence", Oxford Press, 1952.
9. E. Hückel, Z.Physik, 83, 632 (1933).
10. M. Pryce, Proc.Phys.Soc., A 63, 25 (1950).
11. A. Abragam and M.H. Pryce, Proc.Roy.Soc., A 205, 135 (1951).
12. K.D. Bowers and J. Owen, Reports Prog.Phys., 18, 304 (1955).
13. E. Fermi, Z.Physik, 60, 320 (1930).
14. S.I. Weissman and D. Banfill, J.Amer.Chem.Soc., 75, 2534, (1953).
15. H.S. Jarrett, J.Chem.Phys., 25, 1289 (1956).
16. S.I. Weissman, J.Chem.Phys., 25, 890 (1956).
17. H.M. McConnell, J.Chem.Phys., 28, 107 (1958).
18. J.E. Nafe and E. Nelson, Phys.Rev., 73, 718 (1948).
19. P. Sogo, M. Nakayaki and M. Calvin, J.Chem.Phys., 26, 1343, (1957).
20. R. Lefebre, H. Dearman and H. McConnell, J.Chem.Phys., 32, 1 (1960). P. Löwdin, Advances in Phys., Vol. 5, 161 (1956); Phys.Rev., 97, 1509 (1955).

21. B. Venkataraman and G. Fraenkel, J.Amer.Chem.Soc., 77, 2707 (1955); J.Chem.Phys., 23, 588 (1955).

22. A. McLachlan, Mol.Phys., 1, 233 (1958).

23. P. Dirac, "The Principles of Quantum Mechanics", Oxford Univ.Press, (1947).

24. D.C. Reitz and S.I. Weissman, J.Chem.Phys., 33, 700 (1960).

25. D. Ingram, "Free Radicals", Butterworths Scientific Press, (1958).

25a. J. van Vleck, Phys.Rev., 74 (1948) 1168. M.H. Pryce and K.W. Stevens, Proc.Phys.Soc., A 63, 36 (1950).

26. P.W. Anderson and P.R. Weiss, Rev.Mod.Phys., 25, 269 (1953). P.W. Anderson, J.Phys.Soc.Japan, Vol.9, No.3, 316 (1954).

27. C. Hutchison, R. Pastor and A. Kowalsky, J.Chem.Phys., 20, 534 (1952).

28. R.I. Walter et al., J.Chem.Phys., 25, 319 (1956).

29. K. Hausser, Ampere Conference, Pisa, 1960.

30. T.R. Tuttle and G. Pake, Phys.Rev.Letters, 3, 423 (1959).

31. R. Karplus, Phys.Rev., 73, 1027 (1948).

32. S.I. Weissman et al., J.Chem.Phys., 21, 2227 (1953).

33. F. Ehlers, M.I.T. Radiation Lab.Series, Vol.11, 361 (McGraw-Hill, 1947).

34. L.B. Young, M.I.T. Radiation Lab.Series, Vol.11, 527 (McGraw-Hill, 1947).

35. B. Bleaney, J. Loubser and R.P. Penrose, Proc.Phys.Soc., 59, 185 (1947).

36. Bell System Tech.Jour., 25, 411 (1946).

37. S.W. Seely and J. Avins, R.C.A.Rev., 8, 201 (1947).

38. Valley and Wallman, M.I.T. Radiation Lab.Series, Vol.18, 431 (McGraw-Hill, 1947).

39. Van Voorhis, ibid., Vol.23, 52.

40. Nyquist, Bell System Tech.Jour., 11, 126 (1932).

41. R.V. Pound, M.I.T. Radiation Lab.Series, Vol.11, 69 (McGraw-Hill, 1947).

42. J.C. Slater, "Microwave Electronics", pages 71, 89, van Nostrand (1954).

43. S. Seely, "Electron Tube Circuits", 359, (McGraw-Hill,1950

44. H. Logemann, M.I.T. Radiation Lab.Series, Vol.11, 69 (McGraw-Hill, 1947).

45. Valley and Wallman, ibid., Ch.10, 384, Vol.18.

46. N.A. Schuster, Rev.Sci.Instrum., 22, 254 (1951).

47. W.A. Edson, "Vacuum Tube Oscillators", 138, Wiley and Sons (1953).

48. D.T.N. Williamson, Wireless World, Vol.LV, 8, 282 (1949).

49. Artree, Electronic Engineering, April 1955.

50. D.W. Rogers, Electronic and Radio Engineer, 34, No.9, 320 (1957).

51. G.C. Lowe, Electronic Engineering, page 138, March 1959.

52. Chance, M.I.T. Radiation Lab.Series, Vol.19, 35 and 258, (McGraw-Hill, 1947).

53. Pound, ibid., Vol.16, 10.

54. Pound, ibid., Vol.16, 238.

55. Pound, ibid., Vol.16, 58.

56. Valley and Wallman, ibid., Vol.18, 660.

57. Pound, ibid., Vol.16, 257.

58. R.S. Mulliken, J.Amer.Chem.Soc., 74, 811 (1952).

59. W. Brackmann, Rev.trav.chim., 68, 147 (1949).

60. J. Weiss, J.Chem.Soc., 245 (1942).

61. M.J. Dewar, Nature, 156, 784 (1945).

62. Y. Matsunaga and C.A. McDowell, Nature, 185, 916 (1960).

63. W.D. Phillips, J.Chem.Phys., 34, 684 (1961).

64. K. Hausser, British Radio Spectroscopy Group, St.Andrews (1961).

64a. J.E. Wertz and J. Vivo, J.Chem.Phys., 24, 479, (1956).

65. R. Foster, Chemistry Department, Queen's College, University of St.Andrews. Private Communication.

66. E.M. Kosower, J.Amer.Chem.Soc., 80, 3253 (1958).

67. W.D. Phillips et al., J.Chem.Phys., 33, 626 (1960).

68. N. Atherton and S.I. Weissman, J.Amer.Chem.Soc., 83, 1330 (1961).

69. Ward and S.I. Weissman, J.Amer.Chem.Soc., 79, 2086 (1957).

70. See J.Amer.Chem.Soc., 80, 2778-2844 (1958).

71. L.Y. Jackmann, Adv.in Org.Chem., (Methods and Results), Vol.2, 333 (Interscience, 1960).

72. H.S. Jarrett, J.Chem.Phys., 21, 761 (1953).

ACKNOWLEDGEMENTS

I should like to record my sincere thanks to:-

Professor J.F. Allen, F.R.S. : for his interest and allowing me the facilities of Edgecliffe Research Laboratory.

Dr D. Bijl, F.R.S.E. : for suggesting the topic, his supervision and his stimulating advice.

Dr R. Foster, Chemistry Department, Queen's College, Dundee. : for samples and for showing me his optical absorption measurements.

Dr C.K. Campbell, McMaster University, Ontario, Canada, and Mr S. Hamilton, University of Manchester. : for most helpful advice with some of the electronics.

Mr J. Gerrard. : for his assistance with the photography.

Messrs. R.A. Beveridge and C.B. Taylor. : with whom the magnet and some of the waveguide components were designed.

Messrs. J. MacNab, T. Marshall, G. Dunsire. : for excellent fabrication of certain waveguide components.

Messrs. J. Campbell (Astronomy Department, St.Salvator's College, St. Andrews), H. Cairns. : for the generous loan of some equipment.

Dr D.H. Reid, Chemistry Department, St.Salvator's College, St. Andrews. : for samples of Dicyanodichloro-p-quinone.

Miss J.M. Lawson : for the efficient typing.

The Department of Scientific and Industrial Research, the University of St. Andrews and The Carnegie Trust. : for the award of maintenance grants.

The Madras College Trustees. : for the award of a grant that enabled me to attend the Summer School in Quantum Chemistry in Uppsala, Sweden (1960).

The Participants and Staff of that Summer School. : for many stimulating conversations.